

# **Influence of the Wall on the Heat Transfer Process in Rotary Kiln**

**Dissertation  
zur Erlangung des akademischen Grades**

**Doktoringenieur  
(Dr.-Ing)**

**von Mr. Yogesh Sonavane**

**Geboren an 10.04.1978 in Malegaon, Indian**

**Genehmigt durch die Fakultät für Verfahrens und Systemtechnik  
der Otto-von-Guericke Universität Magdeburg**

**Promotionskommission Prof.Dr.-Ing Eckehard Specht (Supervisor & Reviewer)**

**Prof. Dr.-Ing Evangelos Tsotsas (Reviewer)**

**Prof. Dr.-Ing. habil. Jürgen Tomas (Head of examination board)**

**eingereicht am 06 April 2010**

**Promotionkolloquium am 15 June 2010**

## **Acknowledgment**

I would like to thank my family for their support to excel in every bit of my life. I want to dedicate this small piece of magnum opus for them; to my Mom and beloved Dad Late Mr. Shiram Vaman Sonavane, who always supported me and encouraged me to get my Doctoral degree.

Meeting the real standards is a monumental task, and I believe that I reached it to some extent. There is no home feeling as I have so many cheerful friends not only from India but also from other countries and their guidance gave me moral support to achieve my goal.

I would like to express the deepest appreciation to my committee chair, Professor E. Specht, who has the attitude and the substance of a genius: he continually and convincingly conveyed a spirit of adventure in regard to research and scholarship, and an excitement in regard to teaching. Without his guidance and persistent help this dissertation would not have been possible.

I would like to thank Dr. Woche, Prof. Xiaoyan Liu and the laboratory people Mr. Timpe, Mr, Suehring for their kind support in design and construction of the pilot plan in our laboratory.

I would like to thank to family members, my friends and good wishers; A. Katariya, A. Nallathambi, D. Pesheva, D. Mote, F. Herz, G. Sandaka, G. Mirajkar, H. Pastagiya, K. Sunkara, N. Birari, O. Chakradhar, S. Mahadik, S. Sheshadri, S. Bakshi, S. Sonavane, S. Pawar, T. Kotsev, X. Eison and Y. Gokhale for their kind support during my research work and stay in Germany.

Yogesh Sonavane

Magdeburg, Germany

# Contents

---

List of symbol used in the study	I
Greek Symbols	III
Superscript	III
Subscript	IV
Summary	1
Zusammenfassung	4

## Chapter 1

### Introduction and Literature review

1.1 Rotary kiln evolution	7
1.2 Introduction	9
1.3 Comparison of the Rotary kiln with other contactors	11
1.4 Direct Fired Rotary Kiln	12
1.5 Indirect Fired Rotary Kiln	13
1.6 Heat transfer Phenomenon in Rotary kiln	14
1.6.1 Principle Phenomenon at bed	14
1.6.2 Transverse bed motion	15
1.7 Some numerical techniques used like CFD models and some design methods	17
1.8 Calculation method of heat transfer coefficient	22
1.9 Measurement of heat transfer coefficient	23
1.9.1 Convective heat transfer coefficient	29
1.9.2 The radiative heat transfer coefficient	30

<b>References</b>	<b>33</b>
-------------------	-----------

## **Chapter 2**

### **Modeling of the temperature fluctuations in the wall of the Rotary Kiln**

2.1. Introduction	38
2.2. Numerical calculation	40
2.3. Analytical calculation	45
2.4 Temperature fluctuation on the wall	50
2.5 Temperature gradient on the wall	60

<b>Conclusion</b>	<b>61</b>
-------------------	-----------

<b>References</b>	<b>62</b>
-------------------	-----------

## **Chapter 3**

### **Design and fabrication of experimental plant of the Rotary Kiln**

3.1 Introduction	64
3.2 Equipment Details	65
3.3 Design and fabrication of the parts	
3.3.1 Stainless steel cylinder	65
3.3.2 Shaft	66
3.3.3 Bearing	66
3.3.4 Electrical Heater	67
3.3.5 Thermo couple arrangements	67
3.3.6 Wireless temperature assembly	68
3.3.7 Supports	69

<b>Conclusion</b>	<b>69</b>
-------------------	-----------

## **Chapter 4**

### **Experimental analysis in the Rotary kiln**

4.1. Experimental setup	70
4.2 Experimental measurement of response time ( $t_r$ )	71

4.3 Comparison of temperature profiles with fixed and rotating thermoelements assembly	73
4.4 Dependency of the placement of the electrical heater	75
4.5 Temperature distribution on the wall and inside of the moving bed	76
4.6 Calculation of the mean temperature of the bed	79
4.7 Experimental analysis of the temperature profile at various time interval	81
4.8 Temperature profiles for very fine material	93
4.9 Temperature profile at various speed of rotation	97
4.10 Heat transfer coefficient of wall to solid	98
4.10.1 Mean temperature of the bed for heat transfer coefficient calculations	99
4.10.2 Evaluation of the heat transfer coefficient of wall to solid	102
<b>Conclusion</b>	<b>106</b>
<b>References</b>	<b>107</b>

## **Chapter 5**

### **Mixing experiments for the heat of granular material in the agitated bed of rotary kiln**

5.1 Mixing in rotary kiln	108
5.2 Model for describing the mixing process	111
5.3 Experimental setup	
5.3.1 Cold experimental	112
5.4 Experimental determination of the mixing in rotary kiln	
5.4.1 Experimental setup for the hot and cold sand	114
5.5 Concept of rotation of the agitated bed with respect to the rotation of the rotary kiln	128
<b>Conclusion</b>	<b>131</b>
<b>References</b>	<b>131</b>

## List of symbols used in the study

A	-	Heat resistance ratio
A	m	Area per unit length
A	m <sup>2</sup>	Surface area
a	m <sup>2</sup> /s	Thermal Diffusivity
Bi	-	Biot number
B	-	Tuning Parameter
b	mm	Effective depth of penetration in the solid bed
c	J/(kgK)	Specific heat capacity
D	m	Diameter
D	%	Percent fill
De	m	Equivalent diameter
d	m	Wall thickness
F	-	Surface area
f	-	Filling degree
G	kg/s	Gas mass flow rate
Gr	-	Grashoff number
H	W/m	Enthalpy per unit length
h	mm	Mean thickness of gas film
L	m	Kiln length
M	-	Mixing quality
Nu	-	Nusselt number

n	rpm	Rotational speed
n	-	Number
Pe	-	Peclet number
Pr	-	Prandlt number
q	W	Heat added
Q	W	Heat flow
$\dot{Q}$	W/m	Heat per unit length of kiln
$\dot{q}$	W/m <sup>2</sup>	Heat flux
R	m	Radius
Re	-	Reynold number
r	m	Radial coordinate
St	-	Stanton number
s	m	Lumped capacity layer
s	m	Wall thickness
s	-	Scattering
T	K	Temperature
t	s	Time
u	m/s	Axial velocity
w	m/s	Tangential velocity
x	rad	Circumferential coordinate
X	-	True concentration
z	m	Axial coordinate along kiln length

## Greek Symbols

$\alpha$	W/(m <sup>2</sup> K)	Heat transfer coefficient
$\beta$	rad	Central angle of solid bed
$\delta$	m	Particle roughness
$\delta$	m	Thickness at the contact point
$\varepsilon$	rad	Filling angle
$\varepsilon$	-	Emmissivity
$\varepsilon$	-	Surface porosity between particles
$\Theta$	degree	Dynamic angle of repose
$\lambda$	W/(mK)	Thermal heat conductivity
$\pi$	-	Constant (3.14)
$\rho$	kg/m <sup>3</sup>	Density
$\sigma$	W/(m <sup>2</sup> K <sup>4</sup> )	Stefan's Boltzman Constant (5.67e-8)
$\tau$	s	Contact time between solid and covered wall
$\varphi$	degree	Angle with circumference
$\chi$	mm	Gas film thickness
$\omega$	1/s	Rotational frequency

## Superscript

ad	advection
cd	Conduction
r	radiant

## Subscript

A	(Tracer) Component A
b, B	Solid bed
c	Critical
c	Contact
D	Diameter
D	Direct
e	Effective heat penetration
eff	Effective
el	Electric
F	Flow
G	Gas
G,0	Initial wall temperature in contact with gas
G0	Convective outer wall
GS	Gas to solid
GW	Gas to wall
g	Gas
i	Inner
i	position
k	Bulk
L	Loss
lam	Laminar

lc	Lumped capacity layer
m	Mean
m	Rotation
n	Number of
o	Unmixed condition
p	Particle
R	Rotational
R	Radius
s	Solid
T	Total
T	Transportation
W	Wall
WS	Wall to solid
WP	Wall to particle
x	Axial region
z	Axial displacement
$\infty$	Final state

## Summary

Rotary kilns are widely used in the chemical and metallurgical industries. Heat transfer is a complicated phenomenon in the case of rotary kiln as it includes conduction, convection and radiation at a same time. Some studies about the heat transfer mechanism have been quoted in the literature. Although many researchers studied the principle phenomena in the kiln, the heat transfer between the particle and wall is not well understood. Therefore, this study has substantiate an analytical solution in a simplified form to understand the inter dependability of the parameters in a more efficient way. The temperature profile on the wall of the rotary kiln depends on various parameter parameters such as diameter of the kiln, total thickness of the kiln wall and the material properties such as thermal conductivity, density and specific heat capacity. The operating parameters such as initial temperature of the gas, initial temperature of the solid, filling degree, number of rotations and also the heat transfer coefficient from wall to solid and from gas to wall have an important role in defining the heat transfer process in rotary kiln.

An uniform analytical equation for the maximum temperature fluctuation on the wall of the kiln has been formed. The formed equation is significantly simplified as reduction of parameters from 11 to 4. A new modified dimensionless Stanton number has been formulated. Temperature fluctuations are independent on the diameter of the rotary kiln and depend on ratio of the heat transfer coefficients from wall to solid to the heat transportation coefficient and gas to the solid to heat transportation coefficient.

Later this model has been verified with two dimensional numerical finite element package ANSYS with an error less than 3 %. The results for temperature fluctuations from numerical and analytical models matches satisfactorily. It has been seen that the temperature fluctuations on the wall in circumferential direction decreases with increase in rotational speed. Due to these temperature fluctuations a thorough study of the temperature gradient at boundary conditions has been studied numerically. High temperature gradients are observed in radial than in circumferential direction.

A thorough investigations are also needed experimentally due to lack of knowledge about temperature distribution and the heat transfer phenomenon inside the agitated bed of solid in the rotary kiln. Hence a pilot scale externally electrical heated rotary kiln made with stainless steel with 0.6 m diameter and 0.45 m length has been designed and fabricated based on the industrial norms. New measurement techniques with fixed and rotating thermoelements have been developed. It is used to measured temperature profile inside agitated solid bed with K type thermoelements. Experiments have been carried out with materials such as 0.2 mm Quartz sand and 0.8 mm Copper pellets. A thorough study of temperature distribution has been done with various time intervals, a cold and hot regions have been observed inside the agitated bed. High temperature has been seen at the top region of the kiln perpendicular to the agitated solid bed. This is due to buoyancy of the hot gas inside the kiln. Temperature of the agitated solid bed can be defined later with the mean value to evaluate heat transfer coefficient.

Heat transfer coefficient from wall to solid have been studied at various filling degrees and the rotational speeds. High value of heat transfer coefficient have been obtained at higher speed of rotations. The comparison of wall to solid heat transfer coefficients have made with available literature. It has been observed that experimental values are higher. This explains the need for a improved model for heat transfer coefficient.

The thermal efficiency of a rotary kiln is influenced by the amount of lateral mixing of the material bed. Hence a new approach of heat transfer mechanism which relates with mixing of solid have been carried out. The mixing can be experimentally determined with hot and cold layer of the solid bed. Experiments were carried out with various filling degrees and rotational speeds. Number of rotations needed for the perfect mixing of hot and cold layer of the sand have been studied thoroughly. New parameter; goodness of mixture has been formulated. It defines how good mixing can be done. These experiments are compared with other experiments which are carried out using solids of two different colors. It has been observed that results with both mechanisms matches perfectly.

Rotation of the agitated solid bed with respect to the rotation of the kiln has been studied thoroughly. This approach can give better understanding of the mixing and heat transfer phenomenon inside the agitated solid bed.

## Zusammenfassung

Drehrohröfen werden häufig in der chemischen und metallurgischen Industrie eingesetzt. Die Wärmeübertragung im Drehrohröfen ist ein kompliziertes Phänomen, da Wärmeleitung, Konvektion und Strahlung gleichzeitig ablaufen. Einige Studien über den Wärmeübertragungsmechanismus in Drehrohröfen werden in der bisherigen Literatur angegeben. Obwohl viele Forscher die Prozesse im Ofen behandelten, wurde der Wärmeübergang zwischen den Teilchen und der Wand nicht eindeutig geklärt. Diese Studie soll daher eine analytische Lösung in vereinfachter Form, zum besseren Verständnis der Abhängigkeit der Parameter, aufzeigen. Das Temperaturprofil an der Wand des Drehrohröfens, hängt von verschiedenen Parameter ab, wie z.B. dem Durchmesser des Ofens, der Dicke der Ofenwand und der Materialeigenschaften, wie thermische Leitfähigkeit, Dichte und spezifische Wärmekapazität. Die Betriebsparameter wie die Anfangstemperatur des Gases und des Feststoffes, der Füllungsgrad, die Drehzahl sowie der Wärmeübergangskoeffizient von Wand zum Feststoff und vom Gas an die Wand, haben einen Einfluss auf den Wärmeübergang im Drehrohröfen.

Eine einheitliche analytische Gleichung für die maximale Temperaturschwankung an der Wand des Ofens wurde aufgestellt. Eine neue modifizierte dimensionslose Stantonzahl wurde eingeführt. Die entstandene Gleichung wurde durch die Kürzung der Parameter von 11 auf 4 wesentlich vereinfacht. Die Temperaturschwankungen sind unabhängig vom Durchmesser des Drehrohröfens, aber abhängig vom Verhältnis des Wärmeübergangskoeffizienten von Wand/Feststoff zum Wärmetransportkoeffizienten und vom Wärmeübergangskoeffizient von Gas/Wand zum Wärmetransportkoeffizienten.

Es hat sich gezeigt, dass die Temperaturschwankungen an der Wand in Umfangsrichtung mit Erhöhung der Drehzahl abnehmen. Das entwickelte Modell wurde mit einem zweidimensionalen numerischen Finite-Elemente-Paket ANSYS mit einem Fehler von weniger als 3% überprüft. Die Ergebnisse für die Temperaturschwankungen vom numerischen und analytischen Modell stimmen gut überein. Aufgrund dieser Temperaturschwankungen wurde der Temperaturgradient an den Randbedingungen umfassend numerisch untersucht. Es wurde gezeigt, dass sich hohe

Temperaturgradienten in radialer Richtung ergeben. Ebenso wurde festgestellt, dass die Temperaturschwankungen an der Wand in Umfangsrichtung mit Erhöhung der Drehzahl zunehmen.

Aufgrund mangelnder Kenntnisse über die Temperaturverteilung und die Wärmeübertragung innerhalb des bewegten Festbettes im Drehrohrofen sind experimentelle Untersuchungen nötig. Daher wurde eine Pilotanlage für einen indirekt elektrisch beheizten Drehrohrofen aus Edelstahl mit 0,6 m Durchmesser und 0,45 m Länge entworfen und entsprechend industrieller Normen hergestellt. Des Weiteren wurden neue Messtechniken mit festen und rotierenden Thermoelementen entwickelt. Unter der Verwendung eines Thermoelementes des K-Types wurden die Temperaturprofile im bewegten Festbett gemessen. Es wurden Versuche mit unterschiedlichen Materialien wie z.B. Quarzsand (Partikelgröße 0,2 mm) und Kupferpellets (Partikelgröße 0,8 mm) durchgeführt. Umfassende Untersuchungen der Temperaturverteilung wurden in verschiedenen Zeitintervallen durchgeführt. Hierbei ergaben sich kalte und heiße Bereiche im Festbett. Hohe Temperaturen konnten am oberen Bereich des Ofens senkrecht zum bewegten Festbett nachgewiesen werden. Dies ist auf den Auftrieb des heißen Gases im Inneren des Ofens zurückzuführen. Die Temperatur des bewegten Festbetts wurde mit einem mittleren Wert definiert, um so den Wärmeübergangskoeffizient zu bestimmen.

Der Wärmeübergangskoeffizient von der Wand zum Festbett wurde für verschiedene Füllgrade und Drehzahlen untersucht. Hohe Werte für den Wärmeübergangskoeffizient wurden bei höheren Drehzahlen erreicht. Die Werte für den Wärmeübergangskoeffizienten wurden mit verfügbaren Daten aus der Literatur verglichen. Es ergaben sich aus den Experimenten höhere Werte für den Wärmeübergangskoeffizient. Dies erklärt die Notwendigkeit eines verbesserten Modells für den Wärmeübergangskoeffizient.

Der thermische Wirkungsgrad eines Drehrohrofens wird durch die Mischung des Materials innerhalb des Betts beeinflusst. Deshalb ist ein neues Konzept, der den Wärmeübertragungsmechanismus unter Einbeziehung der Mischung beschreibt, entwickelt worden. Das Mischen kann experimentell mit warmen und kalten Schichten des Festbetts bestimmt werden. Die Experimente wurden mit verschiedenen Füllgraden und Drehzahlen

durchgeführt. Die Anzahl der Umdrehungen für die perfekte Mischung von kalten und warmen Schichten für Quarzsand wurden ausreichend untersucht. Ein neuer Parameter; die Güte der Mischung wurde formuliert. Sie ist ein Maß die Durchmischung des Betts. Zusätzlich werden Versuche zur Durchmischung des Festbettes aus Schichten mit unterschiedlichen Farben durchgeführt. Es zeigte sich eine gute Übereinstimmung der Ergebnisse.

Ebenso wurde die Rotation des bewegten Festbettes in Bezug auf die Rotation des Ofens untersucht. Dieser Ansatz erlaubt ein besseres Verständnis der Misch- und Wärmeübertragungsphänome innerhalb des bewegten Festbetts.

# Chapter 1

## Introduction and literature review

---

### 1.1 Rotary kiln evolution

Rotary kilns have been synonymous with cement and lime kilns probably because of the history of their evolution and development. It has been reported that cement deposits characterized by Israeli geologists in the 1960s and 1970s place cement making at 12,000,000 BC when reactions between limestone and oil shale occurred during spontaneous combustion to form a natural deposit of cement compounds [1].

Between 3000 and 300 BC the cement evolution had continued with the Egyptians who used mud mixed with straw to bind dried bricks to carry out massive projects such as the pyramids. This evolution continued with the Chinese who used cementations materials for the building of the Great Wall. Projects such as the building of the Appian Way by the Romans later led to the use of pozzolana cement from Pozzuoli, Italy, near Mt. Vesuvius. However, it is reported that the technology that uses the burning of lime and pozzolan to form a cementations admixture was lost and was only reintroduced in the 1300s. In the United States, projects such as the construction of a system of canal in the first half of the nineteenth century, particularly the Eire Canals in 1818, created the first large-scale demand for cement in this country that led to various cement production business to compete for the market share. By 1824 Portland cement had been invented and developed by Joseph Aspdin of England; this involving the burning of finely ground chalk with finely divided clay in a lime kiln yielding carbon dioxide as an off-gas [2]. In these early days, stationary kilns were used and it is said that the sintered product was wastefully allowed to cool after each burning before grinding. In the late 1870s one Thoman Millen and his two sons, while experimenting with the manufacture of Portland cement in South

Bend, Indiana, burned their first Portland cement in a piece of sewer pipe [1]. This perhaps marked the first experimental rotary kiln use in America. By 1885, an English engineer, F. Ransome, had patented a slightly tilted horizontal kiln that could be rotated so that material could move gradually from one end to the other. The underlying principle of this invention constitutes the rotary kiln transport phenomenon we know of today.

Because this new type of kiln had much greater capacity and burned more thoroughly and uniformly, it rapidly displaced the older type of kilns. It has been further mentioned that the factor that contributed to the tremendous surge of Portland cement between 1880 and 1890, reportedly from about 42,000 to 335,000 barrels, was the development of the rotary kiln [1]. Like most early inventions in the United States, it is said that Thomas A. Edison played a role in furthering the development of the rotary kiln. He is credited for introducing the first long kilns used in industry at his Edison Portland Cement Works in New Village, NJ, in 1902. His Kilns are believed to have been about 150 ft long in contrast to the customary length at that time of 60-80 ft. Today, some kilns are more than 500 feet long with applications ranging far wider than cement and lime making. By the 1900s, most of the advances in the design and operation of cement and lime kilns had undergo a systematic evolution since the days of the ancient Egyptians. By this time, almost countless variations of patented kilns had been invented and promoted although some of these never found useful application.

Currently, rotary kilns are employed by industry to carry out a wide array of material processing operations; for example, reduction of oxide ore, reclamation of hydrated lime, calcining of petroleum coke, hazardous waste reclamation, and so on. These widespread usages can be attributed to such factors as the ability to handle varied feedstock, spanning slurries to granular materials having large variations in particle size, and the ability to maintain distinct environments, for example, reducing conditions within the bed coexisting with an oxidizing freeboard (a unique feature of rotary kiln that is not easily achieved in other reactors). The nature of rotary kiln, which allows flame residence times of the order of 2-5 s and temperature of over 2000K, makes such kilns a competitive alternative to commercial incinerators of organic wastes and solvents.

Although generally the long residence time of the material within the kiln (typically greater than one hour) aids in achieving an acceptably uniform product as the early users had intended, there is considerable scope for improving this aspect of kiln performance. In order to achieve this improvement a more quantitative understanding of transport phenomena within the bed material is required; specifically of momentum transport, which determines particle motion and energy transport, which, in turn determines the heating rate for individual particles [3].

## **1.2 Introduction**

Rotary kilns are ubiquitous fixtures of the chemical, metallurgical, and pharmaceutical process industries. They are commonly used for three purposes: heating, reacting, and drying of solid material, and in many cases they are used to achieve a combination of these aims [4]. Within recent years, rotary kilns have become widely used for the thermal treatment of waste material. ( e.g. the incineration of hazardous waste [ 5 - 7 ], the gasification of waste tires or wood to achieve activated carbon [ 8, 9 ] and the thermal adsorption of carbonated soils [ 10 ]). This widespread usage can be attributed to factors such as the ability to handle varied feedstock, for example slurries or granular materials having large variations in particle size, or the ability to maintain distinct environments, for example reducing conditions within the bed coexisting with an oxidizing freeboard [ 11 ].

Slow rotation of an inclined kiln enables the thorough mixing of wastes during their transport from inlet to outlet and flexible adjustment of the residence time can yield the optimum conditions for the thermal destruction of solid wastes [12, 13]. In the design and modelling of rotary kilns, two important aspects should be considered from a process engineering point of view; heat transfer and reaction kinetics. Heat transfer is the most important of these aspects because in many practical cases heat transfer limits the performance of rotary kilns. [11, 14].

Compared with the other gas/solid reactors, such as packed bed fluidized bed, the intrinsic features of heat transfer in rotary kiln include:

I .Heat transfer coefficient between the gas and rotating wall and between the gas and rolling bed surface are all influenced by the rotation rate of the drum.

II. The inner wall contacts periodically with the high temperature gas and at intervals with the bulk bed, so heat from the high temperature gas absorbed by the wall is delivered indirectly to the bed. This heat transfer process is described as a “storage-release mechanism” which is dependent on the heat transfer mechanism between the inner wall and bulk bed [15]. Thus, it is very important to determine the heat transfer coefficient between the inner wall and solid bed.

III. Radiation heat transfer cannot be ignored in a relatively higher temperature environment, especially when the temperature exceeds 1000<sup>0</sup>C.

In general, a rotary kiln can be classified as internally heated and externally heated, which we will discuss it later in detail. The internally heated mode mainly used as a waste incinerator, has high temperature flue gas as its heat source. This kind of heating mode makes use of coal, gas, or oil directly. The fuel goes through a combustor or burner where it is mixed with air or oxygen to generate high temperature gas. The high temperature gas then introduced into the drum in a direction either co-current or counter-current to the solid flow. However the externally heated rotary kiln can use either electrical heat flux or the outer wall that is indirectly heated by the high temperature flow as its heat source. The externally heated kiln is often adopted as a pyrolyser or gasifier of a special kind of waste. The largest difference between the two modes is that the heat loss from the outer wall to the environment should be considered in an internally heated mode, while the heat sourced from outer wall should be consider in an externally heated mode.

Solids retention time in the kiln is an important design factor and is set by proper selection of the diameter, length, speed, slope and internal design.

### 1.3 Comparison of the Rotary kiln with other contactors

As can be seen from the history of its evolution, the design and operation of rotary kilns have undergone a systematic evolution since the days of the ancient Egyptians. Improvements include reduced labor, increased productivity, mixing, heat transfer, and product quality.

Mineral processing kilns can be classified as vertical, horizontal, or other miscellaneous mixed types. At one extreme, vertical kilns operate in the packed-bed mode whereby the material being processed (calcined) is charged from a top hopper and contained in a vertical chamber in which the static bed moves downwards in plug flow.

Typical feature of Rotary and Other Contact Kilns

Vertical Kilns	Horizontal Kilns	Other/Mixed
Traditional shaft-type kilns	Conventional long wet, dry rotary kilns	Fluidized-bed type kilns
Indirect gas fired	Direct or Indirect fired	Gas suspension type kilns or flash calciners
Large capacity, mixed feed, canter burners	Noncontact externally heated small capacity kilns used for niche applications	Rotary hearth with traveling grate or calcimatic kilns
Parallel flow regenerative type	Modern with recuperators such as cooler type, preheater kilns and internals cylinder	Horizontal ring type, grate kilns etc.

Of the modern day rotary kilns can be distinguished such as, wet kilns, long kilns, short dry kilns, coolers and dryers and indirect fired kilns.

Several types of kiln designs have evolved, each specific to the process application it is intended for. They also come in several forms and shapes. Although the majority consist of straight, cylindrical vessels, dumbbell-shaped designs takes advantage of the benefits that variable drum sizes can bring to process application.

#### **1.4 Direct Fired Rotary Kiln**

A direct fired rotary kiln has the combustion gases going through the rotary kiln / dryer. The combustion can either take place in a combustion chamber (normal for a dryer) or the flame can be directed down the length of the rotary kiln (typical for calciners).

In a drying application, the contact between the gases and the solids is the primary form of heat transfer. In a calcining application, the radiation from the flame is the primary form of heat transfer. Rotary kilns can operate in either the co-current mode where the gases and solids move in the same direction or in the counter-current mode where they move in opposite directions.

The kiln can also be operated in either the reduction or oxidation mode. In this type of the rotary kiln, heat source is placed inside of the kiln. Advantage of this type is, kiln gives more efficiency. The modes of heat transfer for internally heated rotary kiln is as shown in figure 1.1.

Heat source has been considered at the centre of the kiln. Solid bed gains heat from the heat source directly, also at the same time kiln wall gains heat from the central heat source. Wall reflects part of the heat reversed on the solid bed and some heat gets stored in the wall in the form of enthalpy. Part of the heat is lost in the atmosphere.

Velocity profile inside the solid bed can be seen as shown in below figure.

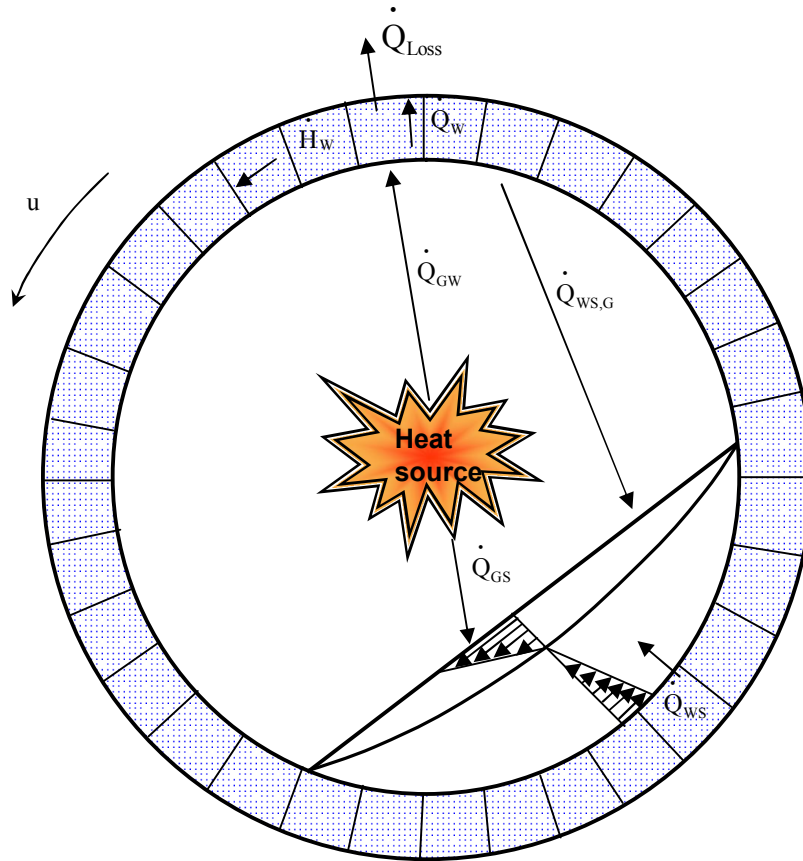


Figure 1.1 Modes of heat transfer in a rotary kiln: internally heated

## 1.5 Indirect Fired Rotary Kiln

With an indirect fired rotary kiln the combustion or other form of heating takes place on the outside of the rotary kiln shell. This way, the material being processed does not come into contact with the combustion gases. This can be important to the product quality or to keeping the product from reacting to the gases. Another advantage is that the amount of gases coming from the kiln that need to go through an emission control system is very small. Indirect rotary kilns can also be used as coolers. Modes of heat transfer for externally heated rotary kiln is as shown in figure 1.2. Heat source present at the outside of the kiln. Most of the time this source can be electrical heat source.

Kiln wall gains heat from the external heat source, Solid bed gains heat from the wall

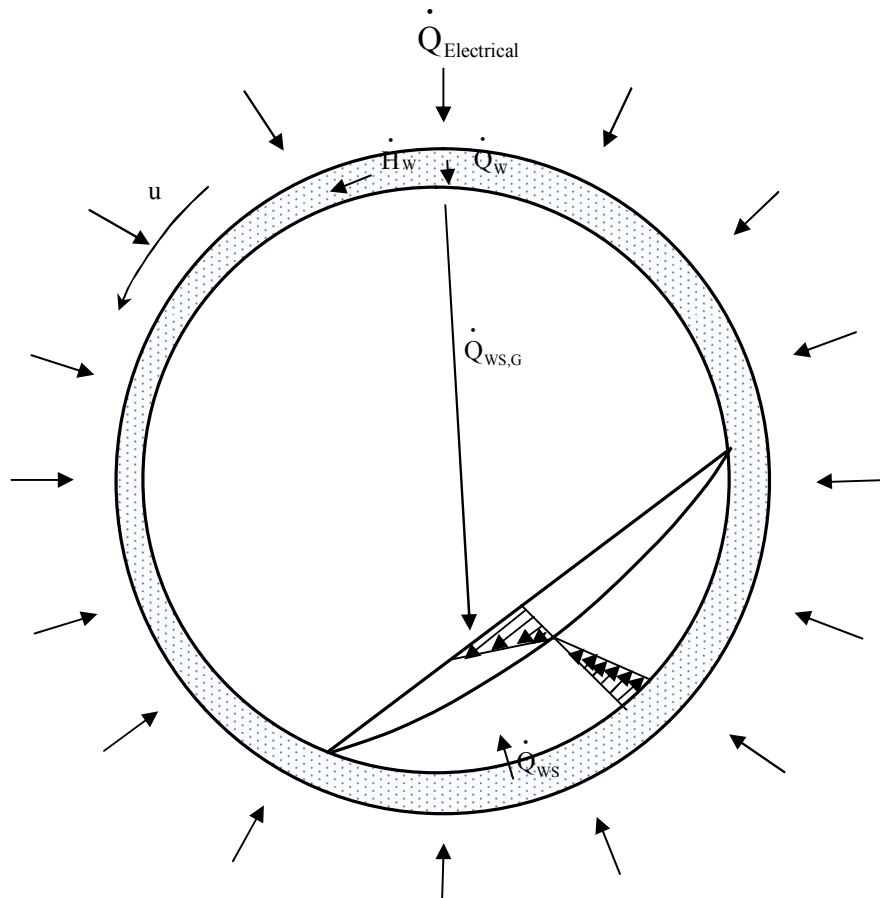


Figure 1.2 Modes of heat transfer in a rotary kiln: Externally heated

indirectly, part of heat get stored in the wall. This stored heat is in the form of enthalpy. Wall reflects part of the heat reversed on the solid bed. Part of the heat is lost in the atmosphere. Velocity profile inside the solid bed have been seen as shown in the figure.

Radiative heat transfer between a non grey freeboard gas and the interior surfaces of a rotary kiln has been studied by evaluating the fundamental radiative exchange integral using numerical methods.

## 1.6 Heat transfer Phenomenon in Rotary kiln

### 1.6.1 Principle Phenomenon inside the bed

During the heat processing of granular materials in rotary kilns, heat transfer within the bed material occurs by the similar mechanisms as in any packed bed and in the shaft kilns.

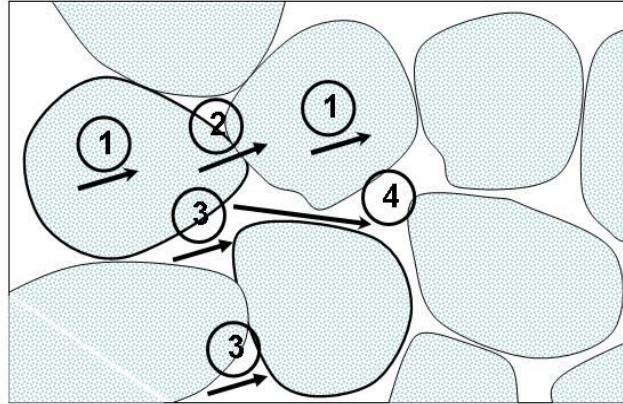


Figure 1.3 Bed heat transfer paths. 1. Internal conduction. 2. Particle to- particle conduction. 3. Particle-to-particle radiation. 4. Interparticle convection.

Heat transfer paths can be particle-to-particle conduction and radiation, as well as interstitial gas-to-particle convection as shown in Figure 1.3. However, the movement of the particles themselves superimposes an advective component for energy transport, which has the potential to dominate heat transfer. Hence the key features of a rotary granular bed is the motion in the transverse plane, which sets the axial flow in motion and is dependent upon the rotation rate, degree of fill (volume of the kiln occupied by material) and the rheological properties of the particulate material. Bed motion plays an important role in the heat transfer phenomenon.

### 1.6.2 Transverse bed motion

Depending on the kilns rotation rate, the bed motion in the transverse plane may be characterized as centrifuging, which occurs at critical and high speeds. This is an extreme condition in which all the bed material rotates with the drum wall. Cascading, which also occurs at relatively high rates of rotation, is a condition in which the height of the leading edge (shear wedge) of the powder rises above the bed surface and particles cascade or shower down on the free surface. Bed motion in cross section is as shown in figure 1.4. It has been established that [16] the dynamic similarity of the rotary drum behavior, and

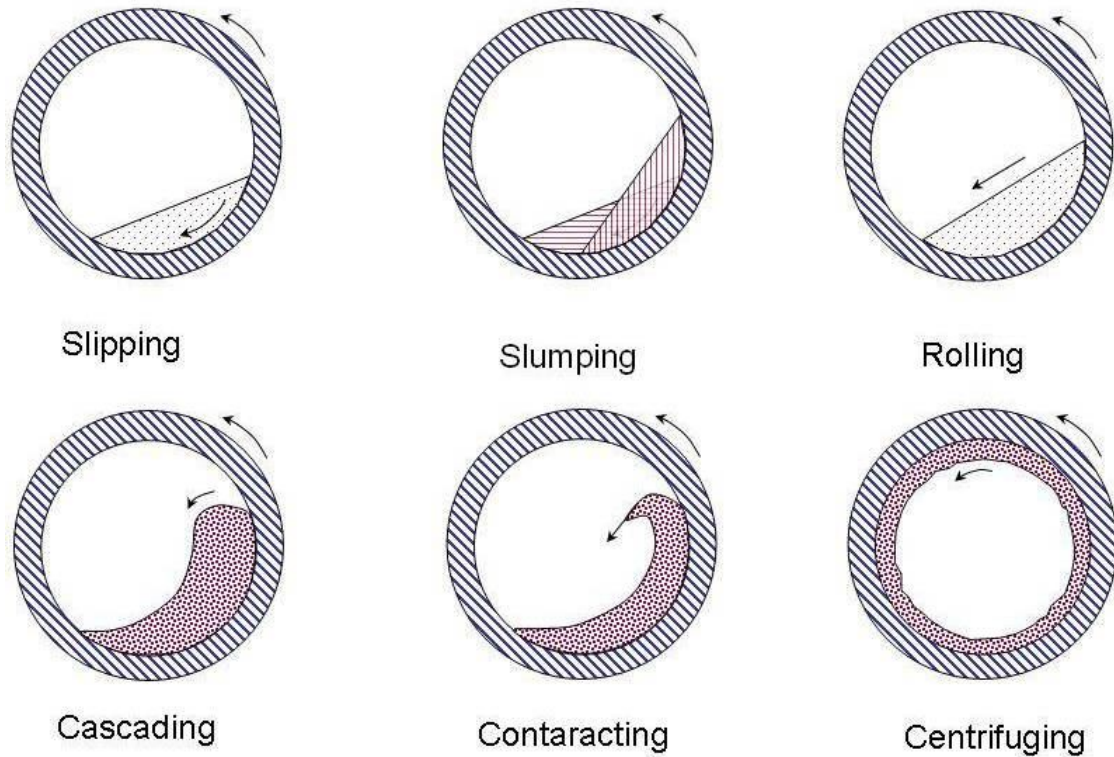


Figure 1.4 Bed motion in cross sectional plane

hence the type of transverse bed motion that occurs during powder processing, is dependent upon the rotational Froude number,  $Fr$ , defined as below,

$$Fr = \frac{\omega^2 R}{g} \quad 1.1$$

Where the critical condition for centrifuging implies  $Fr = 1$ . In the rolling mode as shown in figure 1.4, where rotary drum mixing is maximized, two distinct regions can be discerned, the shearing region, called the active layer, formed by particles near the free surface, and the passive or plug flow region at the bottom where the shear rate is zero.

Studies involving rotary kiln bed behavior have resulted in many ways of estimating how the bed will behave at any given operational condition. One such tool is a bed behavior diagram [17] as shown in figure 1.5, which presents a typical behavior of a sand bed for a 41 cm diameter pilot kiln.

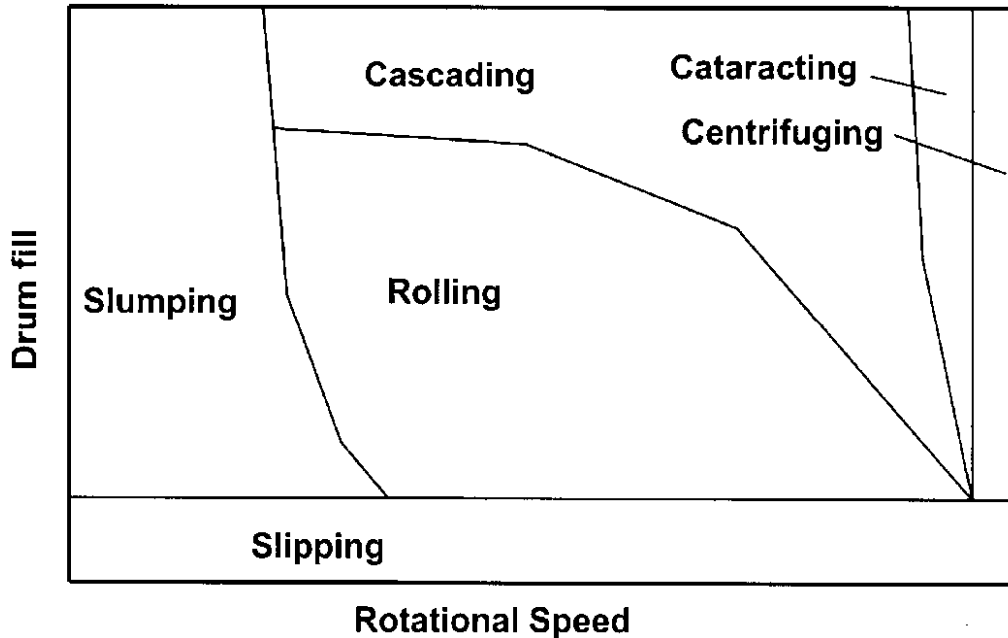


Figure 1.5 Bed behavior diagram. Mapping of bed behavior regimes for different operation conditions. ( Henein, 1980 )

More details about some experimental determination of the two different colored particles and mixing time have been well explained in Chapter 5.

## 1.7 Some numerical techniques used like CFD models and some design methods

Modeling has aided the design and operation of rotary kilns over the years. Many one dimensional models are available in the literature [18-29]. A three dimensional steady state model to predict the flow and heat transfer in a rotary kiln is presented [30]. There are others but these are generally available to the public. The common dimension of interest in one-dimensional models is the kiln longitudinal axis. A series of equations representing conservation of mass, energy and species averages over the cross section are solved using appropriate numerical methods. The critical assumption that must be made is that uniform conditions exist across the cross-section in the freeboard gas, the wall and bed. The bed for example is assumed to be well mixed and isothermal in any given transverse plane. Although these models have been successfully used in industry, they are

limited in the amount of information that can be extracted. Flame positioning for example can be predicted in multi-dimensional models rather than used as an input.

As a result a number of researchers have begun the quest for a more encompassing modelling effort. Boateng and Barr [31] have coupled a conventional one dimensional plug flow model with a two-dimensional reorientation of the beds transverse plane. This improves the ability to simulate conditions within the bed.

Alyaser [32] has modeled for axisymmetric conditions. The model was validated using thermal measurements from UBC's pilot kiln. This effort demonstrates how a model may be used to capture flame phenomenon for Rotary kilns (adjustments of primary air ratio, primary jet momentum, extracting flame length, etc.)

Bui et al.[33-35] were the first to construct a three dimensional model for a rotary petroleum coke calciner, Four submodels (gas, bed, refractory and radiation) were coupled using four grid domains. The model takes into account the major phenomenon of interest including the gas flow, all modes of heat transfer, combustion, bed motion and thermal effects of the refractory.

A numerical simulation involving fluid flow and heat transfer is presented in order to improve the understanding of rotary furnace [36]. The finite element model is employed to simulate the furnace rotation and analyse the energy flow inside the furnace. A transient dynamics analysis is carried out to predict the evolution and distribution of temperature in a rotary furnace by modelling and analyzing the furnace under different flame positions. The finite element modelling system ELFEN is used to develop models of the furnace. The results clearly indicate the temperature distribution for different angular velocities along with a comparison of temperature variation under different flame positions.

In order to improve the design in terms of energy efficiency and productivity a numerical study is necessary to build a mathematic model involving fluid heat transfer.

The first model for the prediction of axial transport in a rotary cylinder was proposed by Sullivan et al.[37] and then developed to study the isothermal transverse motion of a bed of particulate materials by Friedman and Marshall [37], Perry et al.[38], Mu and perlmutter[39] and Perrron and Bui [40]. Since the early 1980s, several numerical approaches have been used to model granular heat transfer methods using Kinetic theory [41], Continuum approaches [40; 41; 42; 43] and Discrete element modelling (DEM) [44, 45, 46, 47, 48, 49].

The constitutive model based on kinetic theory incorporates assumption such as isotropic radial distribution function, a continuum approximation and purely collision interactions amongst particles, which are not completely appropriate in the context of actual granular flow. The discrete element method originally developed by [50,51] has been used successfully to simulate chute flow.

Clinker formation in coal-fired rotary cement kilns under realistic operation conditions has been modeled with a commercial axisymmetric CFD code for the gaseous phase including a Monte Carlo method for radiation, a finite volume code for the energy equation in the kiln wall and a novel code for species and energy conservation equations, including chemical reactions, for the clinker [52].

The single phase forced convective heat transfer and flow characteristics of water in microchannel structures/plates with small rectangular channels having hydraulic diameter of 0.133-0.367mm and distinct geometric configurations were investigated experimentally[53].

The procedure used to correlate the convective heat transfer coefficient data can be described [54]. Heat added by electrical heater. Heat transfer coefficient of Lithium bromide water solutions can be measured with the help of apparatus tube test section in which 25 thermocouples were used to measure the fluid temperature while another 25 thermoelements were used to measure the surface temperature

$$\alpha_{ws} = \frac{q}{A(T_s - T_m)} \quad 1.2$$

Where

q = heat added, W

A= Area surface, m<sup>2</sup>

T<sub>s</sub>, T<sub>m</sub> = Surface and Fluid mean temperature respectively , °K

In his study heat transfer coefficient correlate as

$$Nu = 0.02844.Re^{0.8} Pr^{0.4} (\mu^*)^{0.327} \quad 1.3$$

$$2300 \leq Re \leq 6000$$

$$1 \leq Pr \leq 6$$

Where  $\mu^*$  = Viscosity 1.4

Experimental study of the radiant heat transfer coefficient of diffusion flames explained well in [55]. The radiation heat transfer in diffusion flame is contributed by soot and gas components. In general, total emissivity with the total radiation heat transfer coefficient with combustion products is given by the relation as,

$$\epsilon_T = \epsilon_G + \epsilon_{Soot} - \epsilon_G \epsilon_{Soot} \quad 1.5$$

Where,

$\epsilon_T$  is total emissivity of combustion product,

$\epsilon_G$  is total emissivity of gas component

$\epsilon_{Soot}$  is total emissivity of soot

The average of temperature and soot fraction on a transversal cross-section of the flame is given by the following formula

$$\bar{T} = \frac{\sum T_i L_i}{L}, \bar{f}_v = \frac{\sum f_{vi} L_i}{L} \quad 1.6$$

T<sub>i</sub>, f<sub>vi</sub> temperature and soot concentration at zone i, L is optical length of the flame at considerable cross-section. A method has been developed for the calculation of heat transfer coefficients for various kinds of surfaces in a multistage thermoelectric cooler exchanging heat with gaseous media and bodies [56].

Heat is supplied to the working site via the leads of the soldered connections of the PSE and by convection, Heat is supplied to the working site via the leads of the soldered connections of the PSE and by convection, conduction, and radiation through the gaseous medium from the vacuum tank and through the sapphire window. The working site (7.3 \* 3 mm) is located at distance , $\delta_0 = 1.6$  mm from the top part of the vacuum tank so that heat transfer occurs in a confined space, which, with the present dimensions, can be considered a horizontal slot filled with a gaseous medium. When the heated surface is located at the top, convection is absent in the horizontal slots, and heat is transferred by conduction through a gas interlayer with thickness,  $\delta_0$ . In this case the heat transfer coefficient  $\alpha = \lambda_{\text{med}} / \delta_0$  and the heat transferred by contact

$$Q_{\text{med}} = \alpha_{\text{med}} S_s (T_{\text{med}} - T_0) \quad 1.7$$

Where  $\alpha_{\text{med}}$  is the heat transfer coefficient of the medium;  $S_s$  is the surface area of the working site;  $T_{\text{med}}$  is the temperature of the medium;  $T_0$  is the temperature of the working site. The thermal conductivity is determined at the average temperature of the medium

$$T = (T_{\text{med}} + T_0)/2, \quad 1.8$$

The radiation heat transfer is defined by the formula,

$$\alpha_r = \sigma \epsilon_{\text{red}} \frac{T_1^4 - T_2^4}{T_1 - T_2} \quad 1.9$$

so total heat transfer coefficient in the medium is as,

$$\alpha_T = \alpha_{\text{med}} + \alpha_r \quad 1.10$$

The Wilson plot is a technique to estimate the film coefficients in several types of heat transfer processes and to obtain general heat transfer correlations. This method is an outstanding tool in practical applications and in laboratory research activities that involve analysis of heat exchangers. Moreover, the application of this method is simple enough to be taught in laboratory practices for students at university and doctoral level of physics and engineering[57]. In this study, they also used the same equation which states above.

## 1.8 Calculation method of heat transfer coefficient

The calculation of heat transfer coefficient was based on a simple but realistic equation with the following assumptions.

1. The gas phase is in plug flow and at uniform temperature at each axial position.
2. Since the solid bed temperature is radially uniform, therefore the solid temperature is a function of axial distance only. Solid moves in plug flow.
3. The wall temperature is taken to be independent of angle and time. The experimental results show insignificant fluctuations of wall temperature under conditions used.
4. The bed surface is assumed flat, and in the calculation of gas/bed coefficient its area is taken equal to the chord length times the bed length.

Heat transfer between the covered wall and Bulk bed can be summarized as,

The total heat transfer coefficient between the covered wall and bed include summation of following 3 resistances.

1. Thermal resistance caused by the solid mixing,
2. Thermal resistance from the bed surface to the bulk bed
3. The contact resistance between the wall and the bed surface

### 1. Covered wall-bed heat transfer

- a) Conduction heat transfer coefficient

### 2. Convection in the free board gas

- a) Convection between the gas and wall
- b) Convection between gas and solid bed
- c) Convection to the outer shell

### 3. Radiation in the free board gas

- a) Radiative heat transfer

## 1.9 Measurement of heat transfer coefficient

In the present study, we focused on the way of calculation of the heat transfer coefficient from the wall to solid in the rotary kiln, and apply the same procedure and equations has been explained in Chapter 4.

Before moving on to a brief explanation of the studies of heat transfer, here we will review some more literature about heat transfer mechanism. Following is the discussion of experimental heat transfer coefficient and model equations were used to calculate same.

The earlier investigation on this heat transfer was by Watchers and Kramers (1964) using heating sand of unspecified size in a rotating copper drum of 0.152 m ID with 0.475 m.

At relatively lower speed ( $n < 10$  rpm), the heat transfer coefficient from wall to the solid is as,

$$\alpha_{ws} = \frac{1}{\frac{\sqrt{\pi a_{ws} t_{ws}}}{2\lambda_b} + \frac{\sqrt{\pi d}}{2\lambda_b}} \quad 1.11$$

$d$  can be obtained by extrapolating the experimental data from the above equation

$$d = 1.12 \times 10^{-3} \sqrt{2\varepsilon} \quad 1.12$$

for 10% filling degree and with 6 rpm speed of rotation, the value of  $d$  is 1.8 mm  $\alpha_{ws}$  can be 151 W/m<sup>2</sup>K.

Other simplified model was applied by Wes et al. (1976) [14] in a drum of industrial scale drum of 9.0 m ID x 0.6 m. The initial boundary condition is illustrated in

$$\begin{aligned}\alpha_{ws} &= 2\sqrt{\lambda_b \rho_b c_b / (\pi \cdot t_c)} \\ &= 2\lambda_b \sqrt{(2\pi/a_b \varepsilon)}\end{aligned}\tag{1.13}$$

$$Nu = 2\sqrt{2}Pe^{1/2}\tag{1.14}$$

$$\text{of which } Nu = \alpha_{ws}L_w/\lambda_b \quad Pe = nR^2\varepsilon/a_b\tag{1.15}$$

The wall temperature was measured at 4.57 m from the entrance by thermocouple placed flush with the wall. Since the drum was heated by steam, the wall temperature was taken to be constant along the drum length. Potato starch or yellow dextrine with particle size of 15-100  $\mu\text{m}$  and filling degree between 11 and 23% were used. The rotation speed was predetermined at 1.6-6.5 rpm.

In the work of Lemberg et al. (1976) [58], a laboratory rotary kiln was used in his work with the dimension of 60 cm length 25 cm diameter and wall thickness of 3 mm. They introduced two regions at the contact between the solid and the wall as shown in figure 1.7

$$\alpha_{ws} = \frac{b_e}{\sqrt{t_c}} \left[ \frac{2}{\sqrt{\pi}} - \frac{1}{h\sqrt{a_b t_c}} + \frac{1}{h\sqrt{a_b t_c}} e^{h^2 a_b t_c} \text{erfc}(h\sqrt{a_b t_c}) \right]\tag{1.16}$$

$$\text{where } h = a_g/\lambda_b\tag{1.17}$$

Boundary conditions,

$$T = T_w = \text{const tan } t, \text{ for } x = 0 \text{ for every } t \quad \text{for region 1}$$

$$T = T_i = \text{const tan } t, \text{ for } t = 0 \text{ and every } x \quad \text{for region 1 and 2}$$

$$\left( \frac{\partial T}{\partial x} \right)_{x=0} = -\alpha_{eff} \cdot (T_w - T_{x=0}) \quad \text{for region 2}\tag{1.18}$$

The overall wall-bed heat transfer coefficient across the two regions

$$\alpha_{eff} = \frac{1}{\frac{1}{\alpha_{ws}} - \frac{1}{\alpha_G}}\tag{1.19}$$

$$\alpha_G = h(1-\varepsilon) \frac{(r_m - \delta u)}{r_m^2} \tag{1.20}$$

$$h = 2\lambda_G \frac{r_m}{(r_m - \delta_s)^2} \left( \ln \frac{r_m}{\delta_g} - 1 + \frac{\delta_s}{r_m} \right) \tag{1.21}$$

1.21

where  $b_b = \sqrt{\lambda_b c_b \rho_b}$  is the effective depth of penetration in the solid bed,  $t_c$  is the contact time between solid and covered wall,  $a_b = \frac{\lambda_b}{c_b \rho_b}$  is the effective thermal diffusivities,  $r_m$  is the mean particle size,  $\delta_g$  is the thickness of the thin gas layer and  $\delta_s$  is the surface porosity between particles.

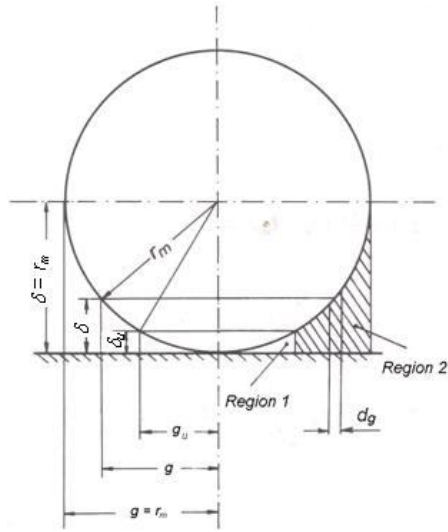


Figure 1.7 Two-region penetration model for wall-bed heat transfer (after Lehmberg et al. 1977)

By adjusting the values of  $h$  and  $\delta u$ , above equation was reported in good agreement with their own experimental data using Quartz sand (mean particle sizes 157, 323, 794 and 1038  $\mu\text{m}$ ) and sodium carbonate (soda)(mean particle size 137  $\mu\text{m}$ ). He reported the value of heat transfer coefficient between wall and solid around 40-400  $\text{W}/(\text{m}^2\text{K})$  for a

short contact time ( $1/t_c = 2s^{-1}$ ). The mean thickness of the gas film ( $\frac{l}{h}$ ) increases with increasing particle sizes. The parameters,  $h$  and  $\delta u$  were determined experimentally, therefore equation is not readily used for design purpose.

Heat transfer coefficient between the wall and solid is  $\alpha_{ws} = 400 \text{ W/m}^2\text{K}$ , from his data,  $h = 1400 \text{ m}^{-1}$

The simple penetration model was proposed by Tscheng S.H. (1979) [59].

$$\alpha_{ws} = 11.6 \times \frac{\lambda_b}{L_{ws}} \times \left[ \frac{n \cdot R_i \cdot 2\varepsilon}{a_b} \right]^{0.3} \quad 1.22$$

$L_{ws}$  is the length of the wall to solid in contact,  $\alpha_{ws} = 637 \text{ W/m}^2\text{K}$

Other simplified model was applied by Wes et al. (1976)[27] in a drum of industrial scale drum of 0.9 m ID with 0.6 m length.

$$\alpha_{ws} = \frac{2\lambda_b}{\sqrt{\pi a_{ws} t_{ws}}} \quad \alpha_{ws} = 400 \text{ W/m}^2\text{K} \quad 1.23$$

Schlünder: heat penetration model (1982) [60] Schlünder and Tsotsas (1988)[61] studied heat transfer in a packed bed and stirred beds from the surface of immersed bodies causes temperature profiles as shown in figure 1.8.

They assumed that there is a thin layer of gas film existing at the contact point of the round particle and slippery wall, which is less than the mean free path of the gas molecule. In the study they introduced two parameters,  $\alpha_{ws}$  as wall surface to bed surface and  $\alpha_{wp}$  as wall to particle heat transfer coefficient,

$$\alpha_{ws} = \phi \cdot \alpha_{wp} + (1 - \phi) \frac{2\lambda_g / d}{\sqrt{2 + (21 + 2\delta) / d}} + \alpha_{rad} \quad 1.24$$

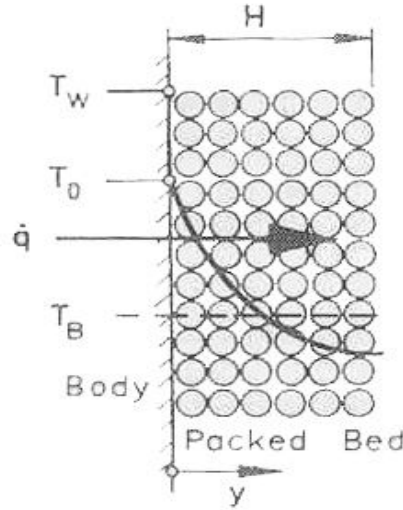


Figure 1.8 Temperature profile in a packed bed heated from the surface of an immersed body (after Schlünder and Tsotsas 1988)

$$\alpha_{rad} = 4 \cdot \sigma \cdot \frac{1}{\frac{1}{\epsilon_w} + \frac{1}{\epsilon_b} - 1} \cdot T_w^3 \quad 1.25$$

$$\alpha_{wp} = \frac{4\lambda_g}{D} \left[ \left( 1 + \frac{2(l+\delta)}{D} \right) \ln \left( 1 + \frac{D}{2(l+\delta)} \right) - 1 \right] \quad 1.26$$

For a low pressure  $l + \delta \approx l$ . Where  $\delta$  is the roughness of particle

The heat transfer coefficient for a single particle in dependence on the pressure is presented in figure 1.9 for smooth  $\delta = 0$  and rough particle ( $\delta = 2$  and  $10 \mu\text{m}$ ). This case was measured for a particle diameter of 2 mm, thermal conductivity 0.0275 W/(mK) and thermal capacity 1008 J/(kgK). The figure shows that the heat transfer coefficient is around 20-400 W/(m<sup>2</sup>K). The empirical equation of Tscheng (1979)[59], Schlünder and Tsotsas (1988) [61] are mostly used in modeling the contact heat transfer in a rotary kiln.

The calculation of the contact heat transfer requires knowledge of numerous parameters, and the approach is difficult to apply in practice. Therefore, it is appropriate to have a range value of this heat transfer coefficient in order to calculate the impact parameter

influencing the heat transfer in the rotary kiln. Thus, based on the above studies, suitable values for typical rotary kiln are in the range of 50 to 500 W/ (m<sup>2</sup>K).

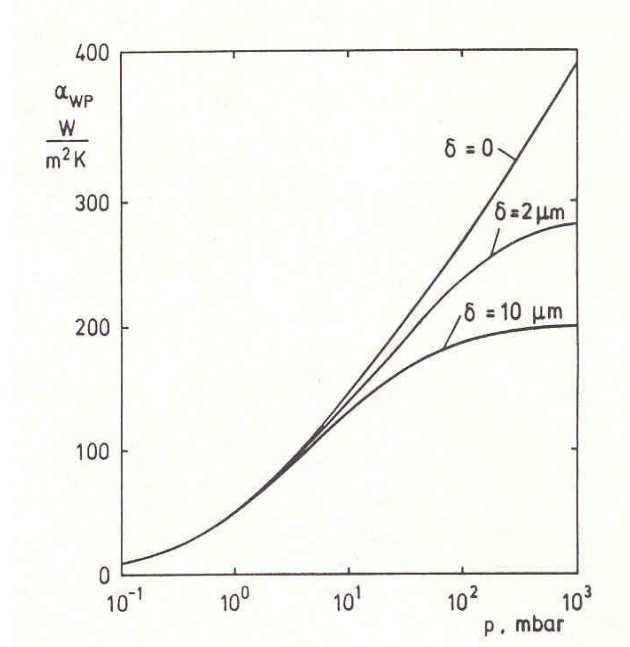


Figure 1.9 Heat transfer coefficient for single particle from kiln wall for different particle surface roughness (after Schlünder and Tsotsas 1988)

Ferron et al.1991 [43] gives following expression for the heat transfer coefficient

$$\alpha_{ws} = Nu \cdot \lambda_b / L_w \quad 1.27$$

$$Nu = \frac{2\sqrt{2}Pe^{1/2}}{1 + \sum_{i=1}^{\infty} \left[ \frac{B_i(\phi_0)}{\pi a_1} \left( 1 - \exp\left( \frac{-j^2 \pi \phi_0^2}{2Pea} \right) \right) \right]} \quad 1.28$$

Basu 1994 gives, Surface renewal model for circulating fluidized bed.

$$h_{cw-cb} = \left( \chi d_p / \lambda_g + \left( 2\sqrt{k_b \rho_b c_{pb} / \pi t_c} \right)^{-1} \right)^{-1} \quad 1.29$$

$$\text{gas film thickness: } \chi = 0.0287(1 - \varepsilon_b)^{-583} \quad 1.30$$

Li et al. used regression analysis of extended penetration theory led to the following equation

$$\alpha_{ws} = \left[ \frac{\chi d_p}{\lambda_g} + \frac{1}{2\sqrt{\frac{n\lambda_b \rho_b c_{pb}}{\varepsilon}}} \right] \quad \text{parameter: } \chi = 0.085 \quad 1.31$$

$$\lambda_g = 0.014 \text{ W / mK}$$

for 10% filling degree and with 6 rpm speed of rotation  $\alpha_{ws} = 161 \text{ W / m}^2\text{K}$

### 1. 9.1 Convective heat transfer coefficient

The convective heat transfer coefficient includes two aspects: Heat transfer between the freeboard gas and exposed wall, and the heat transfer between the freeboard gas and exposed upper bed surface.

The classic equation for turbulent convection in a non-rotating drum,  $\alpha_{GW} = 0.023(\lambda_g / D) \text{Re}_F^{0.8} \text{Pr}^{0.4}$  is not suitable for the calculation of  $\alpha_{G-EW}$  and  $\alpha_{G-Eb}$ . Tscheng and Watkinson [59] conducted a series of experiments on the influence of the rotation rate, gas flow rate, and percent fill on the convective heat transfer in a rotary kiln. Regression analysis of the experimental data led to the following dimensionless form.

$$\text{Nu}_{GW} = \frac{\alpha_{GW} D_s}{\lambda_G} = 1.54 \text{Re}_F^{0.575} \text{Re}_R^{-0.292} \quad 1.32$$

$$\text{Nu}_{GS} = \frac{\alpha_{GS} D_s}{\lambda_G} = 0.46 \text{Re}_R^{0.535} \text{Re}_F^{0.104} f^{-0.341} \quad 1.33$$

Where the flow Reynolds number  $\text{Re}_F = V_g D_e / \nu$ , rotational Reynolds number  $\text{Re}_R = D_s^2 \omega / \nu$ , percent fill  $f = (\phi_0 - \sin \phi_0) / (\pi - \phi_0 / 2 + \sin \phi_0 / 2)$  where introduced. Actually  $D_s$  is the percent fill of solids. Provided  $1600 < \text{Re}_F < 7800$  and  $20 < \text{Re}_R < 800$  then above equations are valid.

## 1.9.2 The radiative heat transfer coefficient

The radiations existing within the freeboard of a rotary kiln is enclosed by the exposed bed surface, inner exposed wall, freeboard gas, and inlet/outlet surface. It is difficult to directly simulate radiation in rotary kiln. In general, radiation is negligible at gas temperature less than 250-350°C, but it is comparable to the convective heat transfer at temperature 800-1000°C.

Gas emissivity depends on various parameters e.g. kiln diameter (mean beam length), concentration of combustion gas, dust, and soot (emissivity of the gas), emissivity of the wall etc. and it is different at each kiln. Among the models for radiation in rotary kilns proposed in the literature, Barr et al. [22] and Gorge et al.[23] gave details descriptions on the heat transfer between the gas . solid and wall by employing the n-zone method. Most of the equations proposed are from VDI wärmeatlas (1997).

The radiative conditions that exist within the kiln free board were simplified by making the following assumptions [62].

1. The surface of the wall and bed are taken to be grey because the spectral emissivity of the solid and wall refractory are not well known.
2. The inlet or outlet surfaces of the kiln are adiabatic.
3. The gas is taken to be radiantly grey, even though it contains CO<sub>2</sub> and H<sub>2</sub>O which emits and absorb radiation in distinct bands. The error due to this assumption is about 20%.
4. The material is mixed sufficiently. The temperature of the surface and gas are uniform at any axial position. The effect of any radial temperature gradient is ignored, while the circumferential wall temperature is approximated by four zones to eliminate its effect.
5. The effect of any axial temperature gradient in the solid, wall, and freeboard gas are negligible. The error brought by this approximation is small due to the large L/D ratio of the kiln.

6. No fire or flame exists in the rotary kiln.

On the basis of the above assumptions , the one-zone wall model to approximate the circumferentially changing inside wall temperature was used to determine the radiant heat flows, and hence the Radiative heat transfer coefficients within the freeboard area.[11,47]

The radiant heat transfer coefficient from the gas to the bed surface is represented by

$$\alpha_{GS}^r = \frac{Q_{GS}^r}{A_b (T_g - T_b)} \quad 1.34$$

The radiant heat transfer coefficient from the gas to the exposed wall is given by

$$\alpha_{GW}^r = \frac{\sum Q_{GW}^r}{A_w (T_g - T_w)} \quad 1.35$$

and the radiant heat transfer coefficient from the gas to the exposed wall to bed surface is expressed as,

$$\alpha_{WS}^r = \frac{\sum Q_{WS}^r}{A_b (T_w - T_b)} \quad 1.36$$

The heat loss from the inner wall to the outer environment includes three heat transfer process: the conduction resistance between the inner wall and the outer wall, the convective resistance between the outer wall and the environment, and the radiant resistance. So the total resistance is the summation of all above resistance for the heat loss [63].

From the above literature survey, a summary of heat transfer coefficient between the wall and the bulk solid has been stated in table 1.1.

Researcher	Heat Transfer coefficient	Validity
Wes et.al. (1976)	(1) $\alpha_{WS} = 2\sqrt{\lambda_b \rho_b c_{pb}} / (\pi t_c) = 2k_b \sqrt{(2\pi/a_b \phi_0)}$ (2) $Nu = 2\sqrt{2}Pe^{1/2}$ of which $Nu = \alpha_{WS} L_{WS} / \lambda_b$ $Pe = nR^2 \phi_0 / a_b$	Rotary kiln
Tcheng and Watkinson (1979)	(1) $\alpha_{WS} = 11.6k_b (nR^2/a_b \phi_0)^{0.3} / l_w^1$ (2) $Nu = 11.6Pe^{0.3}$ of which $Nu = \alpha_{WS} l_w^1 / k_b$ $Pe = nR^2 \phi_0 / a_b$	Rotary kiln
Lehmberg et.al (1976)	$\alpha_{WS} = \sqrt{\frac{\lambda_b \rho_b c_{pb}}{t_c}} \left( \frac{2}{\sqrt{\pi}} - \frac{1}{h\sqrt{a_b t_c}} + \frac{1}{h\sqrt{a_b t_c}} \exp(h^2 a_b t_c) \operatorname{erfc}(h\sqrt{a_b t_c}) \right)$ of which parameter $h = a_g / \lambda_b$	Rotary kiln
Wacheters & Kambers 1964	$\alpha_{WS} = \left( \sqrt{\pi a_b t_c} / 2\lambda_b + \sqrt{\pi d^1} / 2\lambda_b \right)^{-1}$ conditions: $n < 10$ rpm, $d = 0.00112\sqrt{\phi_0}$	Rotary kiln
Ferron et al.1991	(1) $\alpha_{WS} = Nu \cdot \lambda_b / L_{WS}$ (2) $Nu = \frac{2\sqrt{2}Pe^{1/2}}{1 + \sum_{i=1}^{\infty} \left[ \frac{B_i(\phi_0)}{\pi a_1} \left( 1 - \exp\left(\frac{-j^2 \pi \phi_0^2}{2Pea}\right) \right) \right]}$	Rotary kiln
Schlünder:H eat penetration model (1982)	(1) $\alpha_{WS} = \left( 1/\alpha_{wb} + \left( 2\sqrt{\lambda_b \rho_b c_{pb}} / t_c \right)^{-1} \right)^{-1}$ of which: $\alpha_{WS} = \phi_p \alpha_{WP} + (1 - \rho_p) \lambda_g / (\sqrt{2}R_p + \sigma) + \alpha_{rad}$ $\alpha_{WP} = \frac{2k_c}{R} \left[ \left( 1 + \frac{\sigma + \delta}{R} \right) \ln \left( 1 + \frac{R}{\sigma + \delta} \right) - 1 \right]; \alpha_{rad} = \frac{4\delta_2}{1/r_w + 1/r_b - 1} T_w^3$	Packed bed and fluidized bed
Schlunder:Si mplified penetration model (1982)	(1) $\alpha_{WS} = \left( \chi d_p / \lambda_g + \left( 2\sqrt{\lambda_b \rho_b c_{pb}} / \pi t_c \right)^{-1} \right)^{-1}$ parameter: $\chi = 0.085$	Packed bed and fluidized bed
Basu ; Surface	$\alpha_{WS} = \left( \chi d_p / \lambda_g + \left( 2\sqrt{\lambda_b \rho_b c_{pb}} / \pi t_c \right)^{-1} \right)^{-1}$ gas film thickness:	Circulating fluidized bed

renewal model(1989)	$\chi = 0.0287(1 - \varepsilon_b)^{-583}$	
------------------------	---	--

**Table 1** Summary of heat transfer coefficient equations between the wall and bulk solid

## References

1. Blezard, R. G., Reflections of the History of the Chemistry of Cement, Society of Chemical Industry (SCI) Lecture Series, UK, 2008.
2. Peray, K. E., The Rotary Cement Kiln, 2<sup>nd</sup> Edition, Chemical Publishing Co Inc., New York, 1986.
3. Boateng A., Rotary Kilns , Transport Phenomena and Transport Processes, Elsevier Publication, Oxford, 2008.
4. R. J. Spurling, Granular flow in an inclined rotating cylinder, Cambridge University 2000.
5. H.W. Schenck, J. O. Wendt, A. R. Kerstein, Combustion Science Technology 1996, 116-117, 427
6. W. D. Owens, Combustion Flame 1991, 86, 101
7. F. Maris, Computational chemical engineering 2003, 27, 813
8. I. Abe, Carbon 2001, 39, 1485
9. G. San Migel, G.D. Flower, M. Dall'Orso, C.J. Sollars, Journal of Chemical Technology biotechnology 2001, 77,1
10. V. A. Cundy, F.L. Larsen, J. S. Lighty, Canadian Journal of Chemical Engineering, 1996, 74,63
11. Boateng, A. A., and Barr, P.V., A thermal model for the Rotary Kiln Including Heat Transfer within the bed, Int.J.Heat Mass Transfer, 39(10), 1996. pp.2131-2147,
12. S.Q. Li et al , Powder Technology, 2002, 126, 217
13. S.Q. Li et al , Powder Technology, 2002, 126, 228
14. L. Yang, B. Farouk, Modeling of solid particle flow and heat transfer in rotary kiln calciners, Journal of Air Waste Management Association, Volume 47, Issue 11, November 1997, Pages 1189-1196

- 15 J. Kern, Heat transfer in Rotary Kiln, International Journal of Heat and Mass Transfer Volume 17, Issue 9, September 1974, Pages 981-990
16. Rutgers, R., Longitudinal mixing of granular material flowing through a rotary cylinder:part:1. Description and theoretical, Chem.Eng.Sci,20, pp. 1079-1087,1965.
- 17 Henein, H., Bed behavior in Rotary Cylinders with Applications to Rotary Kilns, PhD Dissertation, University of British Columbia, Vancouver,1980.
18. Perron, J., and Bui, R.T., Rotary Cylinders: Transverse bed motion prediction by Rheological Analysis, Can. J. Chem. Eng, 70, pp. 223-231, 1992.
19. Perron, J., Bui, R.T., and Nguyen. T.H., Modelisation du four de calcination du coke de petrole: 1-Le Modele, Can. J. Chem. Eng, 70, pp. 1108-1119, 1992.
20. Perron, J., Bui, R.T., and Nguyen. T.H., Modelisation du four de calcination du coke de petrole: 2- Le Model, , Can. J. Chem. Eng.70, pp. 1120-1131, 1992.
21. Brooks, D.G., Mathematical Simulation of a Rotary Coke Calciner, Light Met.,Proc. Tech.Sess.TMS 118<sup>th</sup> Annual Meeting, Las Vegas, NV, pp. 461-469, 1989.
22. Baar, P.V., Brimacombe,J.K., and Watkinson, A.P., A heat transfer Model for the Rotary Kiln: Part .II Development of the cross section model, Met. Trans.B, 20B, pp.403-419, 1989.
23. Gorge, J.P., and Adams T.N., Design of performance of rotary kilns in the pulp industry, TAPPI Kraft Recovery Operations Seminar, pp.37-70,1987.
24. Gorge,J.P., Brimacombe, J.K., and Adams, T.N., Radiative heat transfer in rotary kilns, Met. Trans.B, 12B, pp. 55-70, 1981.
25. Tscheng, S.H., and Watkinson, A.P., Convective heat transfer in Rotary Kilns, Can. J. Chem. Chem.Eng, 57, pp. 433-443
26. Brimacombe,J.K., and Watkinson, A.P., heat transfer in direct fired Rotary kiln-I Pilot plan and experimentation, Met.Trans.B, 9B,pp. 201-208, 1978.
27. Wes, G.W.J., Drinkenburg, A.A. H., and Stemerding, S., Heat transfer in a horizontal Rotary drum reactor, Powder Technology, 13, pp.185-192, 1976
28. Li,K.W., and Friday, J.R., Simulation of Coke calciners, Carbons,12,pp.225-231, 1974.

29. Sood, R. R., Clark, R., and Stokes, D.M., Computerized model to determine Operating Parameters for Rotary Kilns for Petroleum Coke Calcinations, Light Met, Proc, Tech. Sess. AIME 101<sup>st</sup> Annual Meeting, Denver, Co, pp.151-161, 1972.
30. Georgallis, M., Nowak, P. Salcudean, M., and Gartshore, I.S., Mathematical modelling of Lime kilns Canadian Journal of Chemical Engineering Volume 83, Issue 2, Pages 212-223, April 2005
31. Boateng, A. A., and Barr, P.V., A thermal model for the Rotary Kiln Including Heat Transfer within the bed, Int.J.Heat Mass Transfer, 39(10), pp.2131-2147, 1996.
32. Alyaser, A. H., Fluid Flow and combustion in Rotary Kilns, PhD Thesis, Faculty of graduate studies, Department of Metals and materials Engineering University of British Columbia, 1998.
33. Bui, R.T., Simard, G., Charette, A., Kocaefe, Y., and Perron, J., Mathematical modeling of the Rotary coke calcining kiln, Can.J.Chem. Eng, 73, pp.534-544, 1995.
34. Bui, R.T., Simard, G., Charette, A., Kocaefe, Y., and Perron, J., A Computer model of the Rotary coke calciner, in Proc. Int. Symp. Comp. Software in Extractive metall.C.W:Bales and G.A: Irons, eds., CIM Proceedings Can.J.Chem. Montreal, pp.237 - 248, 1993.
35. Bui, R.T., Simard, G., Kocaefe Y., Charetee A., Lacroix, M., Jain, S., Perron, J.Proulx, A., and Barr, P., "3D Simulation of the Thermal Performance of a coke Calcining Kiln", in Proc. Int.Symp. on Extraction Refining and Fabrication of Light Metals, Sahoo, M., and Pinfeld, P., eds., CIM Proceedings, Montreal, 24, pp.367-380, 1991.
36. Khoei A.R., Masters, I., and Gethin, D.T., Numerical modelling of the rotary furnace in aluminium recycling processes, Journal of material processing technology, 139, pp. 567-572 , 2003.
37. Friedman, E., and Marshall, A., Studies in rotary drying, chem. Eng. Prog, 45 pp.928-934, 1980.
38. Perry, R.H., Chilton, C.G., and Kirkpatrick, S.D., Chemical Engineers' Handbook, McGraw-Hill, New York, 1961
39. Mu, J., and Perlmutter, D.D, The mixing of granular solids in a rotary cylinder, AIChE J. 26(6), pp.928-934, 1980.

40. Parron, J., and Bui, R.T., Rotary cylinders: solid transport prediction by dimensional and rheological analysis, *Can.J. Chem Eng*, 68, pp.61-68, 1990.
41. Natarajan, V.V.R.; Kinetic theory analysis of heat transfer in granular flows, *International Journal of Heat and Mass transfer*, 39, pp.1929-1944, 1998.
42. Michaelides, E.E., Heat transfer in particulate flows. *International Journal of Heat and Mass transfer*, 29, pp.265-273, 1986.
43. Ferron J.R., and Singh D.K., Rotary kiln transport processes *AIChE journal* 37, pp.747, 1991.
44. Hunt M.L., Discrete element simulations for granular material flows: effective thermal conductivity and self-diffusivity, *International Journal of Heat and Mass Transfer*, 40, pp.3059-3068, 1997.
45. Kaneko, Y., Shiojima, T., and Horio, M., DEM simulation of fluidized beds for gas-phase olefin polymerization, *Chemical Engineering Science*, 54, pp.5809-5821, 1999.
46. Li, J., and Mason, D.J.; A computational investigation of transient heat transfer in pneumatic transport of granular particles, *Powder Technology*, 112, pp.273-282, 2000.
47. Vargas, W.L., and McCarthy, J.J., Heat conduction in granular materials, *AIChE journal*, 47, pp.1052-1059, 2001.
48. Vargas, W.L., and McCarthy, J.J., Stress effects on the conductivity of particulate beds, *Chemical Engineering Science*, 57, pp.3119-3131, 2002
49. Skuratovsky, I., Levy, A., and Borde, I., Two-dimensional numerical simulation of the pneumatic drying in vertical pipes, *Chemical Engineering Science*, 44, pp.187-192, 2005.
50. Cundall P.A., A computer model for simulating progressive large scale movements in blocky rock systems, *Processing of Symposium International Society of Rock Mechanics*, 2, pp.129, 1971
51. Cundall, P.A., and Strack O.D.L., A discrete numerical model for granular assemblies, *Geotechnique*, 29, pp.47-65, 1979.
52. Mastroakos, E., Massias, A., Tsakiroglou, C.D., Goussis, D.A., Burganos, V.N., and Payatakes, A.C., CFD predictions for cement kilns including flame modelling heat transfer and clinker chemistry, *Applied mathematical modelling*, 23, pp.55-76, 1999.

53. Peng, X.F., and Peterson, G.P., Convective heat transfer and flow friction for water flow in micro channel structures, *International journal of Heat Mass Transfer*, 39(12), pp. 2599-2608, 1996.
54. Al-Bazroon, H.A., Experimental determination of heat transfer Coefficient for Water-Lithium Bromide Mixture, PhD thesis, King Fahd University, Dhahran, Saudi Arabia, Jan, 1992.
55. Ga, B.V., Le, V.T., Vang, H., and Linh, N.N., Experimental study of the radiant heat transfer coefficient of diffusion flames, *Vietnam Journal of Mechanics, VAST*, 29(1), pp. 98 – 104, 2007.
56. Shabashkevich, G., A method for calculation of heat transfer coefficient for optimization thermoelectric coolers, *Journal of Engineering Physics and Thermodynamics*, 69(4), pp.489-495, 1996.
57. Vhia, F.J., Sieres, J., and Campo, A., Experimental apparatus for measuring heat transfer coefficients by the Wilson plot method, *European Journal of Physics*, 26, N<sub>1</sub>–N<sub>11</sub>, 2005.
58. Lemberg, J., Untersuchungen zum Wärmeübergang Zwischen der Wand und der Feststoffschicht eines Drehrohrofens, PhD Thesis, TU Hannover, Germany, 1975
59. Tscheng, S.H., and Watkinson, A.P., Convective Heat Transfer in a Rotary kiln, *Canadian Journal of Chemical engineers*, 57, pp.433-443, 1979.
- 60 Schlünder, E.U. Particle heat transfer. In: Griggall, U., Hahne, E., Stephan, K., Straub, J. (Eds.), *Proceedings of the Seventh Heat Transfer Conference, Munich*, vol. 1. Hemisphere, New York, pp. 195–211, 1982
61. E. Tsotsas, E. U. Schlünder, On axial dispersion in packed beds with fluid flow : Über die axiale dispersion in durchströmten festbetten, *Chemical Engineering and Processing Volume 24, Issue 1, July-August 1988, Pages 15-31*
62. Gorog, J.P., Brimacombe, J.K., and Adams, T.N., Radiative heat transfer in rotary kilns, *Met. & Mat Trans.B*, 12, pp.55-70, 1981.
63. Kim, N.K., Lyon, J.E., and Suryanarayana, N.V., Heat shield for high - temperature kiln, *Ind. Eng. Chem Process Des. Dev*, 25, pp.843-849, 1986.

## Chapter 2

# Modeling of the Temperature Fluctuations at the Wall of the Rotary Kiln

### 2.1. Introduction

The rotary kilns are horizontal cylinder with internal or external heating arrangement. It rotates with specific speed of rotation. They are being used for many applications in the chemical, pharmaceutical, cement and metallurgical process industries. It is basically a rotating inclined cylinder, used to heat the processed solids. For the flat and shaped products, roller hearth kilns become more and more important for the heat treatment [1, 2, and 3]. Rotary kilns can be operated in either the co-current mode where the gases and solids move in the same direction or in the counter-current mode where they move in opposite directions. Brimacombe and Watkinson (1989) have shown that in an internally heated kiln of small diameter which is operating at solid temperature up to 1100 K,

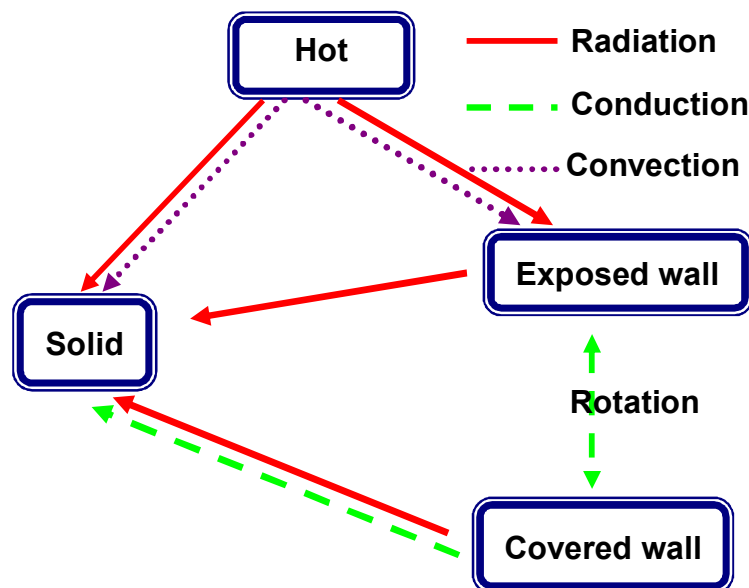


Figure 2.1 Mechanism of heat transfer

convection from the gas is the primary mode of heat transfer [4]. Heating medium is usually a gas stream running over the solid bed which is moving inside the kiln. Temperature fluctuation across the wall of cylinder is a key to explain the heat transfer phenomenon in the rotary kiln. The process parameters include; heat transfer coefficient, temperature of the wall and the solid bed, kiln diameter, the contact time, filling degree and the kiln wall thickness.

In the design and modeling of the rotary kilns four important aspects should be considered from a process engineering point of view: heat transfer, flow of material through the rotary kiln, gas-solid mass transfer, and the reaction kinetics. Among these, heat transfer is the most important phenomenon because in many practical cases heat transfer limits the performance of the rotary kilns [5, 6].

The heat transfer between the particle and the wall has been investigated and can be explained well in Schlünder and Tsotsas [7] and Tsotsas [8]. Also modeling of the heat transfer of transport rollers in kilns is thoroughly explained in E. Specht et al [1]. All the three modes of heat transfer occur simultaneously in the various parts of the kiln as shown in figure 2.1. The freeboard gases come across convective and radiative heat transfers to and from the wall and the solid bed surface. In addition to the heat transfer through the surface, the solid bed follows conductive and convective heat transfer inside the bed as well as to and from the wall. Conduction occurs within the wall, while radiative and convective heat transfer takes place on both inner and outer surfaces.

Purpose of this study is to describe fundamental understanding of the distribution of the temperature fluctuations at the boundary conditions and to build a model that simulate the temperature distribution in circumferential and in radial direction. Temperature distribution across the circumferential and radial direction for the rotary kiln can be studied analytically and in order to predict and improve the evolution and the distribution of temperatures in the rotary furnace. A numerical analysis is undertaken using finite element package ANSYS 11. A comparison have been made within the analytical and the numerical calculations. Fluctuation of the dimensionless temperature across the

circumference depends on the parameter ratio of the heat transfer coefficients, which described in detail later in this work.

Thermal stresses arises in materials when they are heated or cooled. The temperature distribution can cause thermal stress effects (stresses caused by thermal expansion or contraction of the material), which affects the operational facilities, both because of the large components subject to stress and because they are affected by the way in which the plant is operated.

Numerous heat transfer models for refractory kilns are available in the literature [9 10, 11, 12 13, 14]. The model of heat transfer presented in these studies has to rely on numerical techniques because of their two dimensional nature which consider the thermal heat conduction in radial and circumferential directions. The first model for the prediction of the axial transport in a rotary cylinder was proposed by Sullivan in 1927 and then developed to study the isothermal transverse motion of a bed of particulate materials by Perron and Bui [14], Friedman and Marshall [15], Peary et al. [16].

A mathematical model was described by Henein et al. [10] to predict the conditions giving rise to the different forms of transverse bed motion in a rotary cylinder such as slumping, rolling, slipping, cascading, cataracting, and centrifuging. Wu et al. [11] developed a 2D mathematical model based on the heat conduction mode in terms of the enthalpy formulation to simulate heat transfer and melting process of the scrap metals. A 3D steady-state mathematical model of a rotary calcining kiln was recently presented by Bui et al. [14].

## **2.2. Numerical calculation**

The equation for the steady state conditions is the Fourier-Kirchhoff differential equation. It is in the form of polar coordinate, where  $\varphi$  is the angle of the circumference with respect to the center of the kiln and  $r$  is the radial coordinate,  $\omega$  rotational frequency as stated in equation 3.1.

$$c \cdot \rho \cdot \omega \cdot \frac{\partial T}{\partial \phi} = \frac{\lambda}{r} \cdot \frac{\partial}{\partial r} \left( r \cdot \frac{\partial T}{\partial r} \right) + \frac{\lambda}{r^2} \frac{\partial^2 T}{\partial \phi^2} \quad 2.1$$

The figure 3.2 shows schematically the symbols used for the modeling of heat transfer in Rotary kiln. It can be reduced to two dimensional problems ( $\phi$ ,  $r$ ) by neglecting axial thermal conduction along the kiln, as the length of the rotary kiln is long enough in comparison with the diameter. This equation gives temperature distribution across the rotary kilns.

Two boundary conditions on the inner surface of the kiln set in  $r$  and  $\phi$  directions. Equation 2.2 represent heat transfer on the internal kiln wall in contact with the solid.  $T_{r= Ri}$  is the inner surface temperature of the kiln wall. Mean temperature of the solid bed is represented by  $T_S$ . In this model we consider mean temperature of the bed so the transverse solid motion [17] and exact temperature distribution is not necessary.

$$-\lambda \frac{\partial T}{\partial r} \Big|_{r= Ri} = \alpha_{WS} \cdot (T_{r= Ri} - T_S) \quad 0 \leq \phi \leq 2\varepsilon \quad 2.2$$

Solid region bound with the two times of the filling degree angle  $\varepsilon$ . The heat transfer in the contact region of gas and wall is mainly described with the law of convection as linearization of the model is required.

$$-\lambda \frac{\partial T}{\partial r} \Big|_{r= Ri} = \alpha_{GW} \cdot (T_{r= Ri} - T_G) \quad 2\varepsilon \leq \phi \leq 2\pi \quad 2.3$$

$$\alpha_{GW} = \varepsilon_{eff} \cdot \sigma \cdot T_G^3 \left[ 1 + \frac{T_W}{T_G} + \left( \frac{T_W}{T_G} \right)^2 + \left( \frac{T_W}{T_G} \right)^3 \right] \quad 2.4$$

$T_G$  is the gas temperature which is assumed to be constant through the cross section.  $\varepsilon_{eff}$  is the effective emissivity. The heat loss is approximated by the stationary heat conduction through the wall.

$$-\lambda \left. \frac{\partial T}{\partial r} \right|_{r=R_o} = q_L \quad 0 \leq \phi \leq 2\pi \quad 2.5$$

Due to the closed ring, the following boundary conditions for the angular direction can be

$$T(\phi = 0^\circ) = T(\phi = 360^\circ) \quad 2.6$$

$$\frac{\partial T}{\partial \phi}(\phi = 0^\circ) = \frac{\partial T}{\partial \phi}(\phi = 360^\circ) \quad 2.7$$

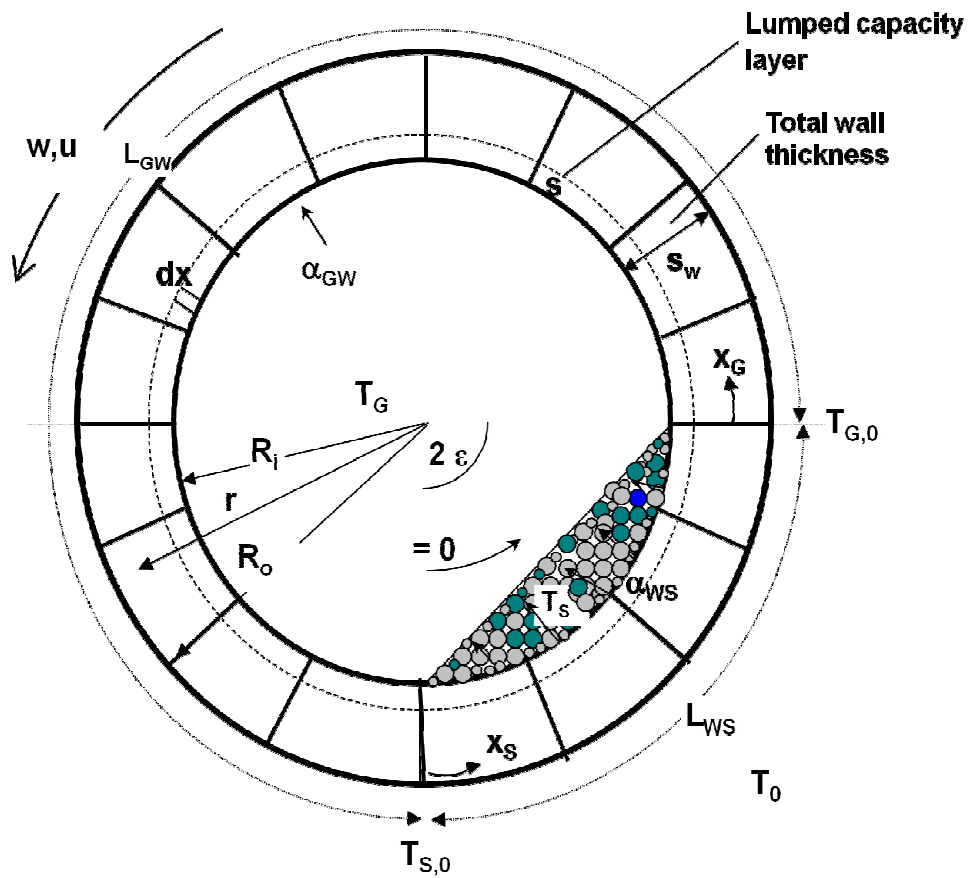


Figure 3.2 Symbol used for the modeling of heat transfer

All these equations with mentioned boundary conditions have been used in all the numerical calculations presented in this investigation.



Figure 2.3a and 2.3b Numerical modeling grid for the Rotary Kiln

Figure 2.3a shows grid for kiln wall and Figure 2.3b represent close view for the finite element grid. 32000 cells used for the calculations. With the help of refined grid in the numerical calculations more suitable temperature distributions can be obtained as shown in figure 2.4a and figure 2.4b.

A dimensionless temperature has been formed in relation with the ratio of temperature difference on the wall and initial temperature of the solid to the temperature difference between initial gas temperature and initial solid temperature. Temperature fluctuations have been measured in two regions; first, the length of the solid bed in contact with the

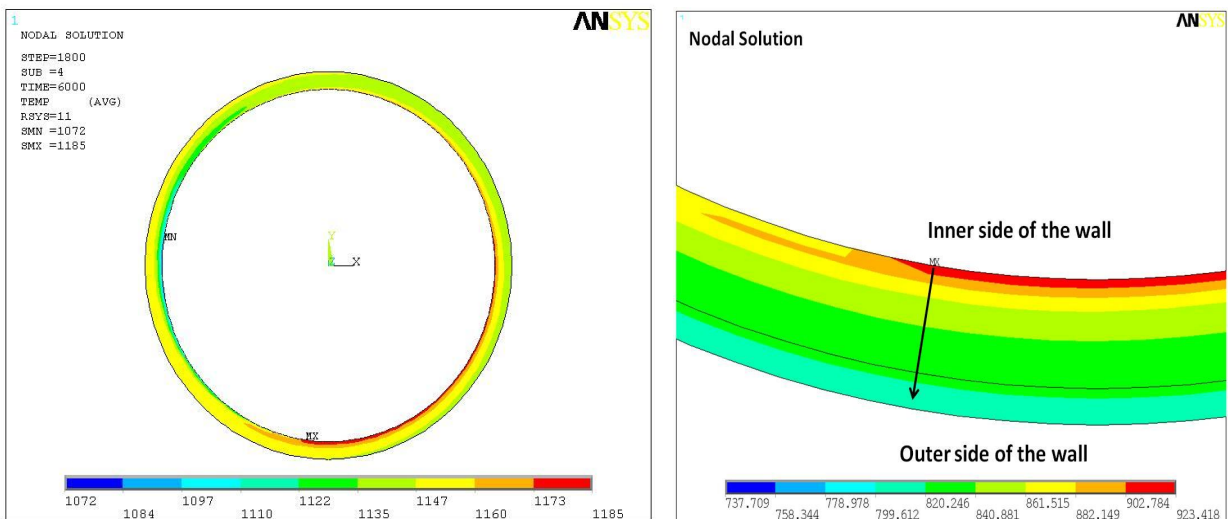


Figure 2.5a and 2.5b Temperature profile on the wall of the kiln

wall  $L_S$  and second, the remaining region where the gas is in contact with the wall  $L_G$ . Heat transfer coefficient from wall to solid and from gas to wall have been considered same for the calculations.

The fluctuations on the internal surface temperature of the kiln wall is presented in figure 2.5a as in the form of dimensionless temperature along the circumference. Kiln with 0.8 m ID with filling degree 10 is used for the simulation with ANSYS. A typical refractory material with a characteristic of  $\rho = 2100 \text{ kg/m}^3$ ,  $c_p = 1040 \text{ J/kgK}$ ,  $\lambda = 2 \text{ W/mK}$ . The thickness of 20 cm was selected for the refractory wall. The rotational speed varies within a range of 0.5 to 10 rpm. Wall to solid and gas to wall heat transfer coefficients have an identical value of  $100 \text{ W/m}^2 \text{ K}$ .

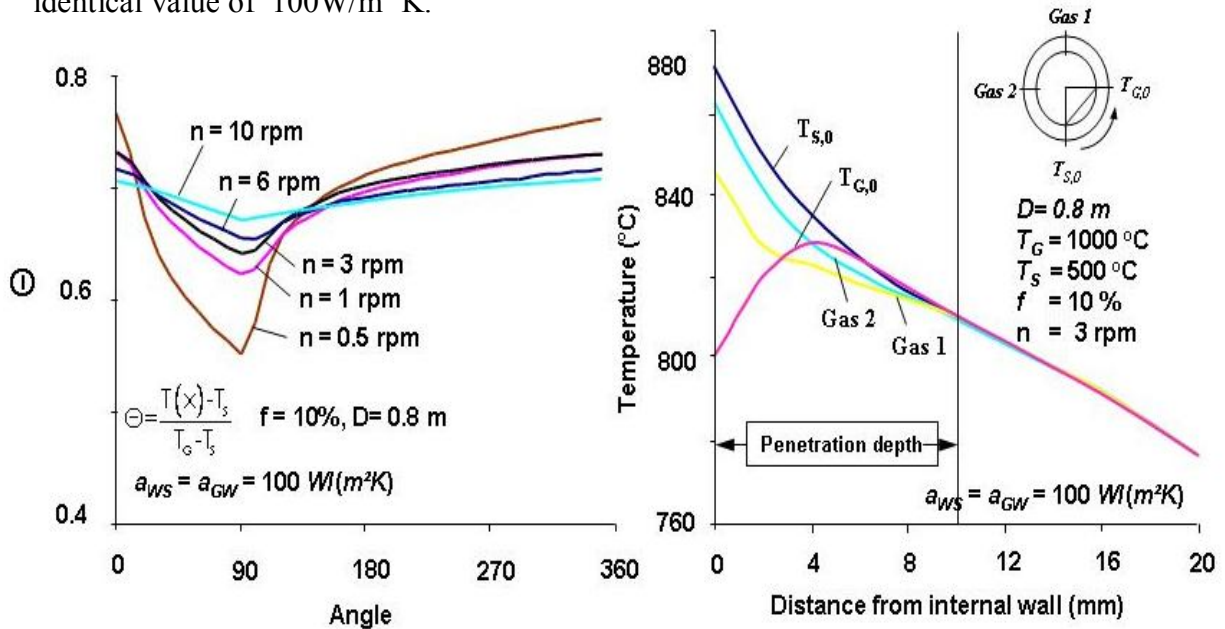


Figure 2.5 a and 2.5 b Temperature distributions across the Rotary Kiln

Temperature are set to be constant for the gas at 1273 K and the solid at 773 K. Kiln wall is alternately cooled and heated during each revolution by the hot gas and the cold solid respectively.  $T_{S,0}$  is the temperature at the inner surface wall at the initial point in contact with the solid and  $T_{G,0}$  is the temperature at a inner surface wall at the initial point in contact with the gas. These two points gives maximum temperature fluctuation of the internal surface kiln wall. The temperature fluctuations of the kiln wall decreases as the kiln speed increases. At the very large speed of rotation of the kiln, there are no

fluctuations on the wall. Figure 2.5b shows temperature profile inside the wall of the rotary kiln. Penetration depth is around 11 mm where all curve of temperature profiles meet together. Only this thickness takes part in the heat transfer process. Temperature of the wall at the solid side decreases continuously and at the gas side it increase due to regenerative heat transfer phenomenon. An analytical equation has been developed to obtain the effect of various parameters on the fluctuations. Following is the brief view of the analytical equations.

### 2.3. Analytical calculation

The temperature profile on the wall of the rotary kiln depends on the following eleven parameters. Diameter of the kiln  $D$ , total thickness of the kiln wall  $s_w$ , material properties like thermal conductivity  $\lambda$ , density  $\rho$  and specific heat capacity  $c$ , operating parameters like, initial temperature of the gas  $T_G$ , initial temperature of the solid  $T_S$ , filling degree  $f$  and number of rotation  $n$  and also on the heat transfer coefficient from wall to solid  $\alpha_{ws}$  and the heat transfer coefficient from gas to wall  $\alpha_{GW}$ . Therefore it is useful to develop an analytical model to evaluate the impact of these parameters and to study their interdependency.

Penetration depth is low in comparison with the total wall thickness. Therefore we introduce an active layer in which the fluctuation of this layer should have  $\lambda = \infty$  in radial direction. So we have uniform temperature in radial direction and only change in circumferential direction. This gives reduction to one dimensional problem.

The wall temperature in the solid region and in the gas region can be calculated with Newton lumped capacity model.

For the solid region it can be written as ,

$$\frac{T(x_s) - T_S}{T_{s,0} - T_S} = \Theta_s = \exp\left(-\frac{\alpha_{ws}}{\rho \cdot c \cdot u} \cdot \frac{x_s}{s}\right) \quad 2.8$$

and for the gas region it can be written as ,

$$\frac{T(x_G) - T_G}{T_{G,0} - T_G} = \Theta_G = \exp\left(-\frac{\alpha_{GW}}{\rho \cdot c \cdot u} \cdot \frac{x_G}{s}\right) \quad 2.9$$

$x_S$  and  $x_G$  are the angular coordinate in solid and gas respectively. And  $s$  is the lumped capacity layer thickness which is explained above.  $L_{WS}$  and  $L_{GW}$  are the angular length of solid side and gas side respectively. For the given filling degree,  $T_{S,0}$  and  $T_{G,0}$  are the initial temperatures where solid and gas first in contact with the wall respectively.

$$T_{G,0} = T(x_S = L_{WS}) \quad 2.10$$

$$T_{S,0} = T(x_G = L_{GW}) \quad 2.11$$

Length at the solid and gas region can be written in the form of filling angle and radius of the kiln as

$$L_{WS} = 2\varepsilon \cdot R_i \quad 2.12$$

$$L_{GW} = 2R_i(\pi - \varepsilon) \quad 2.13$$

Velocity is the function of speed of rotation and diameter of the kiln can be given as

$$u = \pi \cdot Di \cdot n \quad 2.14$$

Heat transportation coefficient  $\alpha_T$ , well explained in [12], which can be written as,

$$\alpha_T = \pi \sqrt{\lambda \cdot \rho \cdot c \cdot n} \quad 2.15$$

The time at which solid bed is in contact with the wall is

$$t_{WS} = \frac{1}{n} \cdot \frac{\varepsilon}{\pi} \quad 2.16$$

$\alpha_{WS}$ ,  $\alpha_{GW}$  and  $\alpha_T$  are mostly participating in the heat transfer process involved in the rotary kiln [19]. Overall heat transfer coefficient can be written with the help of heat transportation coefficient as,

$$\alpha_R = \frac{1}{\frac{1}{\alpha_{WS}} + \frac{1}{\alpha_{GW}} \cdot \frac{\varepsilon}{\pi - \varepsilon} + \frac{1}{\alpha_T} \cdot \frac{\varepsilon}{\pi}} \quad 2.17$$

The Biot number can be written in the form of heat transfer coefficient for wall to solid as follows,

$$Bi = \frac{\alpha_{WS} \cdot \sqrt{\varepsilon \cdot \pi}}{\alpha_T} \quad 2.18$$

To evaluate the equations 2.8 and 2.9, thickness of the lumped capacity layer is required. From figure 2.6, the nature of the temperature profile is similar to the semi infinite body. Carslaw [18] has presented temperature distribution in a semi infinite body. In the radial direction and for the region where solid and wall are in contact, temperature profiles can be calculated using equation 2.19, where  $Z_{lc}$  is the lumped capacity layer thickness,  $t_{WS}$  is the contact time between the rotating wall and the solid bed, 'a' is the thermal diffusivity of the wall. It can be seen that the thermal active layer depends on the material properties of the wall, heat transfer coefficient of wall-to-solid ( $\alpha_{WS}$ ), speed of rotation ( $n$ ), filling angle ( $\varepsilon$ ) and is independent of the kiln diameter.

$$\frac{T(r) - T_s}{T_{s,0} - T_s} = \text{erf}(Z) + \left[ \exp(\text{Bi} \cdot (2 \cdot Z + \text{Bi})) \right] \cdot \left[ 1 - \text{erf}(Z + \text{Bi}) \right] \quad 2.19$$

$$\text{Where, } Z_{lc} = \int_0^{\infty} \left[ 1 - \frac{T - T_s}{T_{s,0} - T_s}(Z) \right] dZ = \frac{s}{2\sqrt{a \cdot t_{WS}}} \quad 2.20$$

Figure 2.6 represent the plot of equation 2.19, at Biot number infinity. The area under this curve represents total heat stored inside the wall of the kiln. With the help of this equation, a relation of  $Z_{lc}$  with the Biot number can be obtained as [19],

$$Z_{lc} = 0.81 \cdot \ln(1 + 4 \cdot Bi) \quad 2.21$$

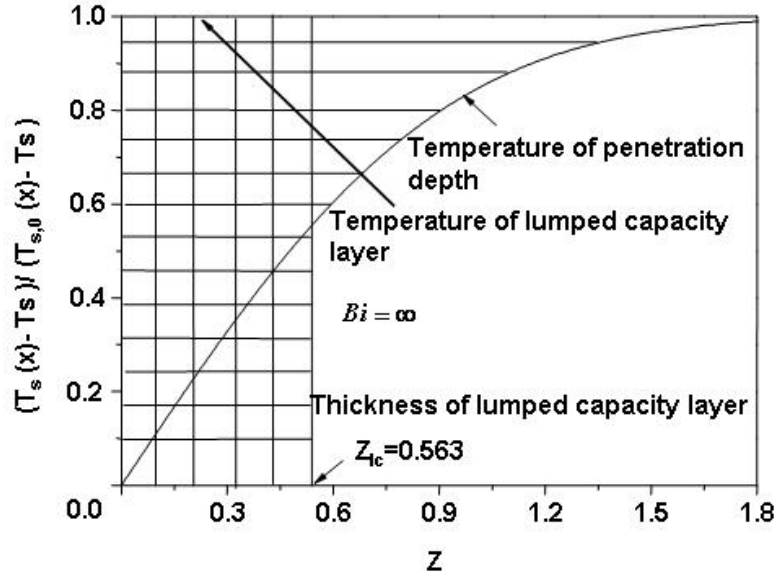


Figure 2.6. Lumped capacity layer characteristics.

From equation 2.21, the lumped capacity layer thickness can be obtained as,

$$s = 2 \cdot \sqrt{a \cdot \frac{1}{n} \cdot \frac{\varepsilon}{\pi}} \cdot 0.81 \cdot \ln(1 + 4 \cdot Bi) , \quad 2.22$$

Stanton number can be written by replacing lumped capacity thickness and adjusting with heat transportation coefficient as,

$$St = \frac{\alpha_{GW}}{2 \cdot \alpha_T} \cdot \sqrt{\frac{\pi}{\varepsilon}} \cdot \frac{(\pi - \varepsilon)}{0.81 \cdot \ln\left(1 + 4 \frac{\alpha_{WS} \cdot \sqrt{\varepsilon \cdot \pi}}{\alpha_T}\right)} \quad 2.23$$

A relationship of Stanton number and a dimensionless parameter A has been formed as,

$$St \cdot A = \frac{\alpha_{WS}}{2 \cdot \alpha_T} \cdot \frac{\sqrt{\pi \cdot \varepsilon} (\pi - \varepsilon)}{0.81 \cdot \ln \left( 1 + 4 \frac{\alpha_{WS} \cdot \sqrt{\varepsilon \cdot \pi}}{\alpha_T} \right)} \quad 2.24$$

$$\text{where } A = \frac{\alpha_{WS}}{\alpha_{GW}} \cdot \frac{\varepsilon}{\pi - \varepsilon} \quad 2.25$$

Equation 2.23 shows that Stanton number depends on speed of rotation, which is slightly different than as explained in [19]. It gives new aspect of process parameter in the heat transfer of rotary kilns.

From the above equations, the dimensionless temperature towards solid side can be written as,

$$\frac{T(x_S) - T_S}{T_G - T_S} = \Theta_S = \frac{\exp[-St \cdot A \cdot x_S^*] \cdot (\exp[-St] - 1)}{\exp[-St \cdot A] \cdot \exp[-St] - 1} \quad 2.26$$

The dimensionless temperature towards gas side can be written as,

$$\frac{T(x_G) - T_S}{T_G - T_S} = \Theta_G = \frac{\exp[-St \cdot x_G^*] \cdot (1 - \exp[-St \cdot A])}{\exp[-St \cdot A] \cdot \exp[-St] - 1} + 1 \quad 2.27$$

where

$$x_S^* = \frac{x_S}{L_{WS}}, \quad x_G^* = \frac{x_G}{L_{GW}} \quad 2.28$$

To the other point of contact where the wall loses the contact with the solid and reaches the onboard gas, the wall gives its heat to the solid bed. Hence the temperature at this point is minimum. Afterwards the wall regains heat from the freeboard gas and starts

heating again till it reaches to the solid bed. It depends on the filling degrees. Less is the filling degree more the length of the wall in contact with gas. Here convection takes important role for the heat transfer. The study of temperature fluctuation across the wall is very important in the heat transfer calculations. Maximum temperature fluctuation can be seen at the boundary conditions shown in equation 2.10 and equation 2.11. Hence the maximum dimensionless temperature can be written as

$$\frac{T_{S,0} - T_{G,0}}{T_G - T_S} = \frac{\exp[-St] + \exp[-St \cdot A] - \exp[-St] \exp[-St \cdot A] - 1}{\exp[-St] \cdot \exp[-St \cdot A] - 1} \quad 2.29$$

From equation 2.17 to equation 2.28, maximum temperature fluctuation is the function of the ratio of heat transfer coefficient of wall solid to the heat transportation coefficient and also heat transfer coefficient from gas-wall to the heat transportation coefficient and the filling angle. It can be written as,

$$\frac{T_{S,0} - T_{G,0}}{T_G - T_S} = f\left(\frac{\alpha_{WS}}{\alpha_T}, \varepsilon, \frac{\alpha_{GW}}{\alpha_T}\right) \quad 2.30$$

From above equation, reduction of parameters from 11 to 4 has been obtained. Temperature fluctuations are independent on, diameter (D) of the rotary kiln and also independent of the total thickness of the wall  $s_w$ .

## 2.4. Temperature fluctuations on the wall

The life time of the refractory wall depends on the fluctuations of the temperature. The fluctuations at the inner wall influences the thermal stresses of the refractory wall. Changes in temperatures causes thermal effects on materials [20]. Some of these thermal effects include thermal stress, strain, and deformations.

Figure 2.7 represents temperature fluctuations on the wall varies with the ratio of the heat transfer coefficient for wall-solid to the heat transportation coefficient. Rotary kilns with

an ID of 0.4 m and 2.0 m with filling degree 10 and a typical refractory material with a characteristic of  $\rho = 2100 \text{ kg/m}^3$ ,  $c_p = 1040 \text{ J/kgK}$ ,  $\lambda = 2 \text{ W/mK}$ . The thickness of 20 cm was selected for refractory wall at typical rotational speed of 3 rpm is used for the simulation with ANSYS. Gas to wall heat transfer coefficient has identical value of  $100 \text{ W/m}^2 \text{ K}$ . Wall to solid heat transfer coefficient varies from 0 to  $1000 \text{ W/m}^2 \text{ K}$ . Temperatures are set to be constant for the gas at 1273 K and the solid at 773 K. Filling degree variation of 5% to 30% has been considered. Similar parameters have also been used for the analytical calculations. Maximum temperature difference from equation 2.29 has been calculated and plotted in comparison with ANSYS simulation results. The heat is transferred perfectly from wall to solid at high value of the heat transportation coefficient wall to solid.

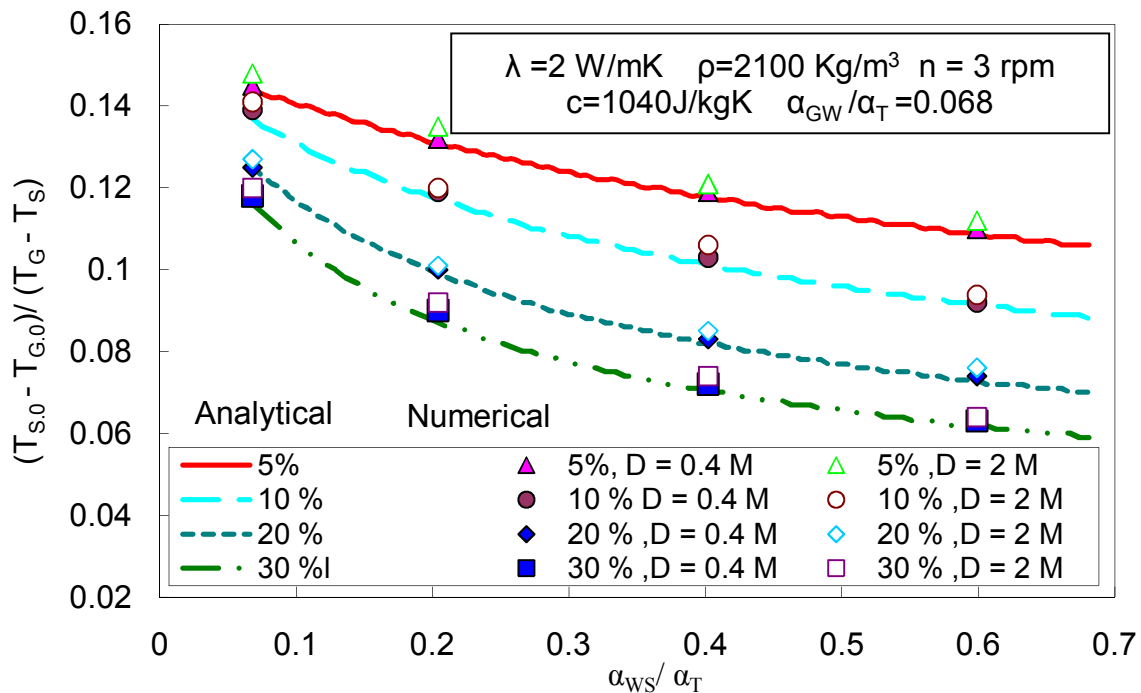


Figure. 2.7 Temperature fluctuations on the inner wall the kiln with ratio of wall solid heat transfer coefficient with heat transportation coefficient

The fluctuations at the inner wall decreases at higher value of the wall to solid heat transfer coefficient. Lower is the filling degree, higher the temperature fluctuations have been observed. It has been seen that analytical values fits very well with numerical

simulation. Especially, it is obvious that the diameter has no influence on the fluctuations. Therefore analytical equations are useful to explain the impact of above mentioned parameters.

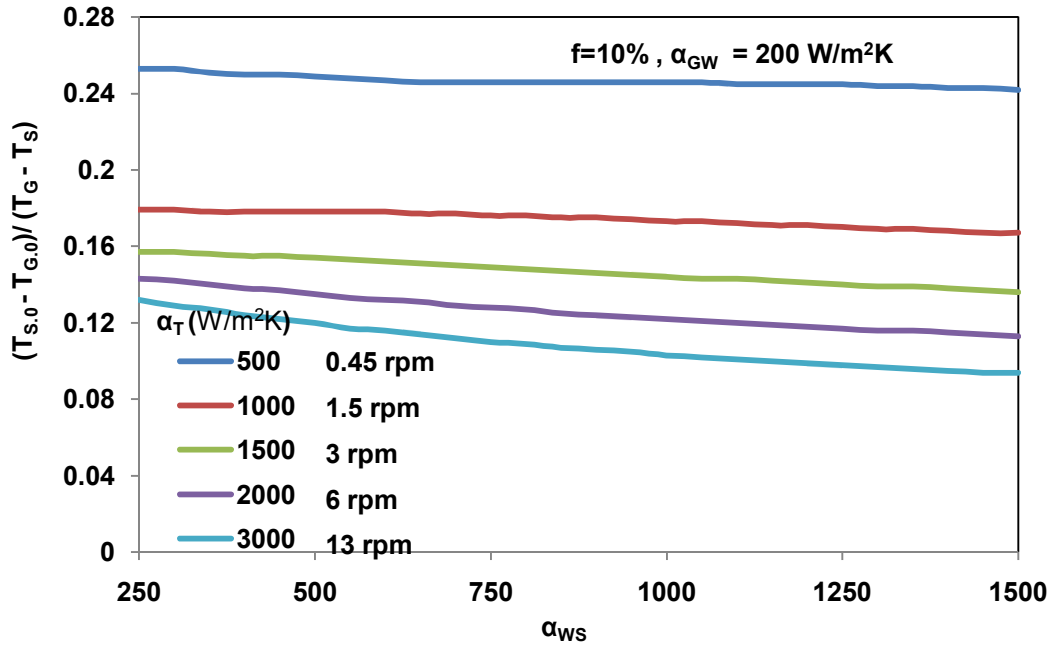


Figure. 2.8 Temperature fluctuations on the inner wall with wall solid heat transfer coefficient for parameter as heat transportation coefficient

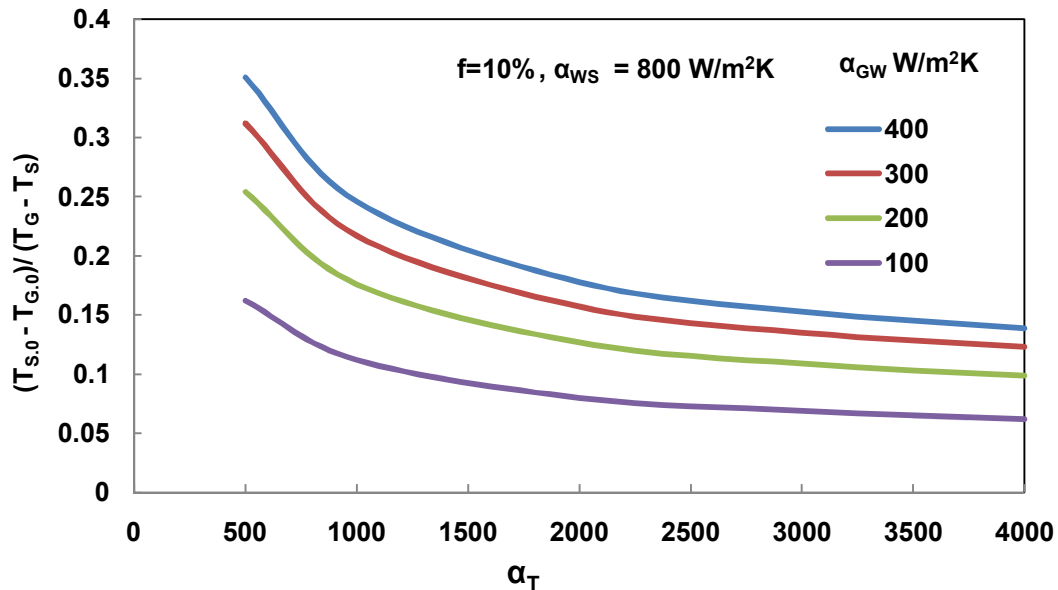


Figure. 2.9 Temperature fluctuations on the inner wall with heat transportation coefficient for parameter as gas to wall heat transfer coefficient

Figure. 2.8 indicates that at higher value of wall to solid heat transfer coefficient gives lower fluctuations. Here we used heat transportation as a parameter. Higher value of heat transportation coefficient gives less temperature fluctuations. Similarly, Figure. 2.9 indicates that by keeping wall to solid heat transfer coefficient constant, fluctuation decreases with increase in rotational speed.

The effect of speed of rotation on the temperature fluctuation is as shown in figure 2.10. Rotary kiln with an ID of 0.4 m, filling degree of 10 %, a typical refractory material with a characteristic of  $\rho = 2100 \text{ kg/m}^3$ ,  $c_p = 1040 \text{ J/kgK}$ ,  $\lambda = 2 \text{ W/mK}$  have been used for the calculations. The speed of rotation varies from 0.5 rpm to 10 rpm. Wall to solid and gas to wall heat transfer coefficients are assumed to be identical value of  $100 \text{ W/m}^2 \text{ K}$ . Temperature are set to be constant for the gas at 1273 K and the solid at 773 K. Temperature fluctuations have been calculated with 5 %, 10 %, 20% and 30 % filling degree. It has been observed that fluctuations decreases as the rotational speed increases.

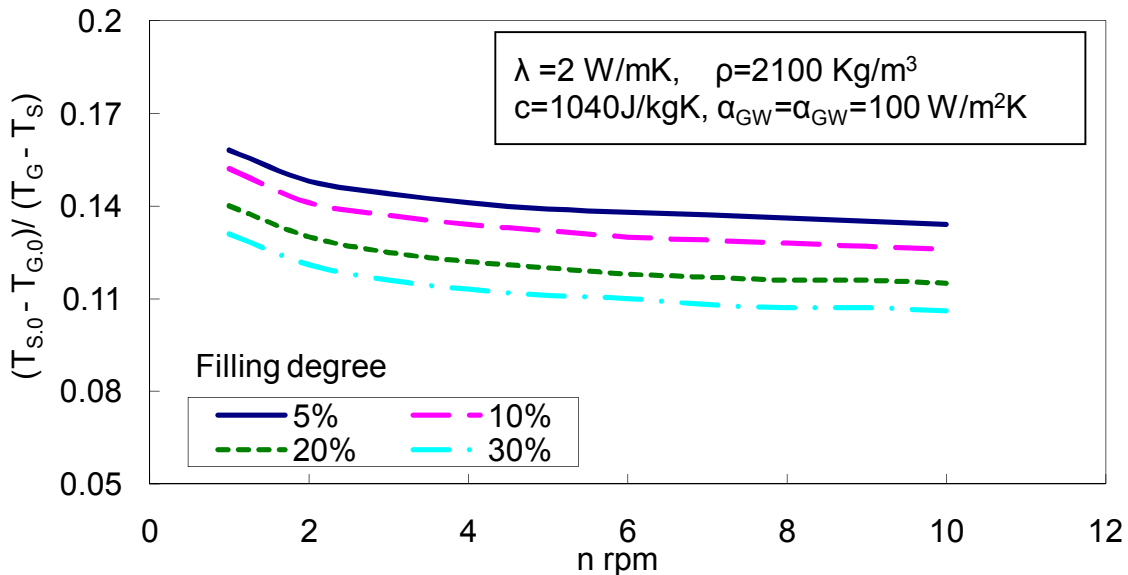


Figure. 2.10 Temperature fluctuations on the inner wall the kiln with various speeds of rotation

The fluctuations become smaller at high rotational speed. For infinite rotational speed, no fluctuation can be observed. Filling degree has an impact on the temperature fluctuations. Higher is the filling degree; lower are the temperature fluctuation at the same rotational speed. Figure 2.11 represents the comparison of temperature profiles using an analytical

and the numerical solution at three different value of gas to wall heat transfer coefficients with typical rotational speed of 3 rpm. A satisfactory match between numerical and analytical results has been observed. High rate of heat transfer gives high dimensionless

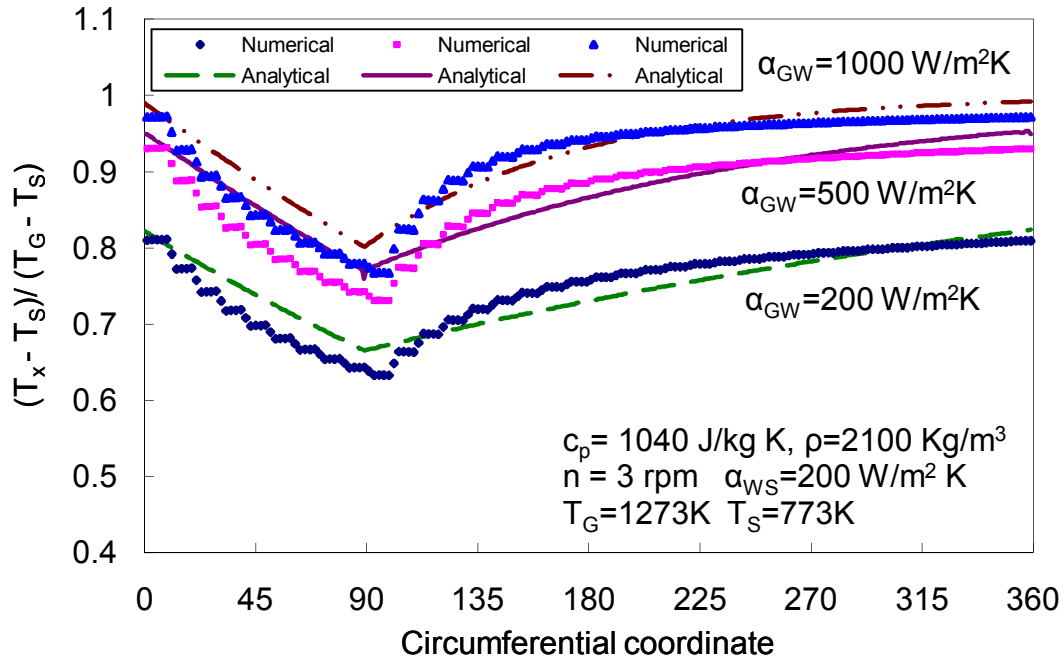


Figure 2.11 Comparison of the Analytical and Numerical temperature profile on the inner wall

temperature. To describe the applicability of the above analytical model, the commercially relevant case of the rotary kiln operation in the cement industry has been considered. A typical refractory material with value of density  $\rho = 2100 \text{ Kg/m}^2$ , specific heat capacity  $c = 1040 \text{ J/kg K}$ , and thermal conductivity  $\lambda = 2 \text{ W/mK}$  is considered. Temperature of the gas  $1950 \text{ }^\circ\text{C}$  and initial temperature of the solid is  $1450 \text{ }^\circ\text{C}$ . Heat transfer coefficient for wall to solid is considered  $200 \text{ W/m}^2\text{K}$ . The effective emissivity  $\epsilon_{\text{eff}}$  has been taken into consideration while deciding gas to wall heat transfer coefficient. It depends on many parameters, e.g. kiln diameter (mean beam length), concentration of combustion gas, dust and soot (emissivity of the gas), emissivity of the wall, etc. and it is different for each kiln. Therefore, this heat transfer coefficient is again taken as a parameter [19]. The range of its value is estimated as follows. For a high value of the gas

temperature of  $1950^{\circ}\text{K}$  and  $\epsilon_{\text{eff}} = 0.5$ , the maximum value of  $\alpha_{\text{GW}}$  is approximately  $1000 \text{ W/m}^2\text{K}$ . The values of speed of rotation are varied within range of 2 rpm to 4 rpm. Filling

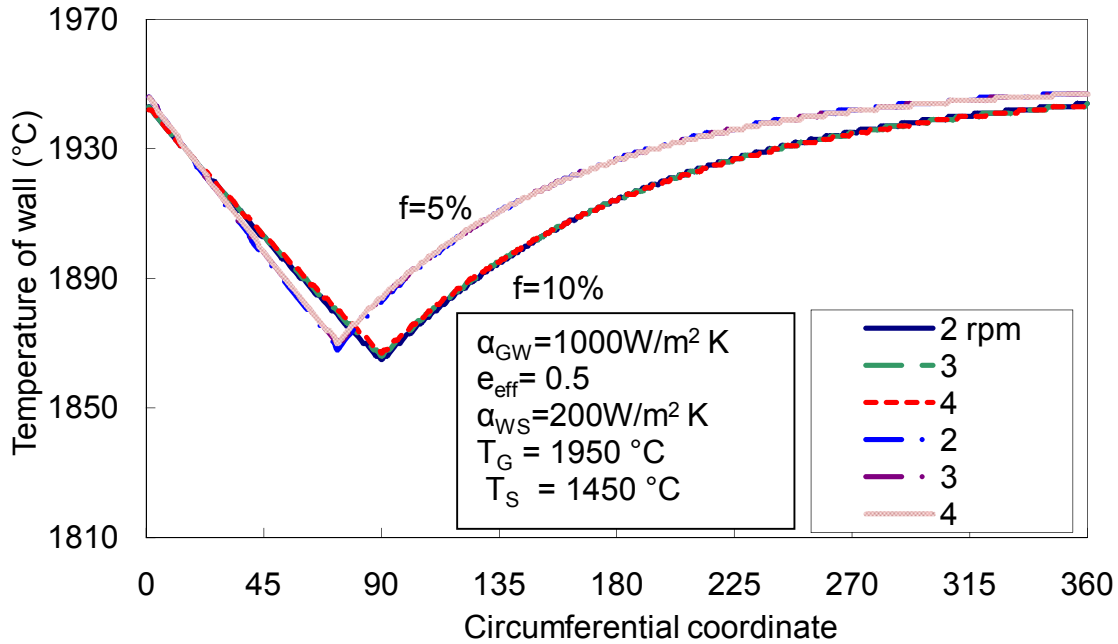


Figure 2.12 Temperature profile on the wall of Rotary kiln

degree of 5 % and 10% has been considered. Results are plotted as temperature of the wall against circumferential coordinates as shown in figure 2.11. The kiln wall is alternately cooled and heated during each revolution by the hot gas and the cold solid respectively. Maximum temperature,  $1945^{\circ}\text{K}$  and  $1940^{\circ}\text{K}$  has been obtained on the wall for filling degrees of 5% and 10% respectively. Lower is the filling degree higher is the wall temperature obtained on the wall.

Figure 2.12 shows temperature profile on the wall with respect to the circumferential coordinate at low value of combustion gas temperature of  $1400^{\circ}\text{C}$  and at initial temperature of the solid is  $900^{\circ}\text{C}$  and at effective emissivity  $\epsilon_{\text{eff}} = 0.35$ . Heat transfer coefficient for wall to solid has been taken around  $200 \text{ W/m}^2\text{K}$ . The values of speed of rotation are varied within the range of 2 rpm to 4 rpm. Maximum temperature of  $1340^{\circ}\text{C}$  and  $1310^{\circ}\text{C}$  on the wall for 5% and 10% filling degrees has been seen respectively. Maximum temperature difference of  $49^{\circ}\text{C}$  for 5% filling degree and  $46^{\circ}\text{C}$  for 10% filling degree has been seen. Maximum temperature difference on the wall at various rotational

speed is as shown in figure 2.13. A typical refractory material with value of density  $\rho=2100 \text{ Kg/m}^2$ , Temperature of the gas is  $1400 \text{ }^\circ\text{C}$  and initial temperature of the solid is  $900^\circ\text{C}$ .

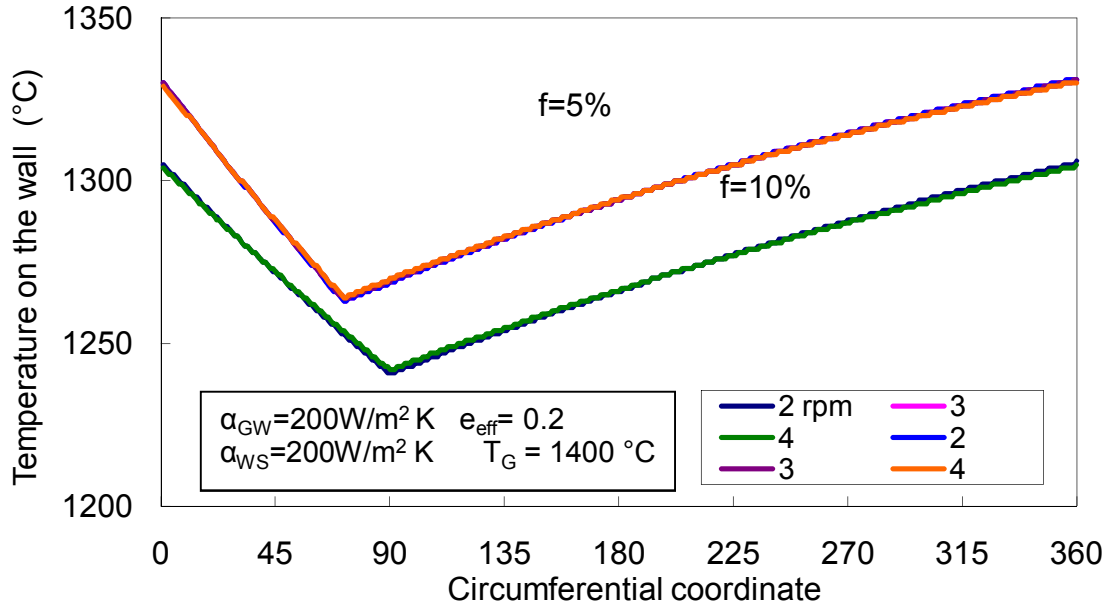


Figure 2.13 Temperature profile on the wall of Rotary kiln

specific heat capacity  $c=1040 \text{ J/kg K}$ , and thermal conductivity  $\lambda= 2 \text{ W/mK}$  is considered.

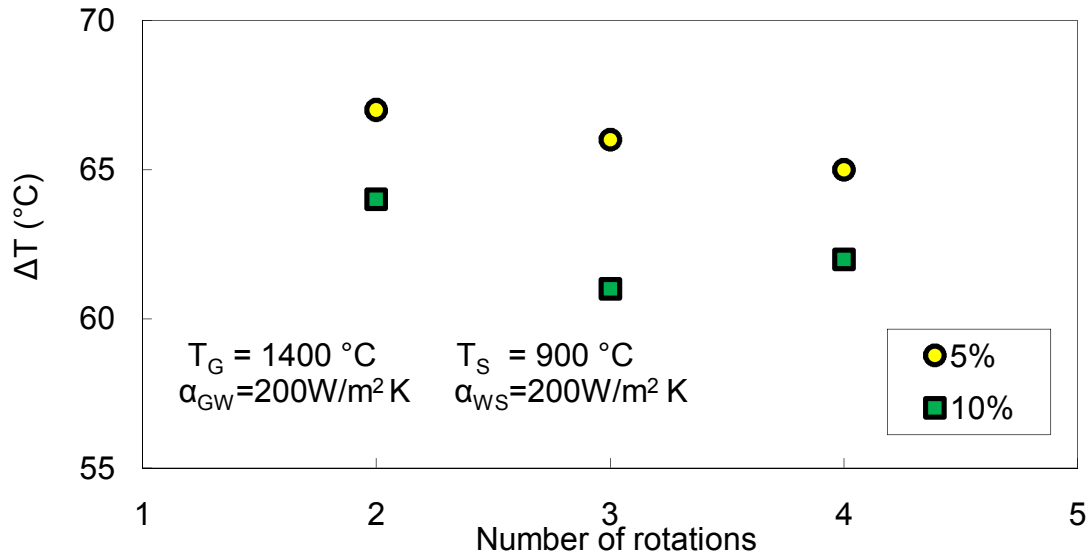


Figure 2.14 Temperature fluctuation with number of rotation

The speed of rotation varies with in 2, 3 and 4 rpm. Heat transfer coefficient for wall to solid is  $200 \text{ W/m}^2\text{K}$ . Filling degree of 5% and 10% has been considered for these

calculations. It has been observed that maximum temperature difference at 5 % filling degree is higher as compared to that at 10% of filling degree as shown in figure 2.14. For lower speed of rotation, high temperature fluctuations have been observed.

Effect of the material property on the maximum temperature difference has been plotted in figure 2.15. Materials such as Stainless steel (Fe-304), Sic, Sapphire (Al<sub>2</sub>O<sub>3</sub>), and Graphite have been considered for the calculations. These are most common material used for the construction of the wall of the rotary kiln. Thermophysical properties are as shown in table 2.1.

Wall material	$\lambda$ ( W/m <sup>2</sup> K)	$\rho$ ( Kg/m <sup>3</sup> )	c ( J/ Kg K)	Emissivity ( $\epsilon$ )
Stainless steel (Fe-304)	29	7530	640	0.2
SiC	40	2700	1650	0.8-0.9
Sapphire (Al <sub>2</sub> O <sub>3</sub> )	6	3600	1260	0.1
Graphite	20	1730	1920	0.7-0.85

Table 2.1. Thermophysical properties of indirectly heated rotary kiln wall. [21]

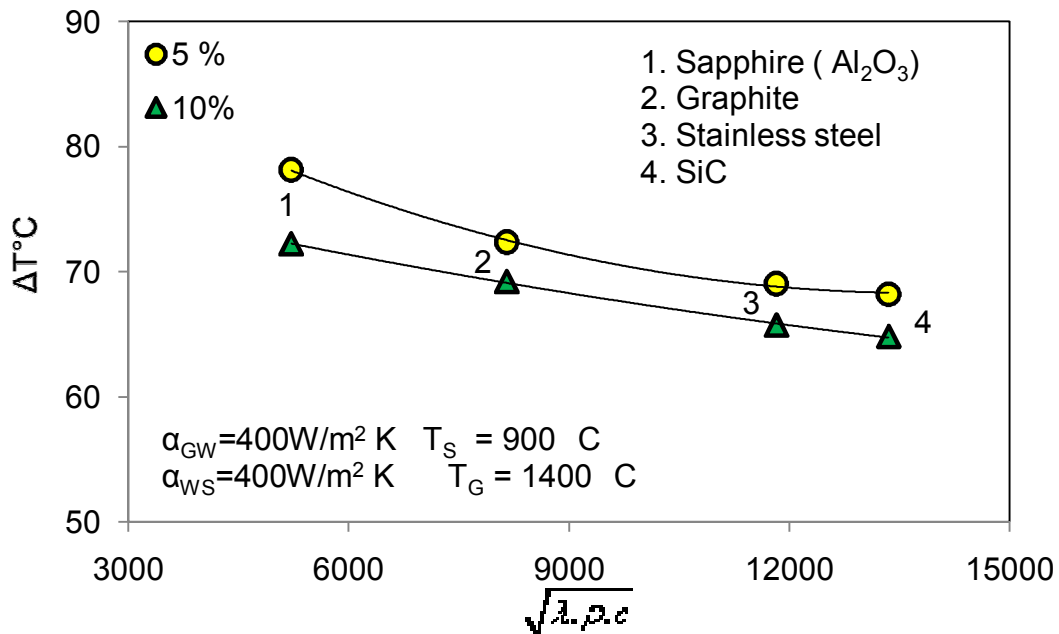


Figure 2.15 Temperature fluctuation with various wall materials

The thermal conductivity of each material is low, so the wall temperature in any axial kiln position is essentially small. Maximum temperature difference on the wall does not

have significant influence on the thermophysical properties of the wall material. Filling degree of 5 % and 10 % gives almost same maximum temperature difference.

The overall heat transfer coefficient as given in equation 2.17, is dependent on the heat transfer coefficient of wall to solid, the heat transfer coefficient of gas to wall, and the heat transportation coefficient [19].

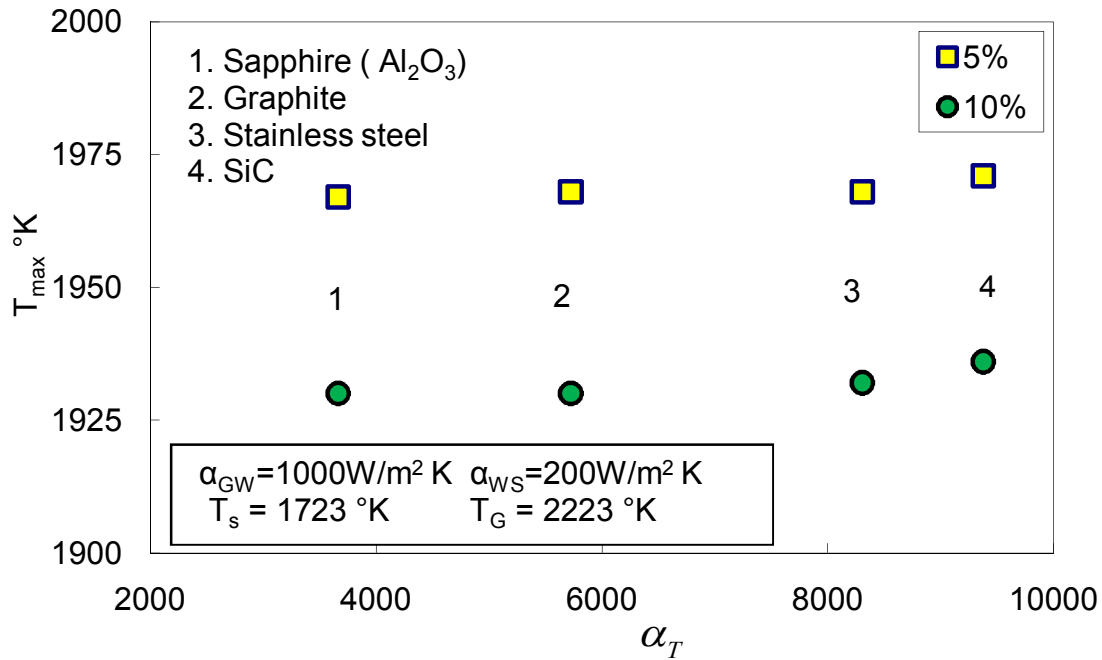


Figure 2.16 Wall maximum temperature with various heat transportation coefficient

The heat transportation coefficient  $\alpha_T$  depends on the material properties of the wall. For typical refractory materials and rotational speed around 2, 3 and 4 rpm, the heat transportation coefficient is in the range of 2000 to 8000 W/m<sup>2</sup>K. These values are much higher than the heat transfer coefficient from wall to solid  $\alpha_{WS}$  and the heat transfer coefficient from gas to wall  $\alpha_{GW}$ . For a high value of the gas temperature of 1950°C, at the initial temperature of the solid 1450°C and  $\epsilon_{eff} = 0.5$ , the maximum value of  $\alpha_{GW}$  is approximately 1000 W/m<sup>2</sup>K. Maximum wall temperature obtained is almost same for all

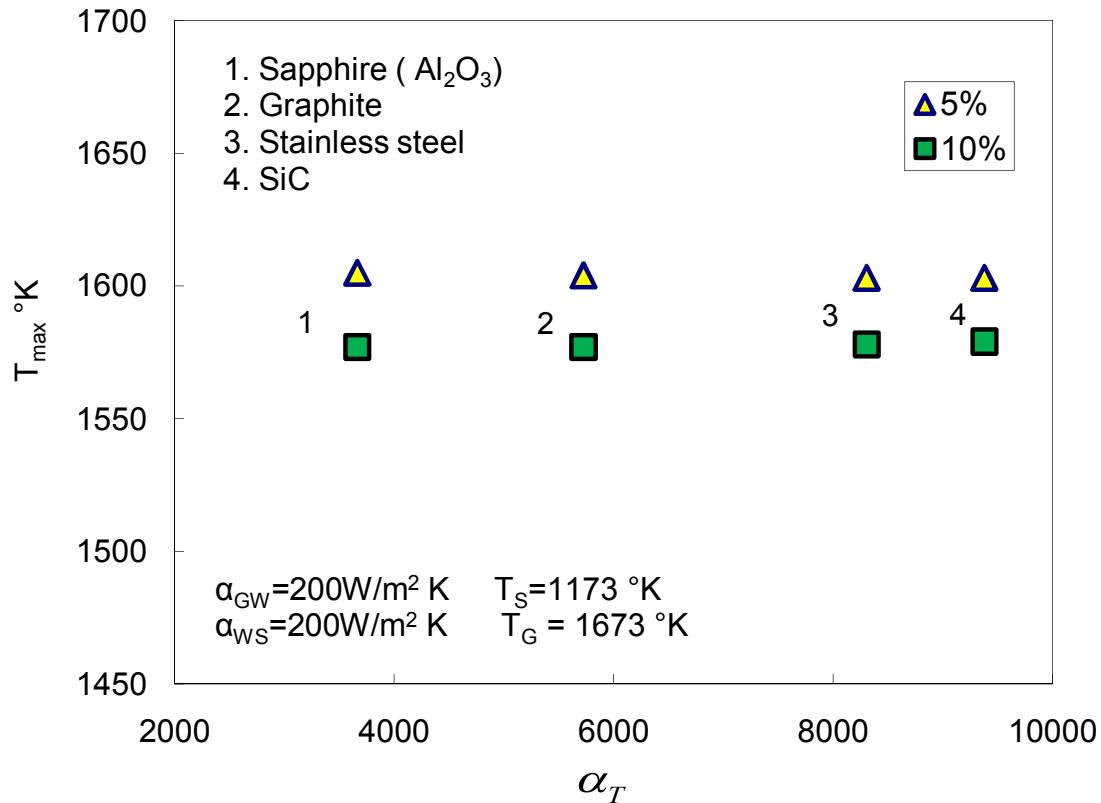


Figure 2.17 Maximum wall temperature with various heat transportation coefficient the materials such as Stainless steel (Fe-304), Sic, Sapphire ( $Al_2O_3$ ), and Graphite as shown in figure 2.16. For lower filling degree of 5%, maximum temperature has been observed to be same as compare to the 10% of filling degree.

Similar calculations have been performed for the low value of combustion gas temperature of  $1400^\circ C$  and at initial solid temperature of  $900^\circ C$ , and  $\epsilon_{eff} = 0.35$ . The heat transfer coefficient from gas to wall and wall to solid is taken as  $200 \text{ W/m}^2 K$ . Stainless steel (Fe-304), Sic, Sapphire ( $Al_2O_3$ ), and Graphite have been consider for the calculations. As seen from figure 2.17, it is observed that for each filling degree the maximum temperature on the wall is independent of the heat transportation coefficient.

Experimental results support the analytical result more satisfactory which has been described in more details in next chapter 4.

## 2.5. Temperature gradients on the wall of Rotary kiln

From the analytical and numerical analysis, it has been observed that temperature gradients exist in the circumferential and the radial direction of the wall for gas and solid side. Temperatures on the wall in circumferential direction decreases in the solid side and increases in the gas side. At the same time, temperatures in the solid side, inside the wall in the radial direction is decreases. In the gas side, the temperature increases first and then it decreases, which happens due to the regenerative heat transfer mechanism as explained before. Due to the above temperature distribution mechanisms, it is important to study temperature gradients for obtaining stress and strain distribution inside the wall of the rotary kiln and also to define the life time of the kiln assembly.

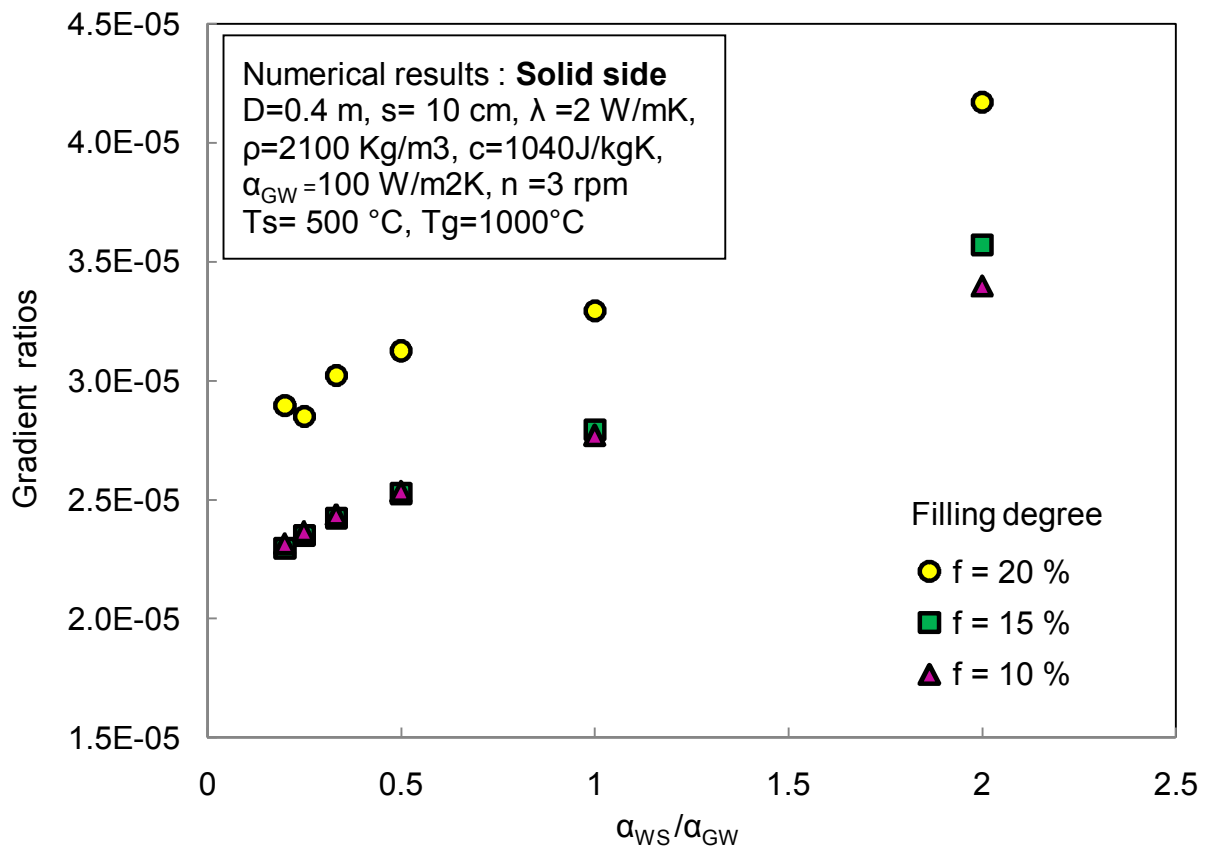


Figure 2.18 Temperature gradients ratio with respect heat transfer ratios

Temperature distribution across the radial direction has been studied with finite element package ; ANSYS as explained earlier. Numerical simulation of gradient ratio of the

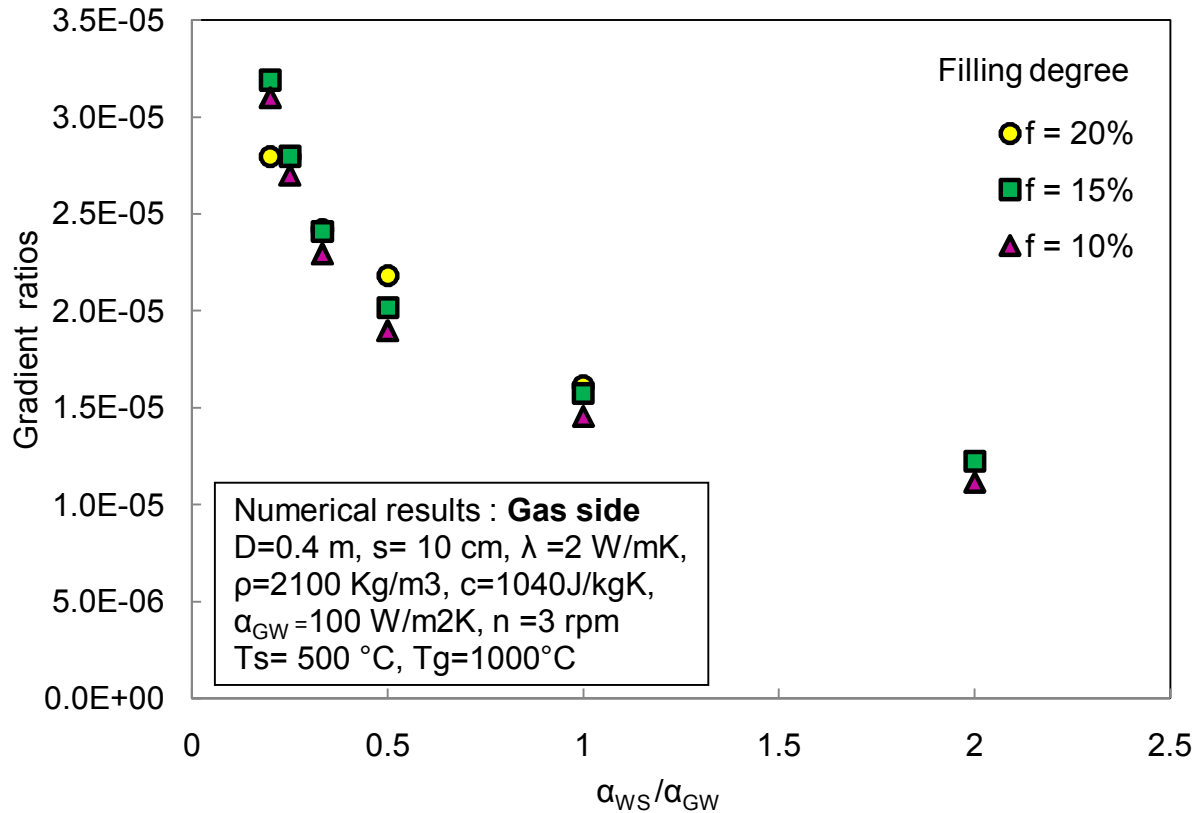


Figure 2.19 Temperature gradients ratio with respect heat transfer ratios

circumferential and the radial direction for various heat transfer coefficients with 10%, 15% and 20% filling degrees has been plotted as shown in figure 2.18 and 2.19. It has been observed that temperature gradients in the radial direction is higher than that in the circumferential direction along gas and solid side.

## 2.5 Conclusion

Maximum temperature fluctuation on the wall has been formulated. New Stanton number has been formed. Reduction of the parameter for the maximum temperature fluctuations from 11 to 4 has been achieved. Analytical model of the maximum temperature fluctuations on the wall is good perfection of parameter dependence. Heat transfer coefficient of wall to sold and heat transfer coefficient of gas to wall and filling degree takes important role in the heat transfer process. Temperature fluctuations decreases with increase in the rotational speed and are independent on the diameter of the rotary kiln.

The fluctuations of the inner wall decreases at higher value of the wall to solid heat transfer coefficient. Temperature gradient at radial directions are more than those in the circumferential directions.

## 2.5 References

1. M. Chmielowski, E: Specht, Modeling of the heat transfer of the transport in kilns, *Applied Thermal Engineering* 26 (2006) 736-744
2. Kai-Umw Holzapfel, E. Specht, Heat transfer between a rotating cylinder and a transported plate, *Experimental Heat transfer*, 19:39-51, 2006.
3. M. Chmielowski, E: Specht, Einfluss der Transportrollen auf die Temperaturverteilung in plattenförmigem gut in Rollenöfen, *Gaswärme International* [53], 397-401, Nr. 7/2005
4. Barr, P.V., Brimacombe, J.K., and Watkinson, A. P., A heat Transfer Model for the Rotary Kiln Part I. Pilot Kiln. Volume 20, Number 3 June, 1989, 391-402
5. A. A. Boateng, P. V. Barr, *Int. J. Heat Mass Transfer* 1996, 39, 2131
6. L. Yang, B. Farouk, *J. Air Waste Manage. Association* 1997, 47,1189
7. E. U. Schlünder and E. Tsotsas, *Wärmeübertragung in Festbetten, durchmischten Schüttgütern und Wirbelschichten*, George Thieme Verlag Stuttgart, New York 1988.
8. E. Tsotsas, Heat transfer From a Wall to granular Products, In *Heat Exchanger Design Update*, Begell Hous Inc., New York, 2000.
9. Sass, A., Simulation of the Heat transfer phenomenon in a Rotary Kiln, I and EC *Process Design and Development*, volume 6 no. 4, PP 532-535, 1967
10. Pearce, K. W. A Heat transfer model for Rotary kilns, *J. of the Institute of Fuel*, no. 7 pp, 363-371, 1973
11. Gardeik, H. O. And Jeschar, R, , Simplified Mathematical Models for calculating the heat transfer in Internally heated adiabatic rotary kiln ( convection models) Part I, Idealized rotary kiln with infinitely large thermal conductivity coefficient of the wall, *Cement lime Gypsum International* , vol 7 pp. 201-210,1979
12. Gardeik, H. O. And Jeschar, R, , Simplified Mathematical Models for calculating the heat transfer in Internally heated adiabatic rotary kiln ( convection models) Part II,

Rotating tube with finite value of thermal conductivity of the wall, Cement lime Gypsum International , vol 7 pp. 434-441,1979

13. Goshdastidar, P. S., Rhodes, C. A., Orloff, D. I. Heat transfer in a rotary kiln during incineration of solid waste, ASME- Papers vol. 8 no.85-HT-85, pp. 1-6,1986

14. Bui R.T., Perron and Read, M., Mode-based optimization of the operation of the coke calcining kiln, Carbon, vol. 31, no. 7, pp. 1139-1147,1993

15. Friedman S. J, Marshall W R. J. Studies in Rotary drying, Part II. Heat and Mass transfer, Chemical Engineering Progress, vol. 45, no. 9, pp. 573, 1949

16. Peary, K. E., Waddell, J.J., The rotary cement kiln, Chemical publishing co., New York, 1972

17. Liu, X., Mellmann, J. and Specht, E., Prediction of rolling bed motion in rotating cylinders, AIChE Journal, vol.50, no. 11, pp 2783-2793, 2004

18. Carslaw, H. S., Jaeger, J.C., Conduction of heat in solid, 2<sup>nd</sup> edition, Oxford clarendon Press, London, 1959.

19. Sri Silvia Agustini, Regeneration action of the wall on the heat transfer for directly and indirectly heated rotary kiln, Dissertation 2006

## Chapter 3

# Design and Fabrication of Experimental Pilot Plant of the Rotary Kiln

### 3.1 Introduction

The Rotary kiln with 600 mm ID and 450 mm length has been fabricated with industrial norms as shown in figure 3.1.

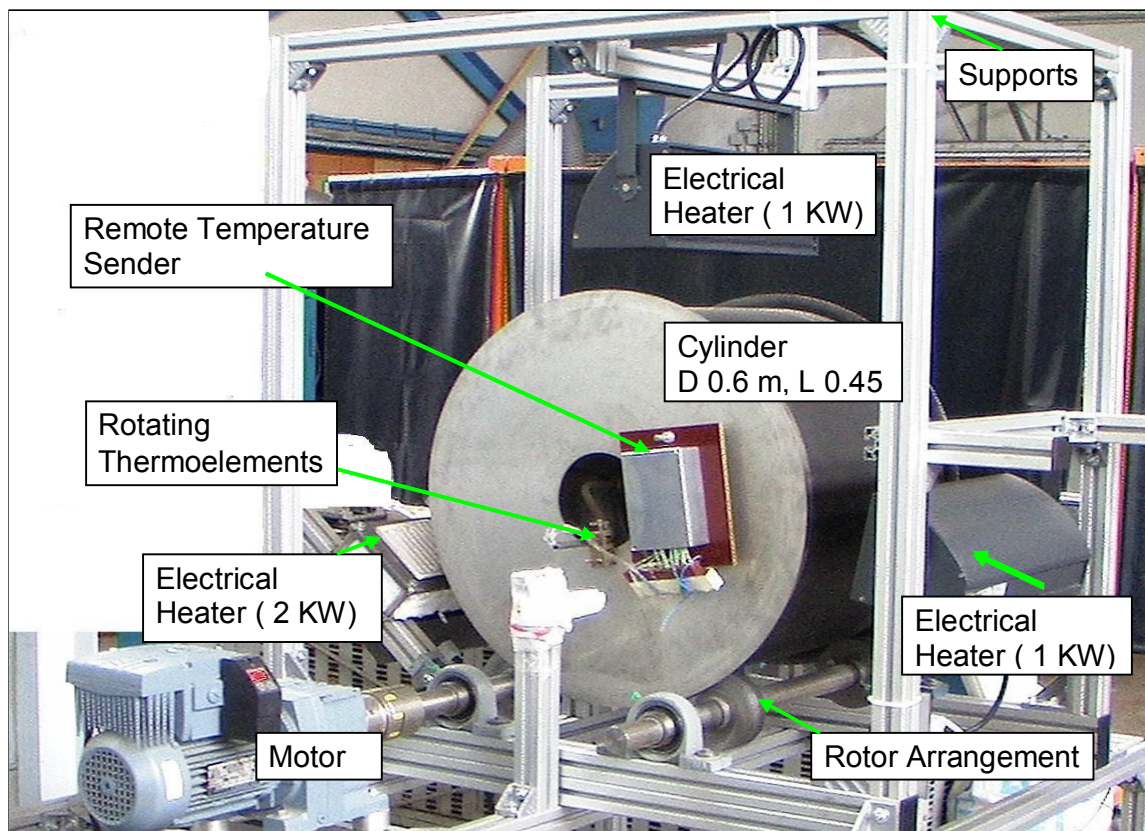


Figure 3.1 Experimental setup for externally heated Rotary Kiln

Accessories and fabrication details of the laboratory scale rotary kiln has been given in the following section.

The rotary kilns consist of long cylinder lying almost horizontally that is rotated slowly and heat is applied to the material being treated inside. It can be used for multiple purposes. The kilns are applied mainly in continuous processes, including cement manufacturing and the drying of granular materials.

### **3.2 Equipment Details**

The aim of the present study is to design the equipment which provides the knowledge of temperature distribution across the wall and inside the moving bed. AutoCAD has been used in the detailed sizing of the equipment which can then be used for the equipment fabrication. Following is the list of the main parts of the equipment;

1. Stainless steel cylinder: Diameter 600 mm, Length 450mm and Thickness 2 mm.
2. Driving assembly:
  - a. Electrical motor
  - b. Shaft
  - c. Bearing
3. Electrical Heater: 2 KW, 1 KW and 1 KW. (Three)
4. Driving power : 1.1 KW, electric motor.
5. Temperature sensors: K type 0.5 mm Diameter.
6. Wireless temperature assembly: This Instrument transfer digital signals to the computer for temperature.
7. Supports for the overall assembly.

### **3.3 Design and fabrication of the parts**

#### **3.3.1 Stainless steel cylinder**

Stainless steel iron-based metal containing 10% chromium (alloy metals) was used to fabricate the drum of the rotary kiln as shown in figure 3.1.

Thickness of the drum is 2 mm. Both sides of the cylinder have been closed with the circular metal plates with boar at the centre. This hole helps to set and to install the rotating thermo elements and also to charge or discharge the solid inside the rotary kiln.

### 3.3.2 Shaft

Stainless steel shafts with diameter 40 mm and length 500 mm have been used. Two ball bearings have been attached to each shaft. One end of the shaft is connected with the chain arrangements and other end to the electrical motor. The drum has been kept on the bearings and it rotates with the frictional force alone as shown in figure 3.2.

### 3.3.3 Bearing

Bearings are made-up of Stainless steel with 40 mm diameter have been used for the assembly. Cylinder is placed directly on the bearing. It is important to have some friction with the surface of the wall and outer surface of the bearings so that cylinder can freely rotate on it.

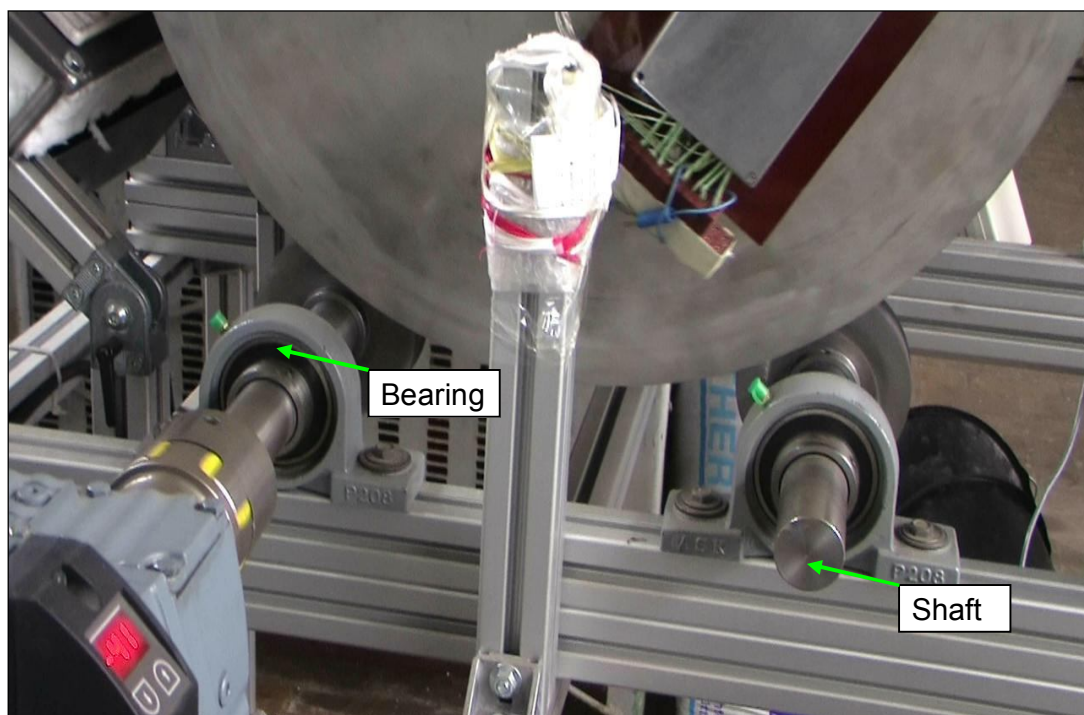


Figure 3.2 Rotating arrangements with Stainless steel bearing

Four bearings are used for the rotating the assembly. This arrangement is as shown in figure 3.2 so that drum with the assembly must be more stable while it is functioning.

### 3.3.4 Electrical Heater

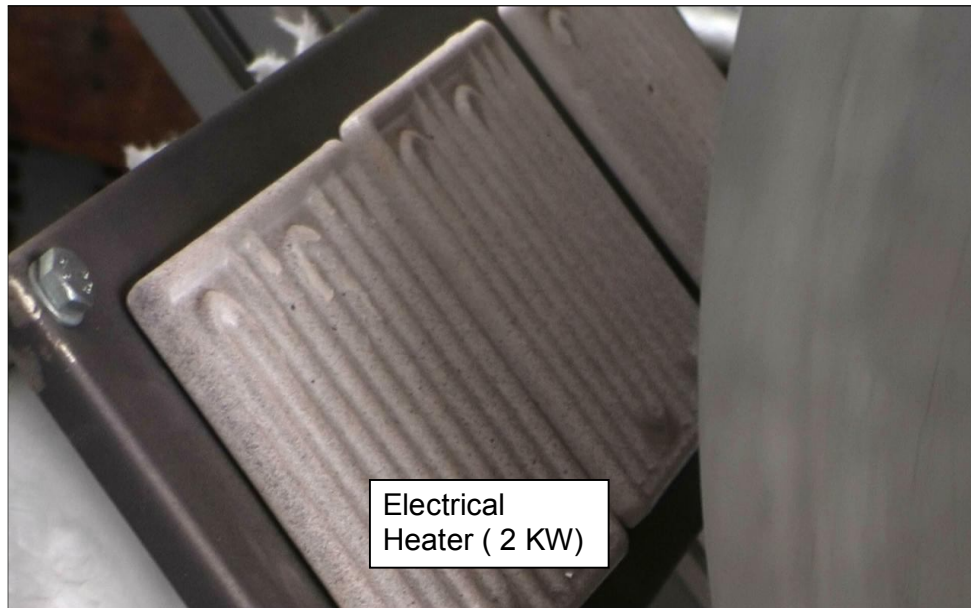


Figure 3.3. Electrical heaters arrangement

Three electrical heaters with capacity of 2 KW, and 1 KW, 1 KW are used for the experiments. It is made of three metal coils connected in series and immersed in the ceramic material. It is placed in one special hub which is filled with glass insulations as shown in figure 3.3. This arrangement reduces heat loss. Location of the these electrical heaters are shown in figure 3.1.

### 3.3.5 Thermo couple arrangements

K type temperature sensors are used for the experiments. K type thermo elements have been



Figure 3.4 Spacing arrangements for the thermoelements

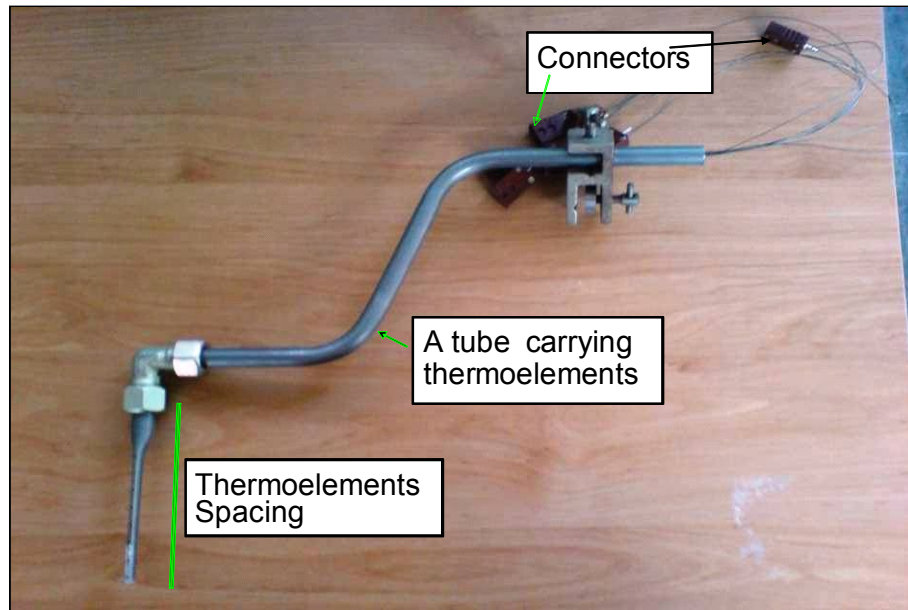


Figure 3.5 Assembly of the thermocouple

used to measure the temperature on the wall and in the moving solid bed. Totally 16 thermo elements have been used. Positions of the thermo elements are as shown in figure 3.4. The first thermo element measures temperature at the wall and the second thermo element placed at is placed at 2 mm from the wall. Thermo elements from 2<sup>nd</sup> till 7<sup>th</sup> are kept at a distance 5 mm from each other. Thermo elements from 7<sup>nd</sup> till 16<sup>th</sup> are kept at distance 10 mm from each other. The purpose of the spacing of the thermo element is to measure the temperature profile at maximum possible position in the moving solid bed and to study in detail where it varies. These thermoelements have been attached to the 7 mm tube. This tube then tightened with rotary cylinder in case of rotating thermoelements arrangement. Similar assembly has been used and fixed to the outside of the kiln in case of fixed thermoelements assembly.

### 3.3.6 Wireless temperature assembly

The wireless temperature assembly is having electrical circuit which measures temperature with respect to the time. One sensor is attached on the outside and it changes its contacts with respect to the position. So the position of the thermoelements have been measured with respect to the time in seconds. Wireless temperature assembly is installed on the side of the rotary kiln as shown in figure 3.6.

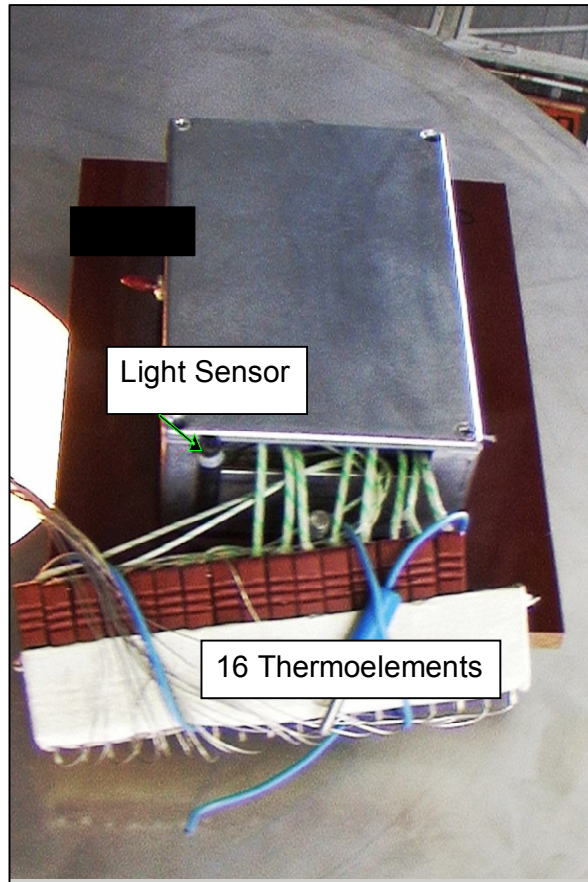


Figure 3.6 Rotating thermoelements arrangement.

### 3.3.7 Supports

Strong supports were provided to the equipments which prevent to move while operating as shown in figure 3.1.

### Conclusion

A pilot plant of externally heated rotary kiln has been successfully fabricated and installed in the laboratory.



The schematic of the externally heated rotary kiln is as shown in figure 4.1 and the details are given in chapter 2. A laboratory scale pilot drum made with stainless steel of diameter 0.6 m and length 0.45 m, with 2 mm wall thickness has been fabricated with the industrial norms. Three electrical heaters are placed at 0°, 90° and 180°. Fixed and rotating arrangement of the thermo elements have been placed inside and its rotating paths are as shown with dotted lines. This path is always constant and it depends on its distance from the wall. Thermoelements close to the wall travel longer path than those which are away from the wall.

The most important thing in the experimental analysis is to select an appropriate thermo element which can withstand at various experimental conditions such as high temperatures, good temperature response and also a very good resistance to oxidation. Low response time defines correctness of selection of the thermoelements.

## **4.2 Experimental measurement of response time ( $t_r$ )**

The thermocouples, which have now been used for a number of years in the range 0-1000°C, are still the most widely used temperature measuring instruments owing to their wide range of use, ruggedness, low cost, high interchange ability. Today the necessity for more accurate temperature determinations in the range from 0 to 1060°C both in process measurements (e.g., in the energy industry and in materials treatments, etc.) and laboratory measurements has renewed the interest for such instruments and stimulated research work, with the twofold purpose of improving the performance of the existing sensors and of studying new types.

Recently, a new base-metal thermocouple, the Nickel-chromium, was introduced [1] and normalized [2]. The experience gained about K type thermocouples has shown the short-range ordering phenomena [3]. K type thermoelements were used in the recent studies to measure temperature profile in the Rotary kilns [4]. Performance of the thermo elements depend on how fast thermoelements indicates the real temperature. Quick response is the

key for the temperature measurement. A simple experiments have been conducted to measure the performance of the thermoelements.

The schematic for the measurement of the response time is as shown in figure 4.2. An experiment has been performed by using 0.2 mm Quartz sand with constant temperature maintained around 74<sup>0</sup> C. The thermo element has been inserted in it and the time required to obtain a constant temperature has been observed as shown in figure 4.3. Thermo element response to the temperature has been measured.

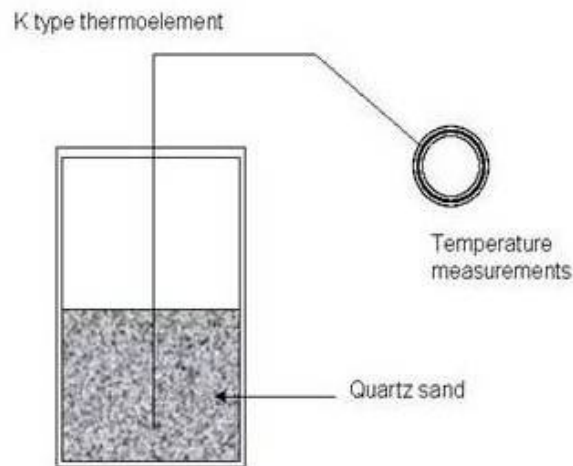


Figure 4.2 The schematic for the measurement of the response time.

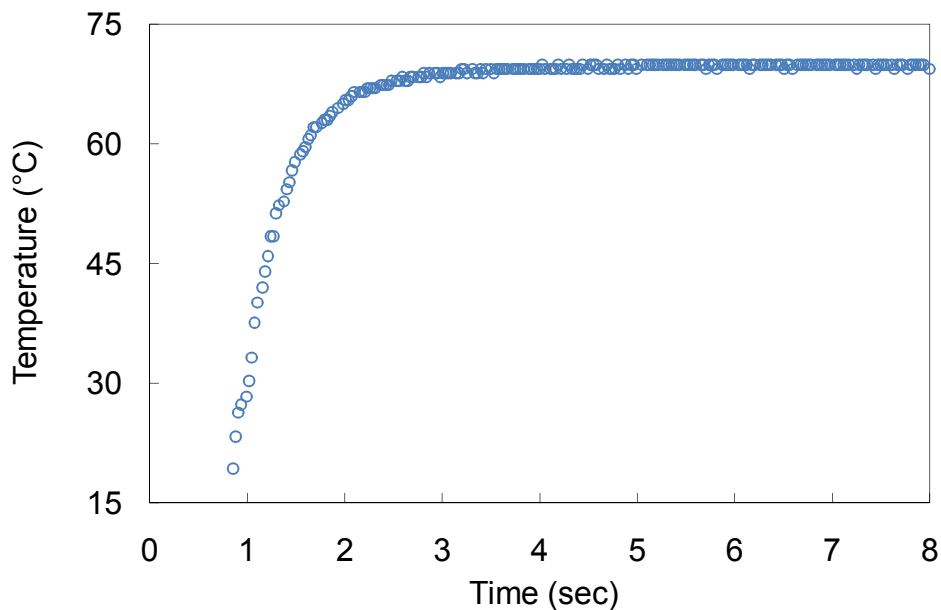


Figure 4.3 Performance time of K type thermo element

It has been found that response time ( $t_r$ ) to get actual temperature of the sand bed is more than one second. In the actual experimental measurement of the temperature has to be performed on the basis of the rotating kiln and agitated bed of the solid. Because of quick response and good anti-oxidation qualities this K type thermoelement ( Ni-Cr ) is useful for the temperature measurement purpose.

### 4.3 Comparison of temperature profiles with fixed and rotating thermoelements assembly

To measure the wall temperature of the rotary kiln, it has been split in to angles from  $0^\circ$  to  $360^\circ$ . It is more convenient to show these measurement points on the circumferential direction depending on the angle.

Depending on the position and rotational speed, thermo element takes various time in contact with the agitated solid bed. The rate of heat transfer is lower in fixed bed than in agitated bed and response time in agitated bed can be lower. Therefore to compare an appropriate output temperature measurement results, it is recommended to measure temperature profiles by two different mechanisms at the same time and positions.

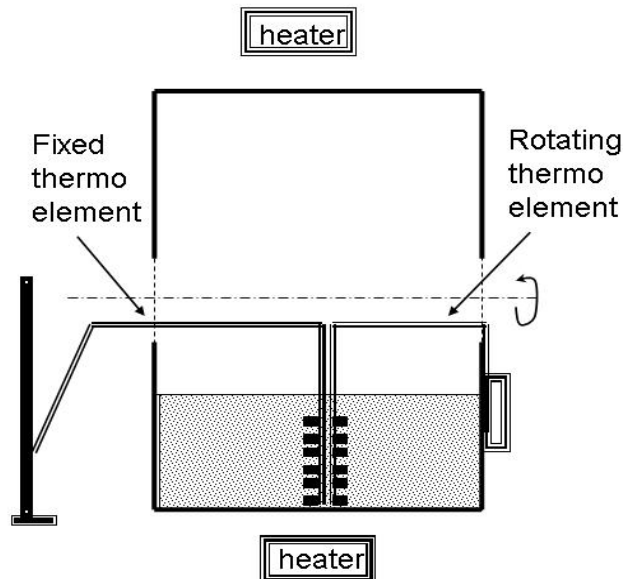


Figure 4.4 Schematic for fixed and rotating thermo elements temperature measuring system

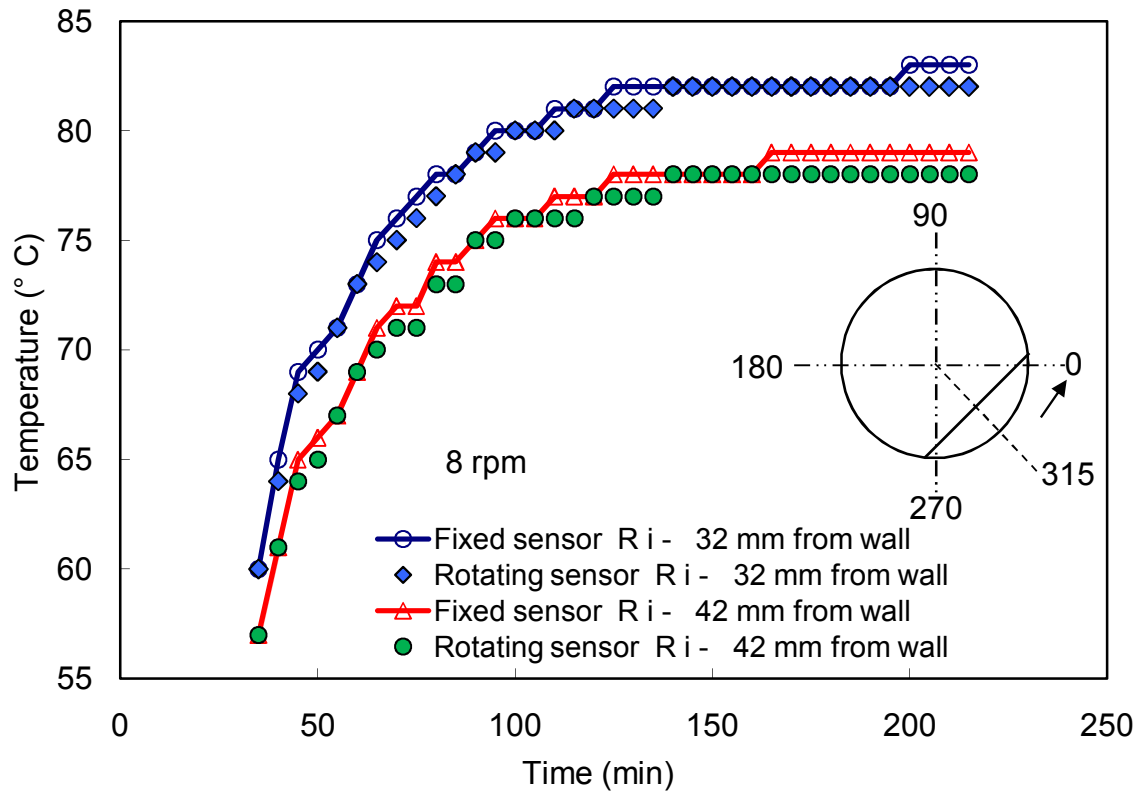


Figure 4.5 Temperature profiles of fixed and moving thermoelements

Among these two mechanisms, the first is to measure the temperature with fixing thermo element at certain position inside the solid bed and second has been measured by rotating the thermoelements at the same position. Schematic of temperature measurement system for fixed and rotating thermo elements is as shown in figure 4.4. Comparison of both temperature profiles with respect to time can predict the reliability of the measurement techniques.

The lesser the temperature difference measured by fixed and moving thermo elements, the better the technique is. Figure 4.5 indicates the temperature profiles inside the solid bed at 32 mm and 42 mm away from the wall for 0.2 mm quartz sand, with 10% of filling degree and rotational speed of 8 rpm. Temperature was measured at an angle 315°. It has been found that there is no significant temperature difference between fixed and rotating thermo elements at the same position. Therefore, temperature measured from rotating thermo elements can be the most appropriate measures for the heat transfer calculations.

#### 4.4 Dependency of the placement of the electrical heater.

Temperature profiles in the agitated bed by changing the position of the electrical heaters have been studied thoroughly. The effect of the position of the electrical heater observed is shown in figure 4.6 and figure 4.7. Electrical heater of 2 KW has been used in the experiments.

Quartz sand of 0.2 mm is used at the filling degree of 10% and rotational speed of 6 rpm. Initially, the electrical heater was placed at the left side of the rotary kiln.

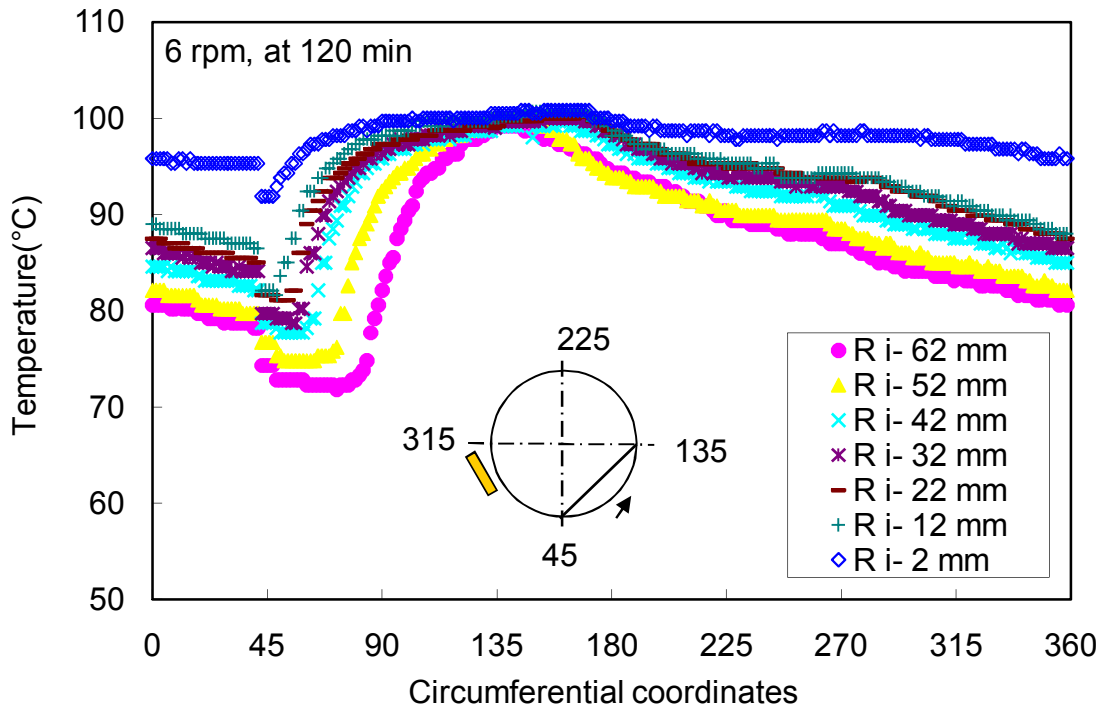


Figure 4.6 Effect of the position of electrical heater on the temperature profiles

The solids in the moving bed gains heat from the wall. Temperature profile along the wall and in the agitated bed of solids has been shown in figure 4.6. Consequently, in the externally heated rotary kiln, heater position was changed to right as shown in figure 4.7.

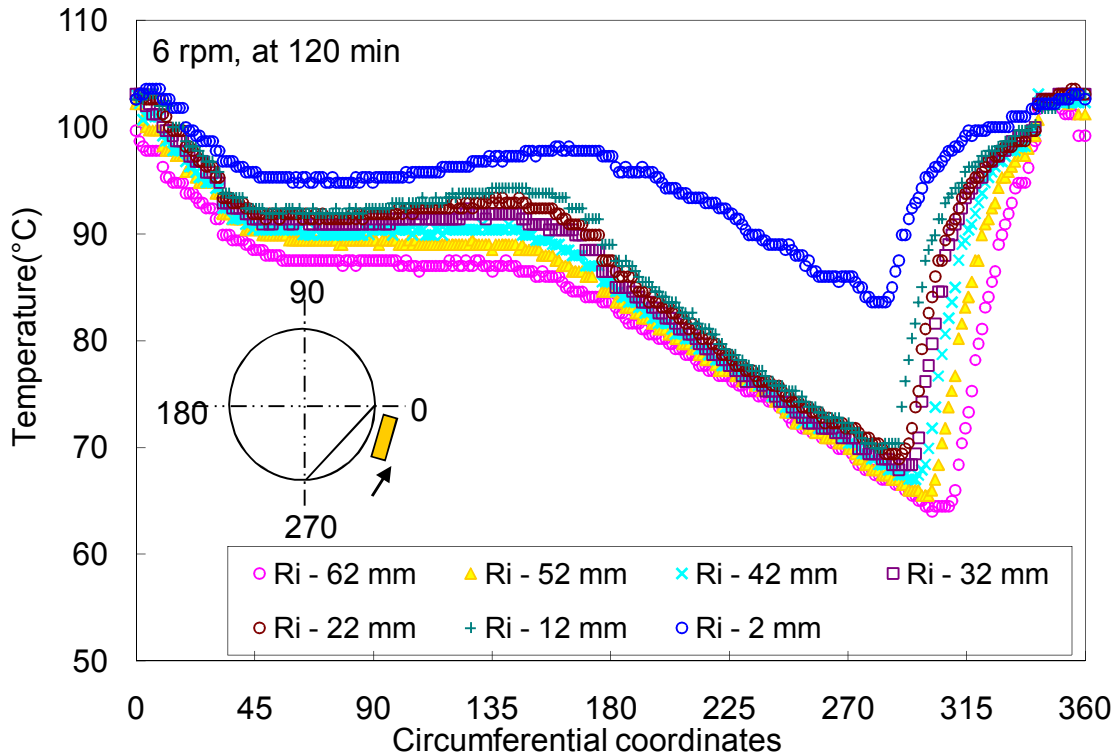


Figure 4.7 Effect of the position of electrical heater on the temperature profiles

Similar nature of the temperature profiles have been observed. It can be concluded that the nature of the temperature profiles is independent of the position of the electrical heater.

#### 4.5 Temperature distribution on the wall and inside the moving bed.

To study the temperature distribution across the wall and inside the agitated solid bed of the rotary kiln, a series of experiments have been performed. Thermophysical properties of sand have been mentioned in Chapter 3. Quartz sand of 0.2 mm and with 3 rpm was used to perform the experiment. Distribution of the temperature profiles across the wall and inside the moving bed is as shown in figure 4.8. Rotary kiln has been divided in 360 parts which includes the air zone and the moving solid bed zone. Angle from 0° to 270° represents the air zone where thermo elements are only in contact with air inside the rotary kiln. Temperature profiles inside the moving solid zone are represented by the angle from 270° to 360°.

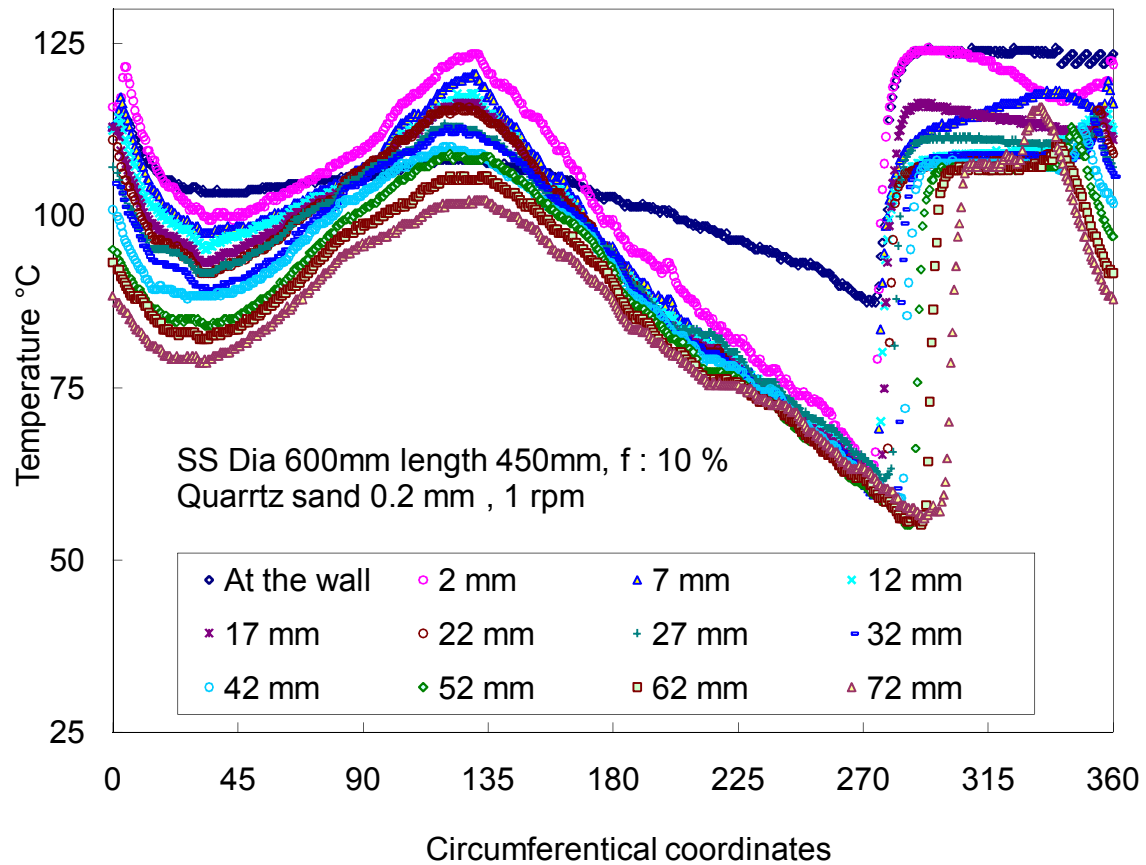


Figure 4.8 Temperature profiles on the wall and inside the moving bed

First, the rotational speed was adjusted to 1 rpm and then the experiment was started at room temperature. Typical motion of an industrial rotary kiln is rolling motion, depends on rotational speed and filling degree. The wall receives heat from the heater and transports it to the solid bed. The dotted blue line in figure 4.9 indicates the temperature profile on the wall. Thermo elements 2 to 12 are designed to measure inside solid bed temperature. The temperature increase is indicated by the thermo elements when it enters into the solid bed.

The solid near the wall is getting heated first and a high temperature difference exist between the wall and the moving solid bed. Temperature across the wall remains nearly constant.

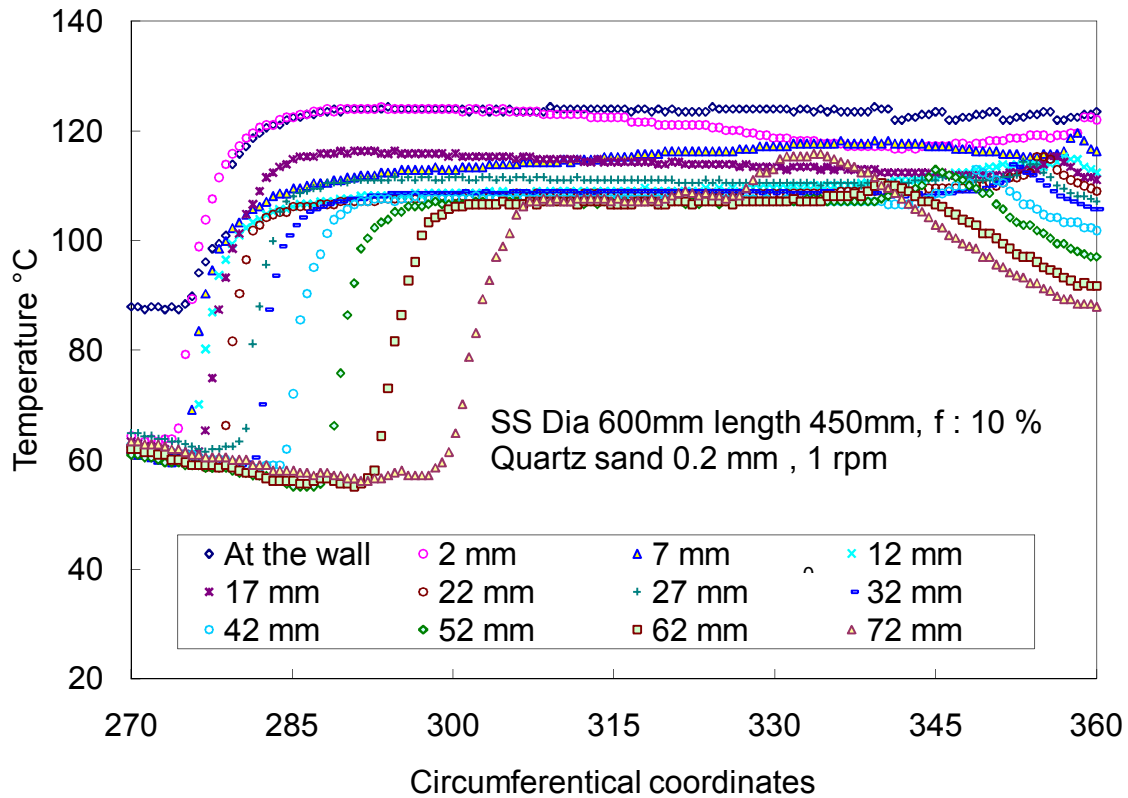


Figure 4.9 Temperature profiles on the wall and inside the moving bed

Thermo elements at distance 2 mm and 102 mm from the wall are immersed first and last respectively inside the solid bed. Temperature profile in the region from 270 to 360 angle represents moving solid bed region. Temperature gradients have been observed in this region. Study of the temperature profile is challenging at this region because of motion of the drum as well as motion of the solid bed at a time. Temperature profile at the wall is almost constant in this region shown by blue line.

The cold and hot region have been observed as shown in figure 4.10a and figure 4.10b. Slight increase in the temperature has been observed before thermoelements end the contact with the solid. This is because solid gets heated from the wall when it moves forward. When it reach at the extreme peak, point B and it slides down towards A.

A slight increase in temperature has been found in the air zone at the angle ranging from

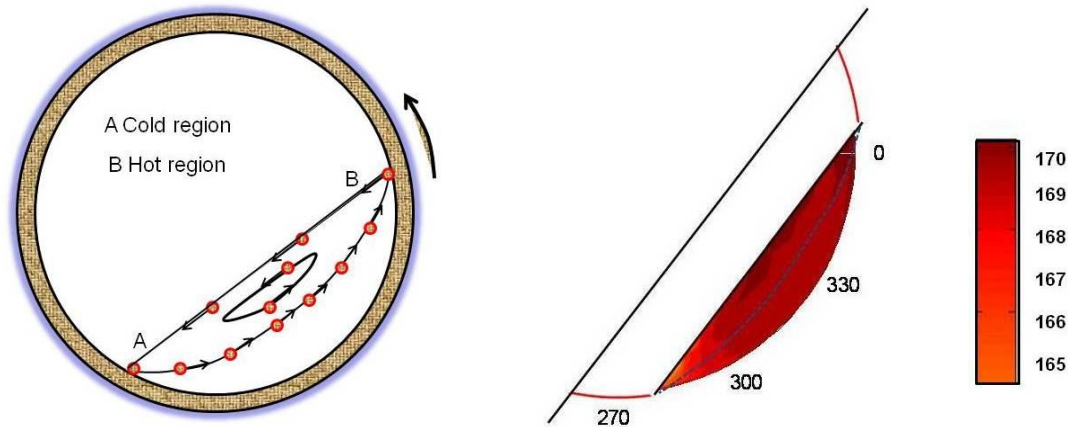


Figure 4.10a 4.10b Path of the solid in rotating solid bed.

90° to 150°. This is due to the high air temperature in this region and the buoyancy. Study of the temperature rise in the agitated solid bed has been studied thoroughly. A series of experiments were performed with 0.2 mm quartz sand and 0.8 mm cylindrical copper pellets at different rotational speed which ranges between 1 rpm, 3 rpm and 6 rpm.

#### 4.6 Calculation of the mean temperature of the bed

Temperature across the wall and the mean temperature of the solid bed plays an important role in heat transfer process. Temperature across the wall continuously increases with time. The solids near the wall surface were heated first and the temperature difference across the solids is found to be high at the beginning of the heating process. After certain time interval, uniform temperature can be obtained at the solid bed.

For the analysis, the bed temperature data are reduced to the mean temperature, defined by equation 4.1. Similar approach has been seen in [5] where  $A_1$  and  $A_2$  are the areas of the solid bed and  $T_1$ ,  $T_2$  are the respective temperatures and  $T_w$  is the temperature at the wall and  $n$  is the number of thermo elements used with respective areas.

Measurement of the mean temperature of the solid bed is practically very critical because

$$T_{meanbed} = \frac{A_1 \cdot \left( \frac{T_w + T_1}{2} \right) + A_2 \cdot \left( \frac{T_1 + T_2}{2} \right) + \dots + A_n \cdot \left( \frac{T_{n-1} + T_n}{2} \right)}{A_1 + A_2 + \dots + A_n} \quad 4.1$$

of the complexity of the equipment. Manually, it is quite difficult to get mean temperature by mixing the moving solid bed which is used to estimate the heat transfer coefficient from the wall to the solid which plays the most important role in the heat transfer phenomenon.

Moreover, one cannot guess when the uniform temperature inside the solid bed can be observed. Figure 4.11 represents the mean temperature of the bed with respect to the wall temperature for 2 KW heating system, 0.8 mm Copper pellets, 10% of filling degree with 3 rpm. Temperature difference at the beginning is high, it starts reducing and finally both temperatures become uniform after certain time. Experimental results indicates that

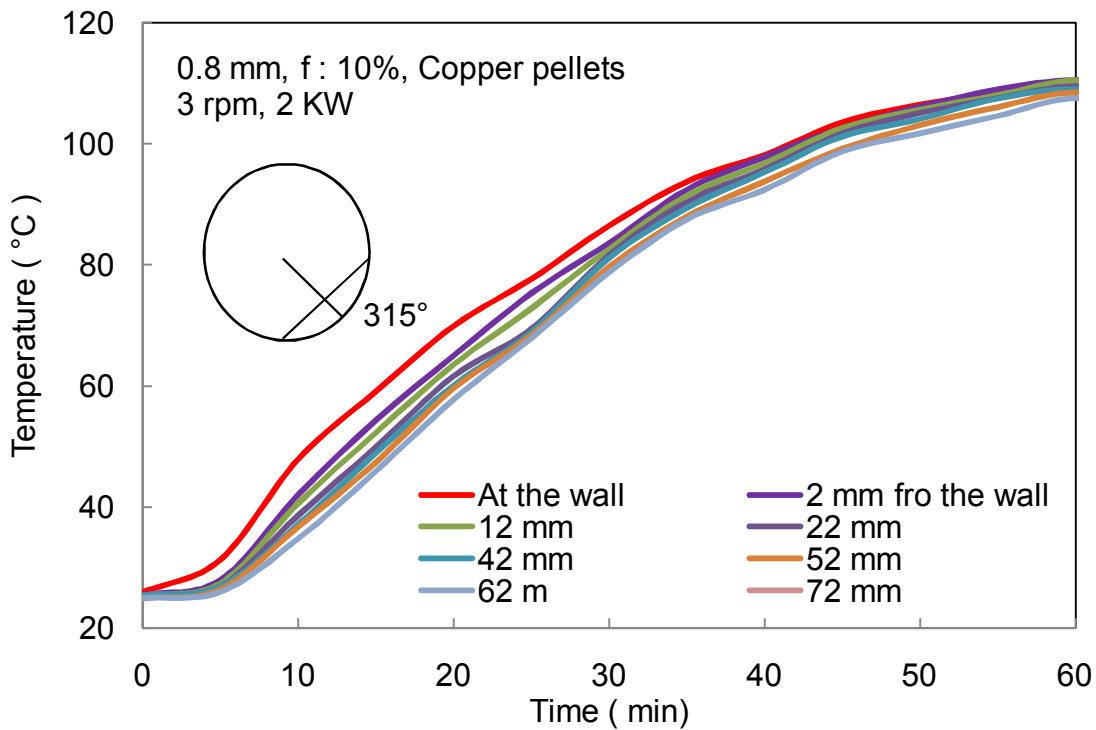


Figure 4.11 Temperature on the wall and inside the moving bed at fixed position with time

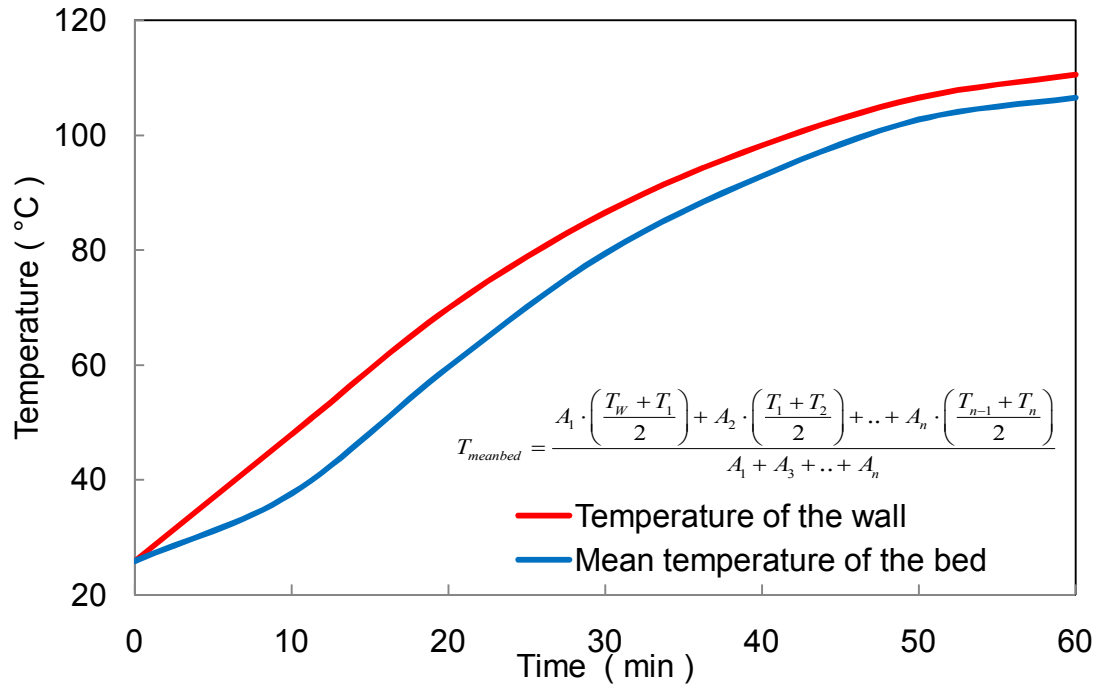


Figure 4.12 Mean temperature of the bed with time

the temperature difference is higher at the time interval of 0 to 30 min and slowly the solid attains the temperature of the wall and uniform temperature distribution can be observed inside the solid bed.

#### 4.7 Experimental analysis of the temperature profiles at various time intervals

Thorough study of temperature distribution inside the agitated solid bed have been carried out. Table 4.1 represents details of the performed experiments. Temperature profile for one whole experiment at different time intervals have been plotted and explained as follows.

No	Material	Filling degree	Rpm
1	Quartz sand 0.2 mm	10 %, 15%, 20%	1, 3 , 6
2	Copper pellets cylindrical 0.8 mm	10 %, 15%, 20%	1, 3 , 6
3	Mehl (cement)	10 %, 15%, 20%	1, 3 , 6

Table 4.1 Experimental analysis

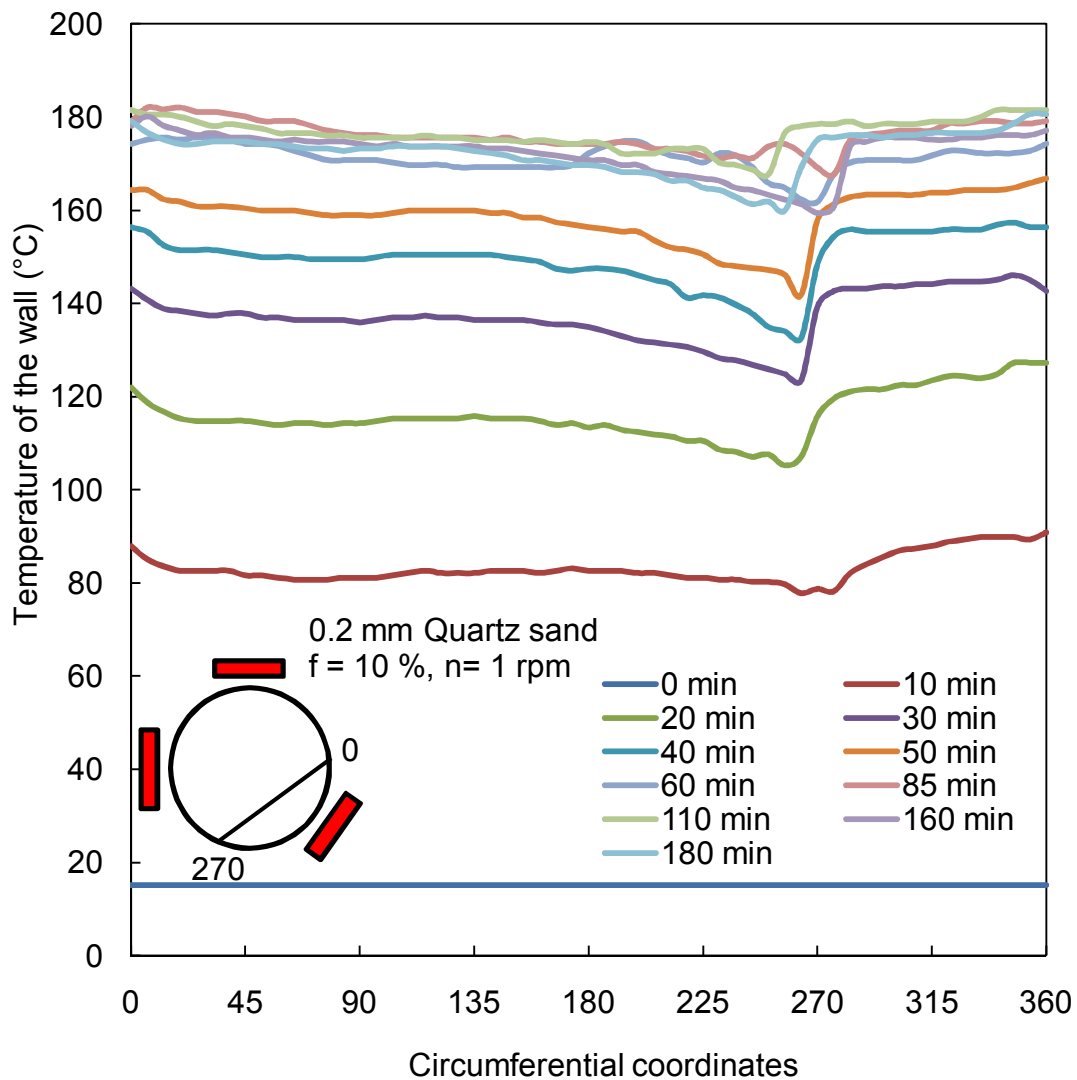


Figure 4.13 Temperature profiles on the wall at the various time intervals

Temperature profiles on the wall at various time intervals for Quartz sand 0.2 mm at 10 % of filling degree, with 1 rpm speed of rotation, have been started from ambient temperature are plotted as shown in figure 4.13. The kiln wall gains the heat from externally placed 3 electrical heaters. Experiment has been started at ambient temperature of  $17^{\circ}\text{C}$ , it has been shown with a straight line. Rotary wall gives heat to the solid bed and the temperature across the wall increases steadily. Around  $180^{\circ}\text{C}$  temperature has been observed at 80 min. Figure 4.14 represents the detailed bed side temperature profiles on the wall and inside the solid bed.

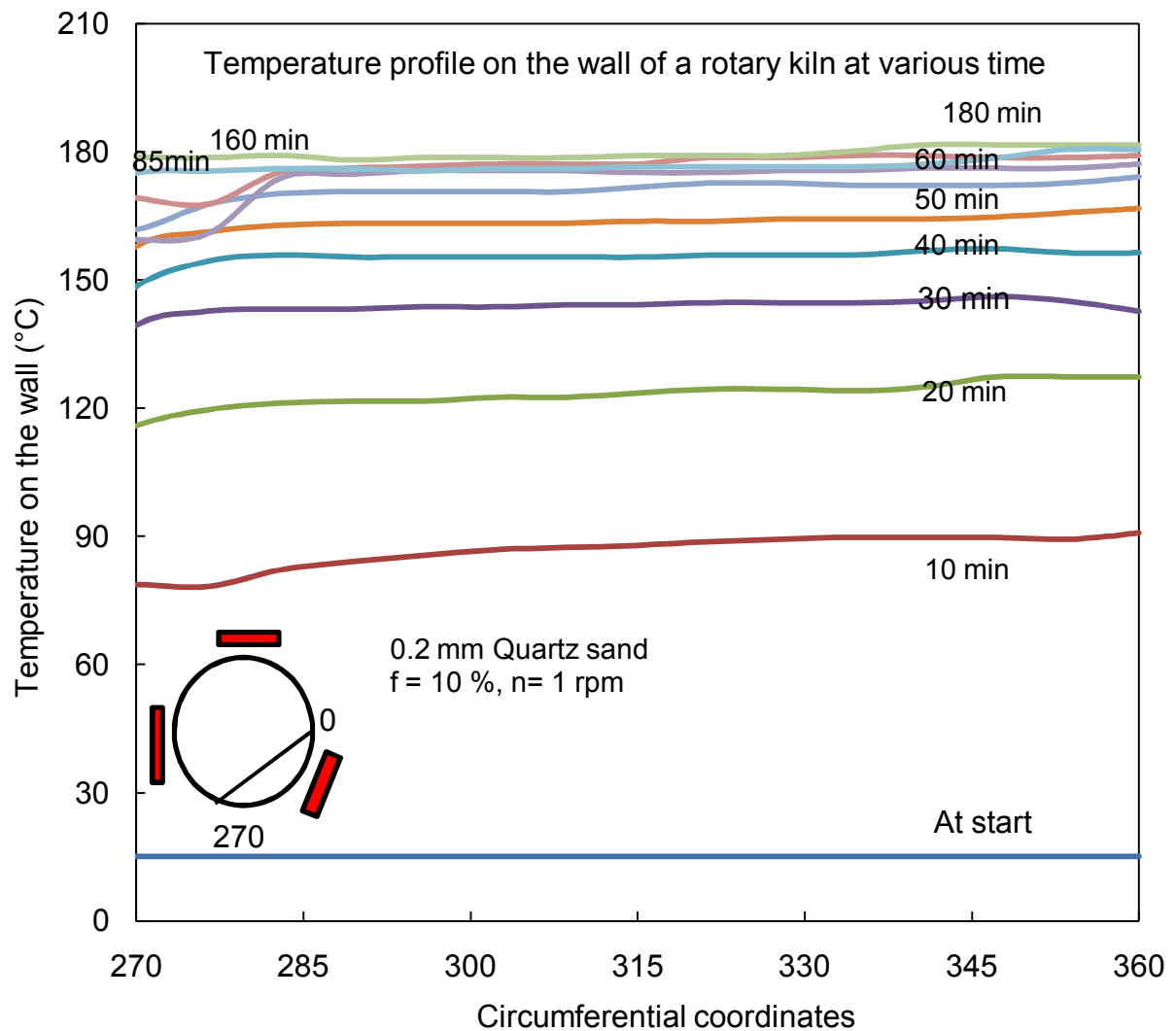


Figure 4.14 Temperature profiles on the wall and inside the solid bed at 10 min

Temperature profile at 10 min, 20 min, 30 min, 60 min, 110 min, 180 min have been shown in figure 4.15 to figures 4.20 respectively. High temperature gradients have been seen at the start of the experiment. Slight rise in temperature at the region where solid ends between angles  $315^{\circ}$  to  $360^{\circ}$  have been observed. This is because of hot particles sliding down from the top of the agitated bed and they get mixed with the following particles in the same direction. In figures 4.18 to 4.20, the temperature gradients decrease as mixing phenomenon dominates the heat transfer. The level of temperature gradient is almost neglected at 180 min.

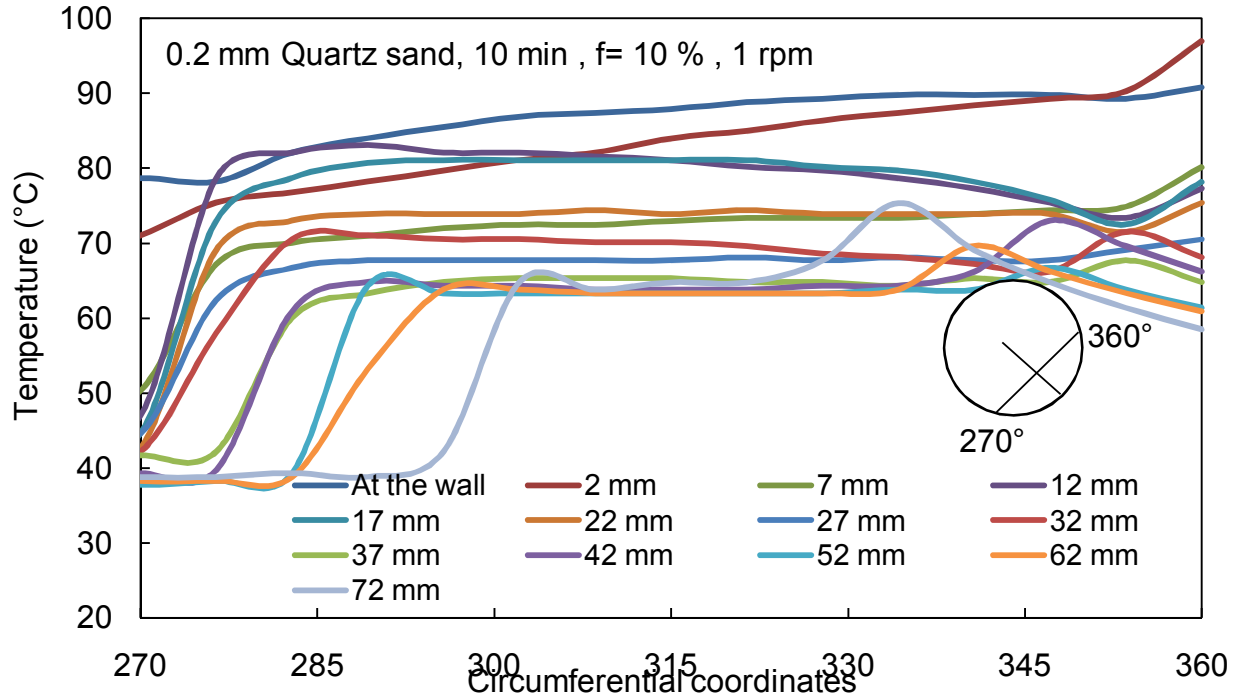


Figure 4.15 Temperature profiles on the wall and inside the solid bed at 20 min

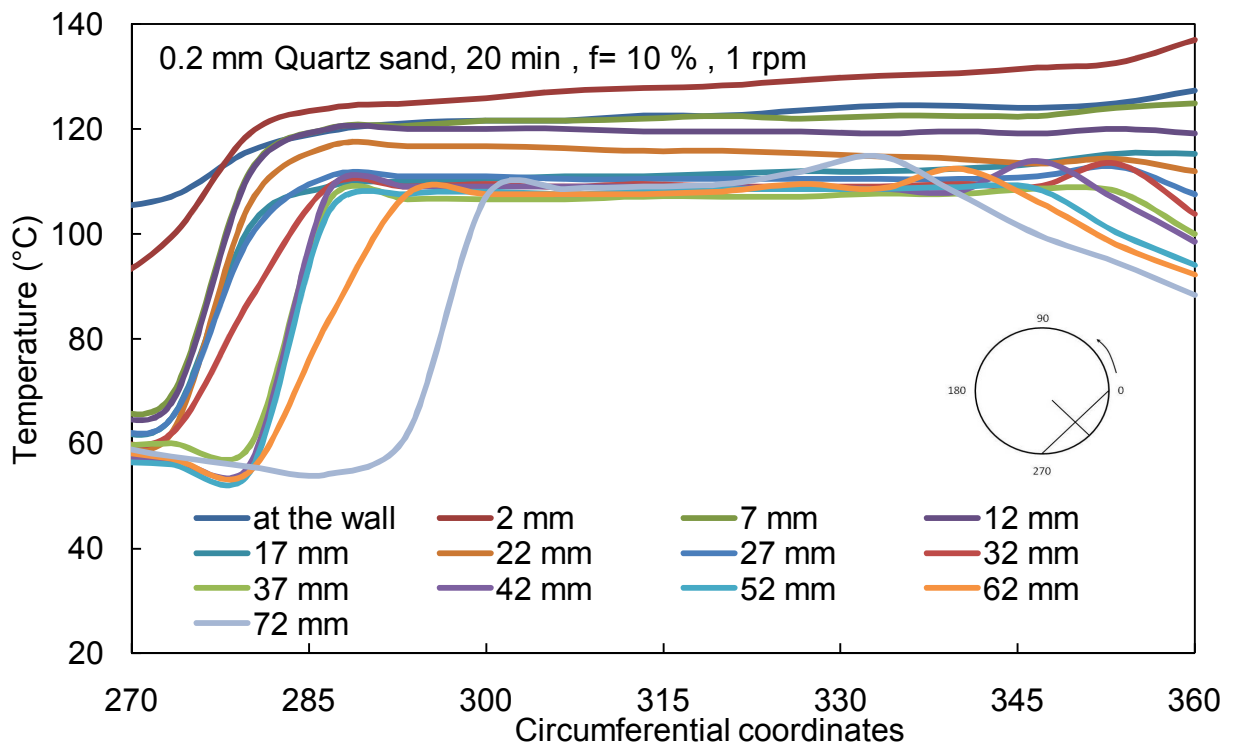


Figure 4.16 Temperature profiles on the wall and inside the solid bed at 20 min

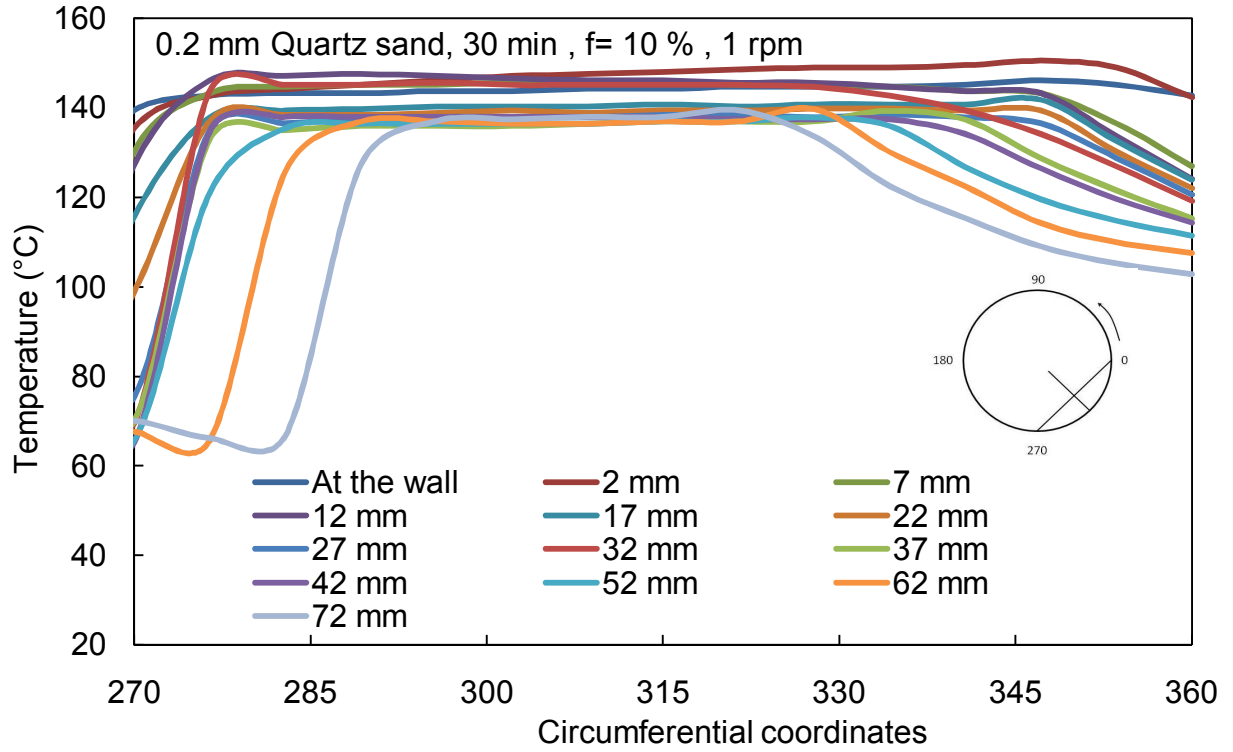


Figure 4.17 Temperature profiles on the wall and inside the solid bed at 30 min

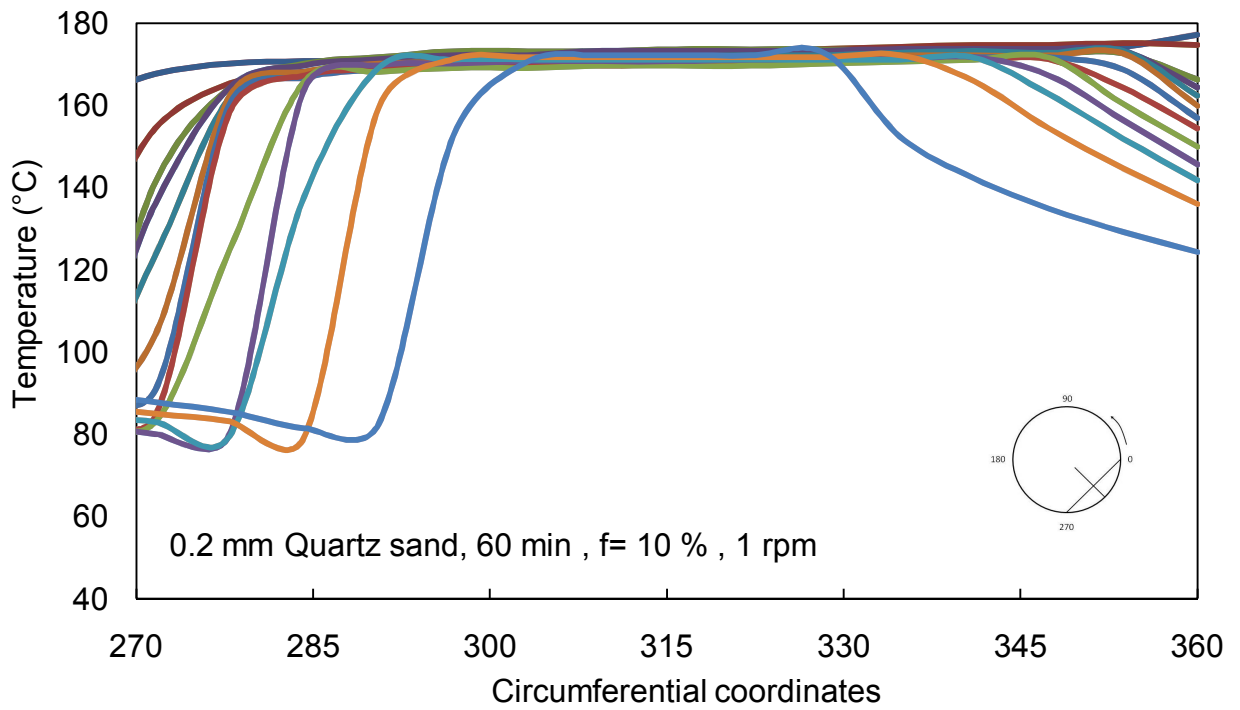


Figure 4.18 Temperature profiles on the wall and inside the solid bed at 60 min

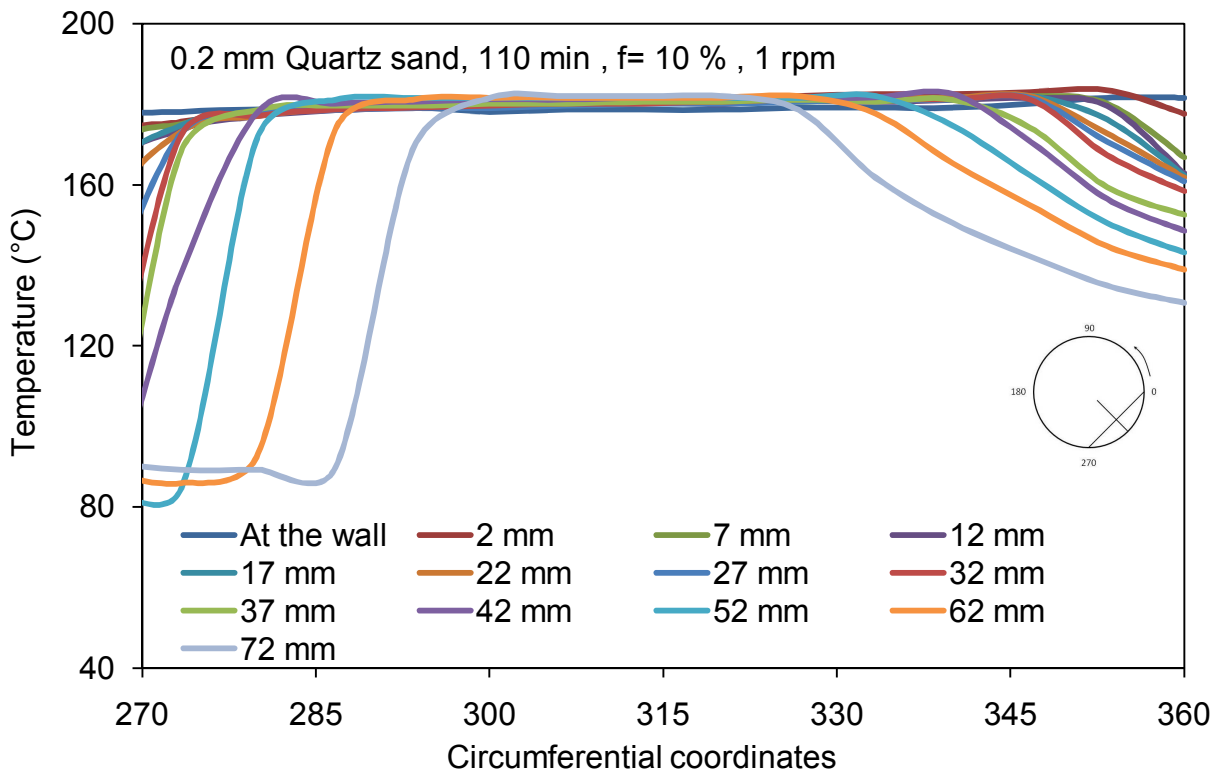


Figure 4.19 Temperature profiles on the wall and inside the solid bed at 110 min

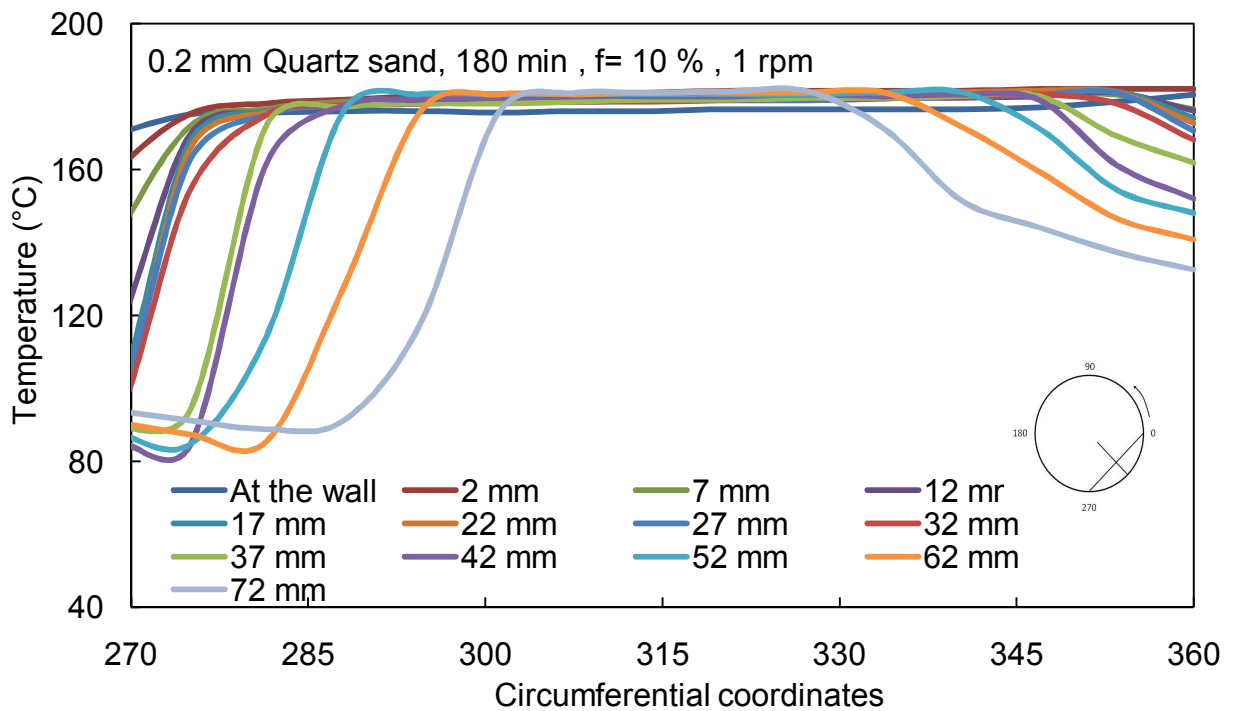


Figure 4.20 Temperature profiles on the wall and inside the solid bed at 180 min

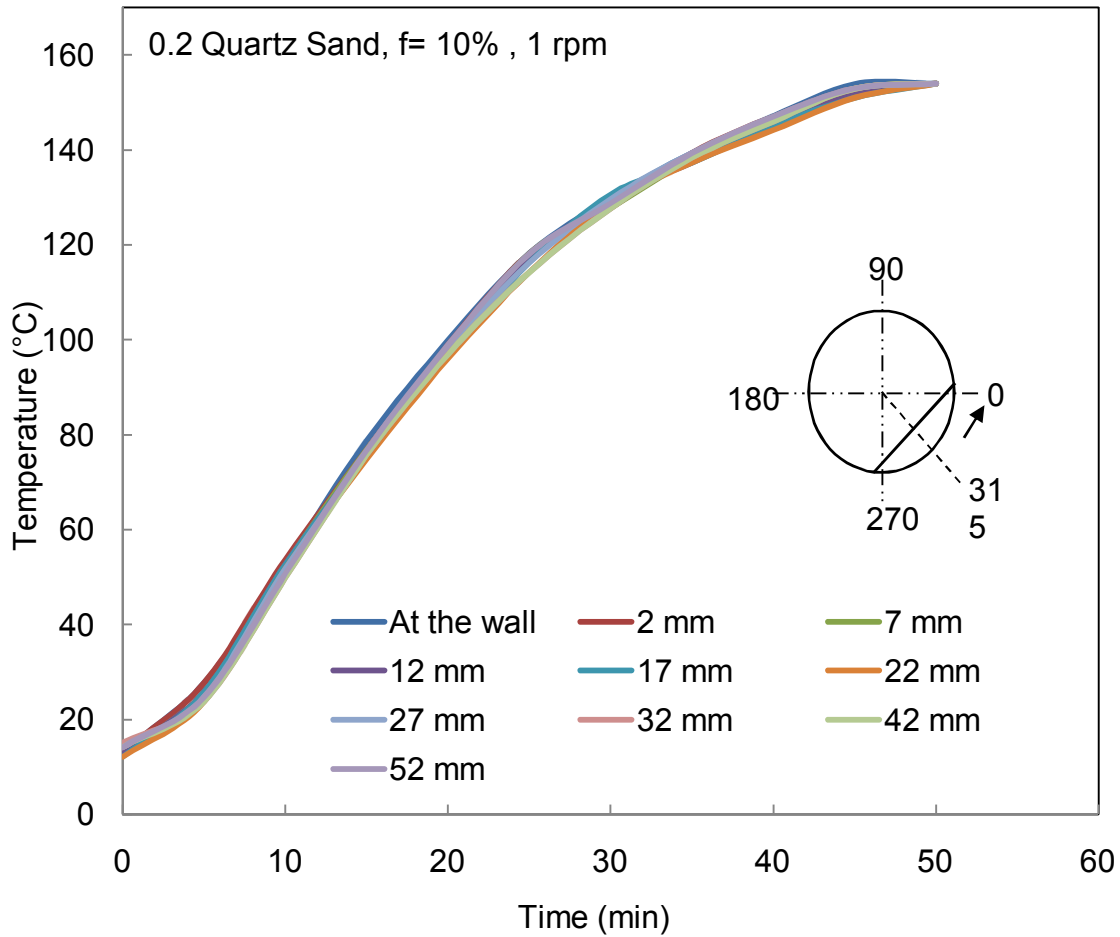


Figure 4.21 Temperature profiles on the wall and inside the agitated solid bed with respect to time (min)

Temperature profiles on the wall and inside the agitated solid bed with respect to time is as shown in figure 4.21.

Temperature profiles for the material, cylindrical copper pellet of 0.8 mm, at the wall for various time intervals for 10% of filling degree with 3 rpm speed of rotation are plotted as shown in figure 4.22. Experiment has been started at ambient temperature of  $19^{\circ}\text{C}$ , it has been shown with the straight line. The kiln wall gains heat from three externally placed electrical heaters. The Rotary kiln wall gives heat to solid bed and temperature across the wall is constantly increases. Around  $170^{\circ}\text{C}$  temperature has been observed in 80 min. Figure 4.23 represents the detailed bed side temperature profiles on the wall and inside the solid bed.

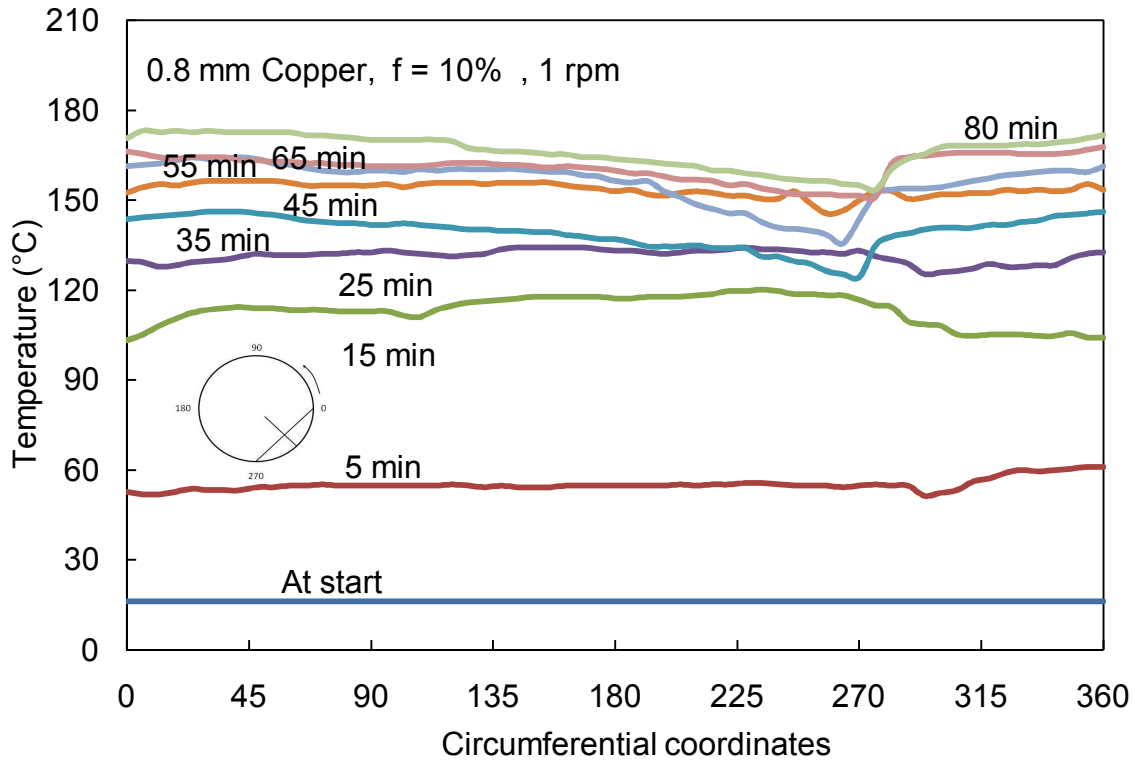


Figure 4.22 Temperature profiles on the wall and inside solid bed at various time intervals

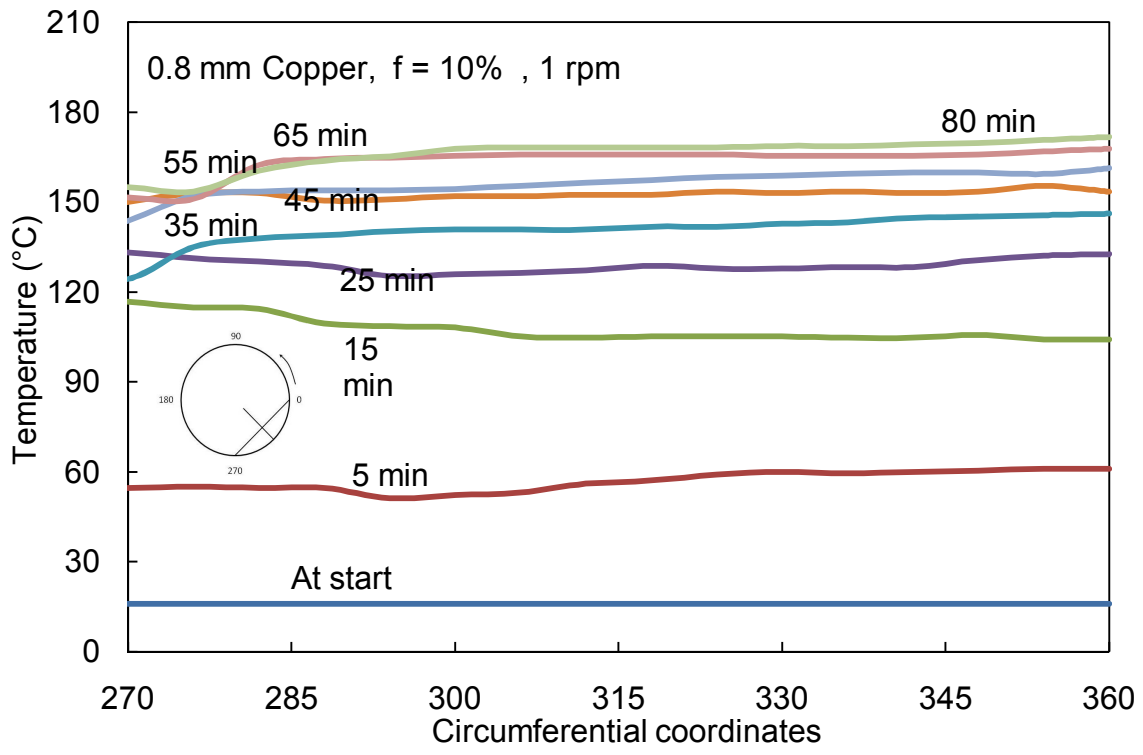


Figure 4.23 Temperature profiles on the wall and inside solid bed at various time intervals

Thorough study of temperature profiles for one whole experiment has been plotted for particular time intervals. Figure 4.24 to figure 4.29 represents temperature profile on the wall and inside the agitated solid bed at 5 min, 15 min, 25 min, 45 min, 65 min and at 80 min respectively.

At the beginning high temperature gradient have been observed. Due to high thermal conductivity of the copper pellets, it acquires higher temperature earlier than the quartz sand.

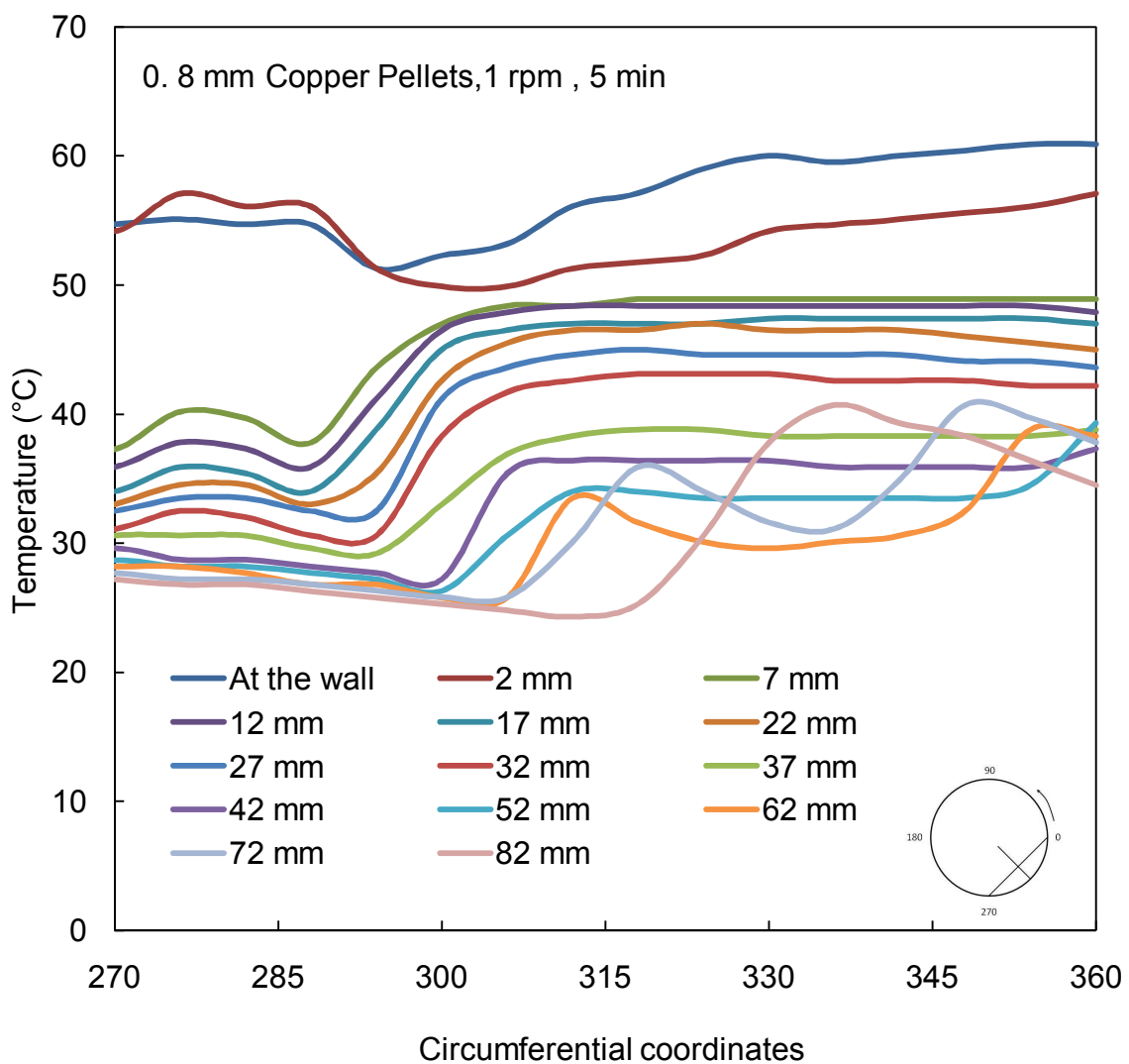


Figure 4.24 Temperature profiles on the wall and inside the solid bed at 5 min

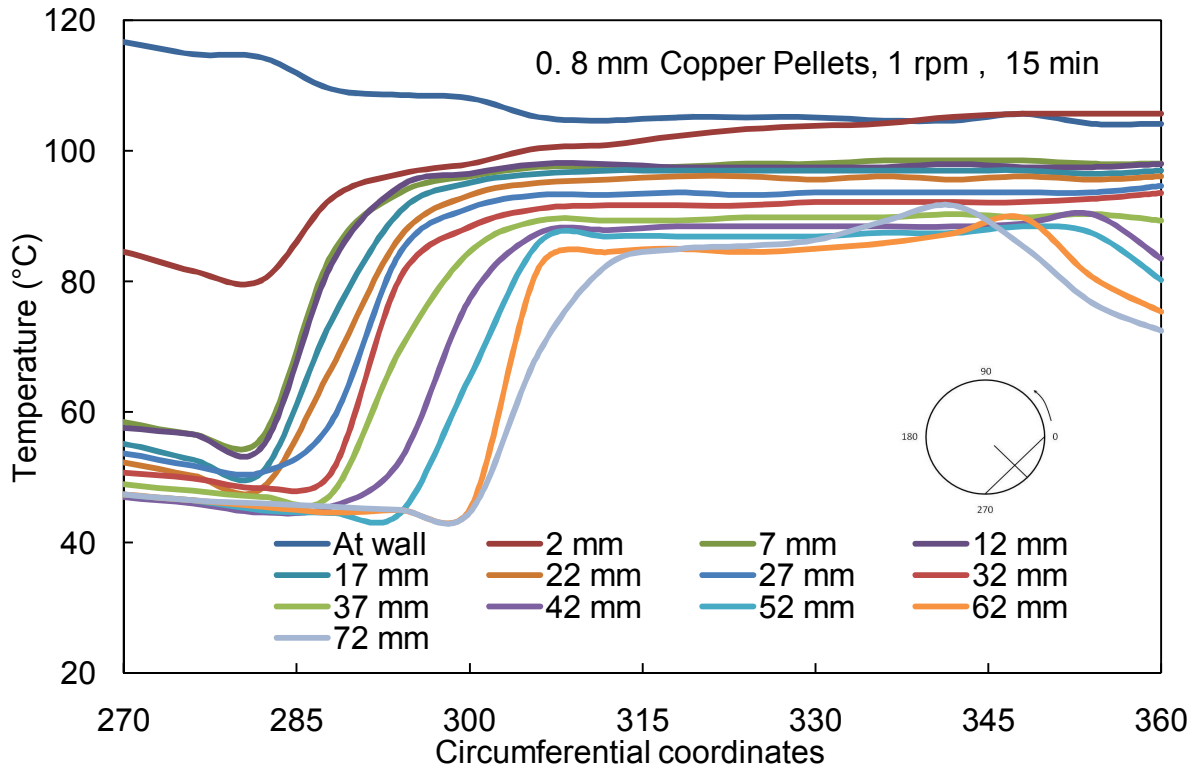


Figure 4.25 Temperature profiles on the wall and inside the solid bed at 15 min

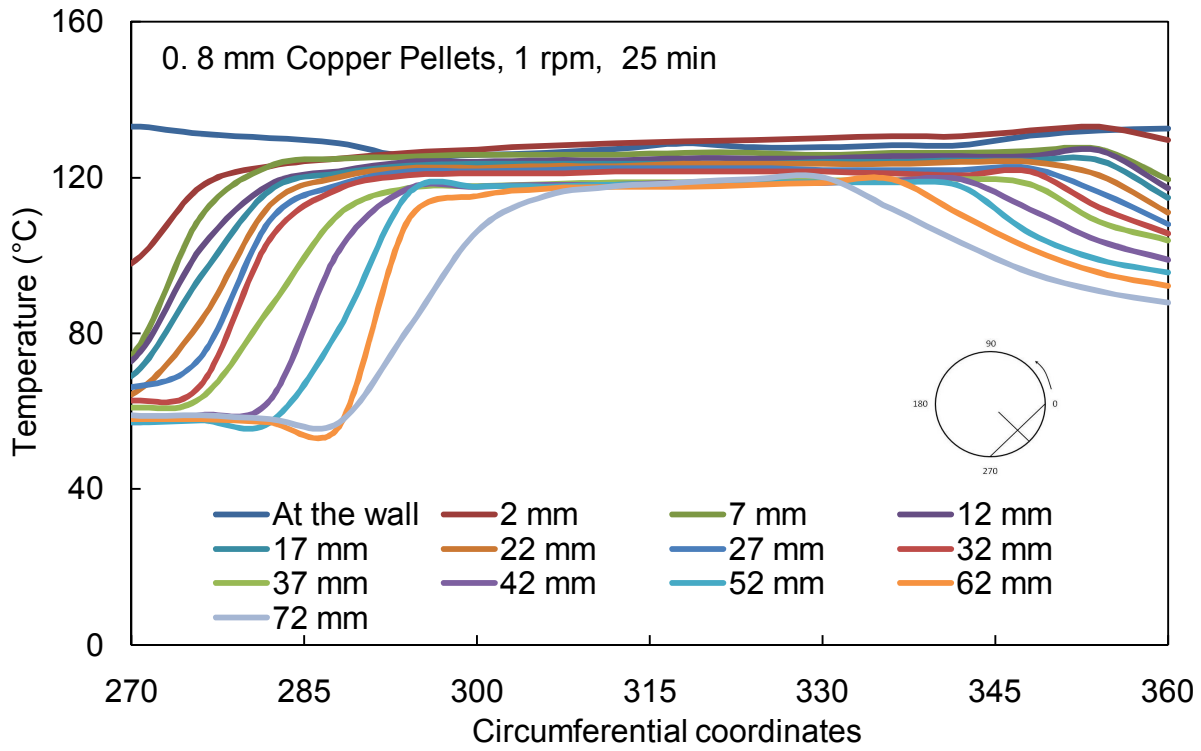


Figure 4.26 Temperature profiles on the wall and inside the solid bed at 25 min

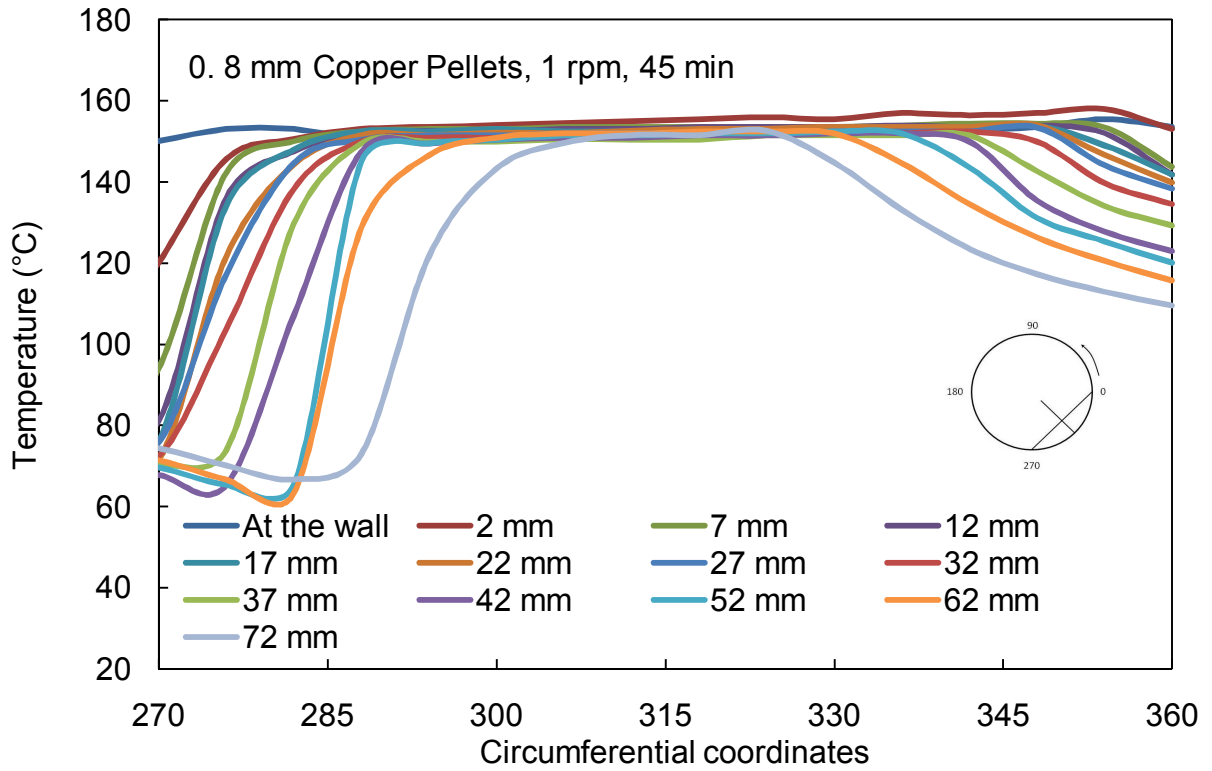


Figure 4.27 Temperature profiles on the wall and inside the solid bed at 45 min

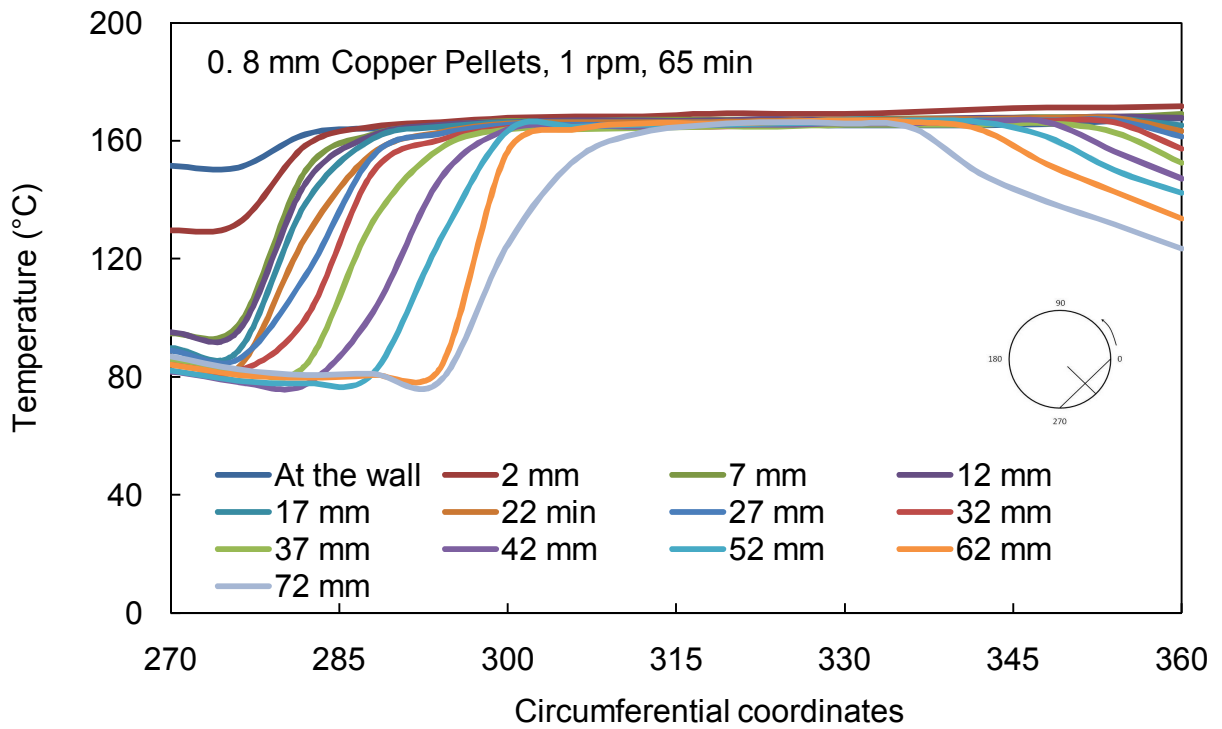


Figure 4.28 Temperature profiles on the wall and inside the solid bed at 65 min

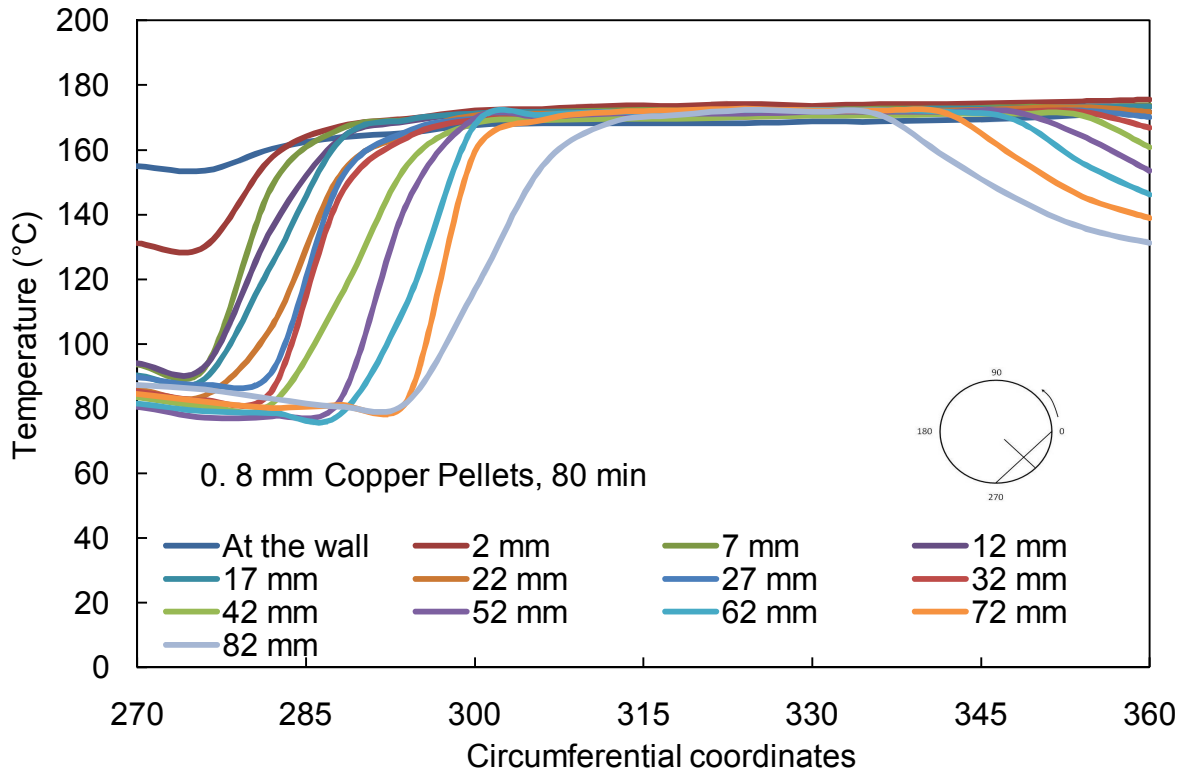


Figure 4.29 Temperature profiles on the wall and inside the solid bed at 80 min

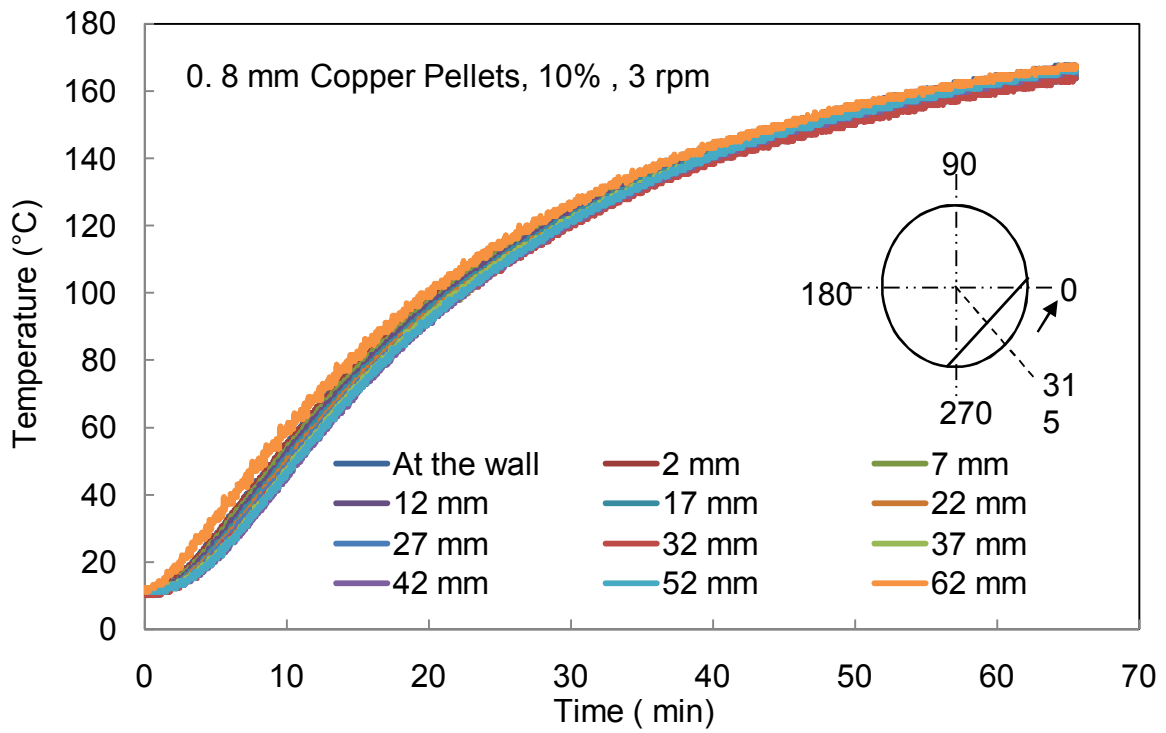


Figure 4.30 Temperature profiles on the wall and inside the agitated solid bed with respect to time (min)

Temperature profiles on the wall and inside the agitated solid bed with respect to time are as shown in figure 4.30.

#### 4.8 Temperature profile for very fine material [ Mehl (Cement) ]

Figure 4.31 represent the temperature profiles across the rotary kiln for a fine material Mehl (Cement). Sliding motion has been observed at rotation speed of 3 rpm and 10% filling degree. It is difficult to see the mixing phenomenon inside the sliding solid bed. No perfect temperature gradient has been observed. Sliding motion is seen due to the polished inner surface of the rotary kiln wall. To convert sliding motion in to the rolling motion, roughness of the surface should increased up to certain extent.

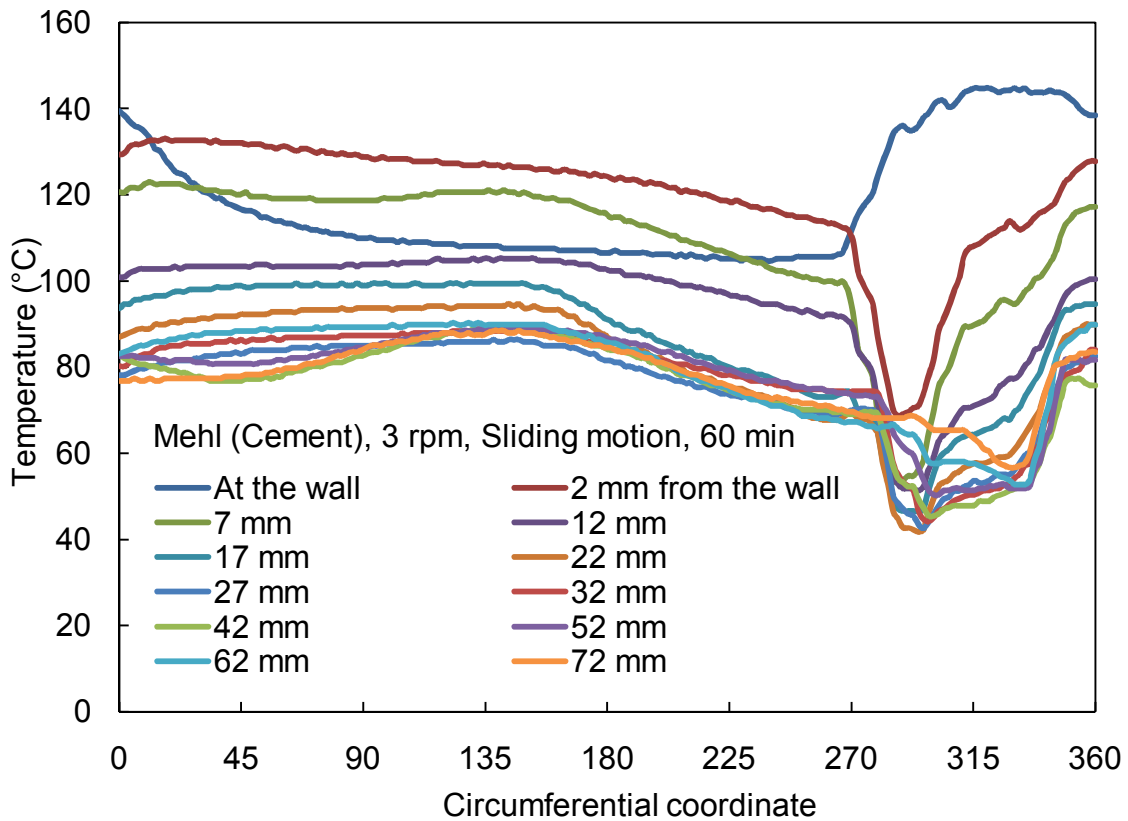


Figure 4.31 Temperature profiles at the wall and inside the solid bed 3 rpm for 60 min

More experiments have been performed at high rotation speed around 6 rpm. No changes in the motion of the solid bed have been observed as shown in figure 4.32.

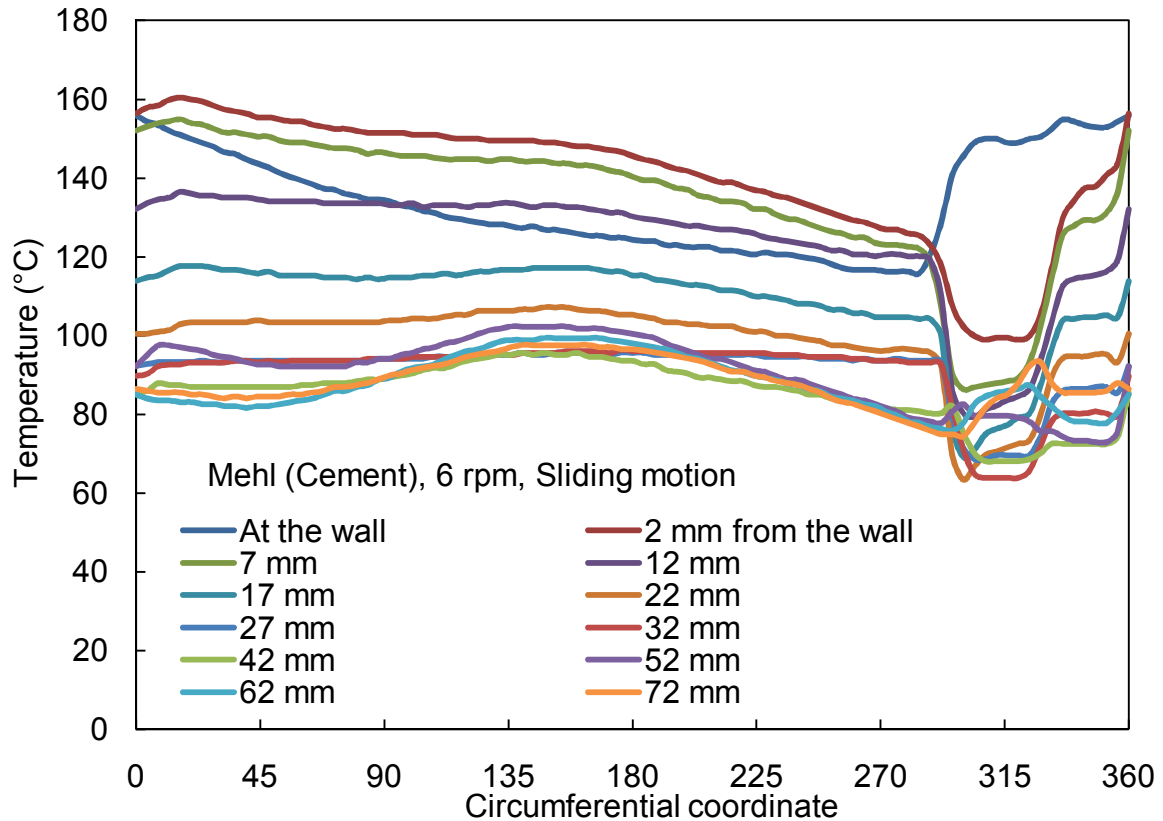


Figure 4.32 Temperature profiles at the wall and inside the solid 6 rpm for 60 min

Temperature profiles inside the Rotary kiln include the air and solid region is as shown in following figures 4.33 to figure 4.38. Temperature contour represents the heat transfer phenomenon inside the Rotary kiln. Various experiments with 0.2 Quartz sand at 1 rpm have been performed in the pilot plant of Rotary kiln. It shows that at the start of the experiments low temperature gradient exist inside the agitated solid bed. After certain extent of the time; temperature gradients found to be very high. The temperature profile for the air side has also been studied.

From all above experiments, one important observation which has been seen is that the temperature at the opposite of the agitated solid bed is high. Hot air goes up because of its lower density hence region of high gas temperature have been seen. The high temperature has been observed due to the buoyancy of the air. During the rotation of the agitated bed, rolling motion has been observed. Temperature at the wall starts increase first. This can be easily seen in following figures.

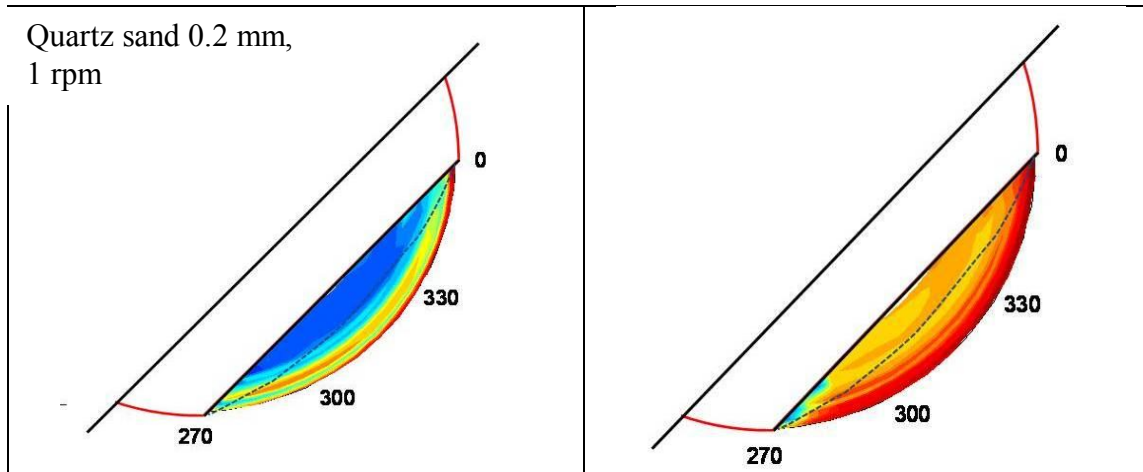


Figure 4.33 & 4.34 Temperature profiles inside the solid bed at 5 and 10 min

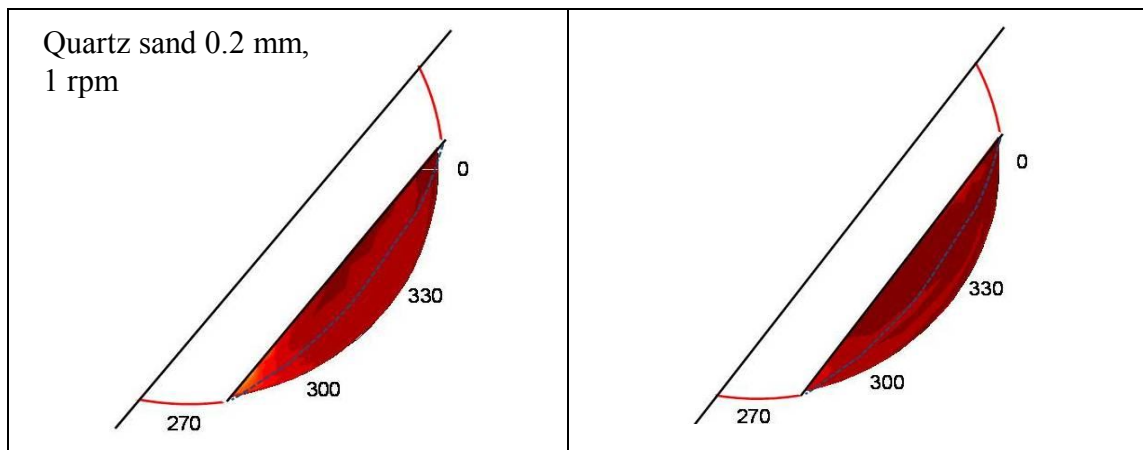


Figure 4.35 & 4.36 Temperature profiles inside the solid bed at 20 and 30 min

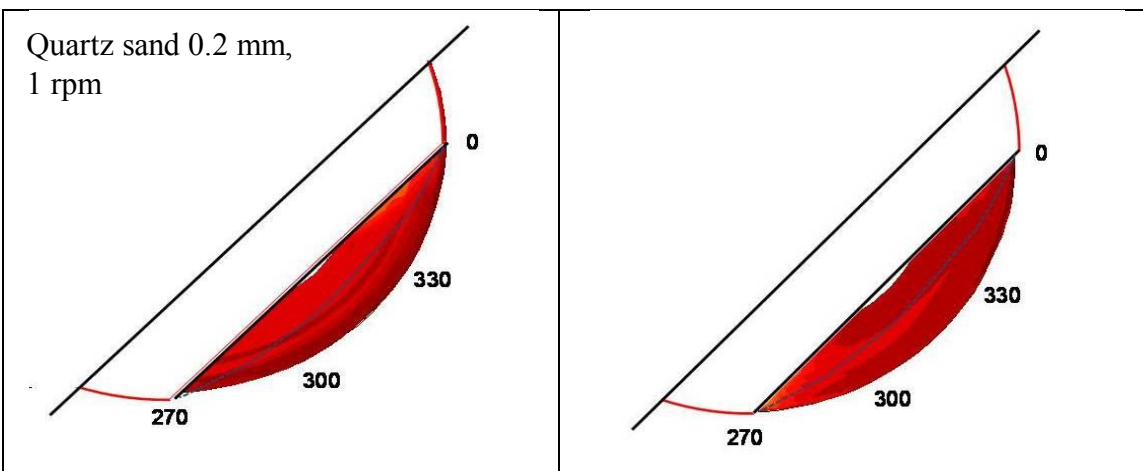


Figure 4.37 & 4.38 Temperature profiles inside the solid bed at 60 and 110 min

Because of continuous rotating motion of the solid bed, hot particles move up and fall down on the free surface of the solid bed. The increase in the temperature at the free surface has been seen in figures 4.37 and 4.38. The heated solid particles pulled up with the passive layer. This hot particle falls down and hot region has been observed.

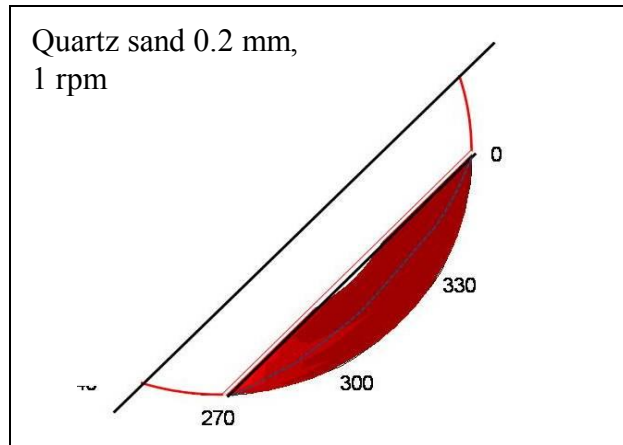


Figure 4.39 Temperature profiles inside the solid bed at 180 min

Similarly temperature profile inside the Rotary kiln for 0.8 mm copper pellets, 1 rpm and 10 % filling degree at various time interval are as shown in figure 4.40 to figure 4.43.

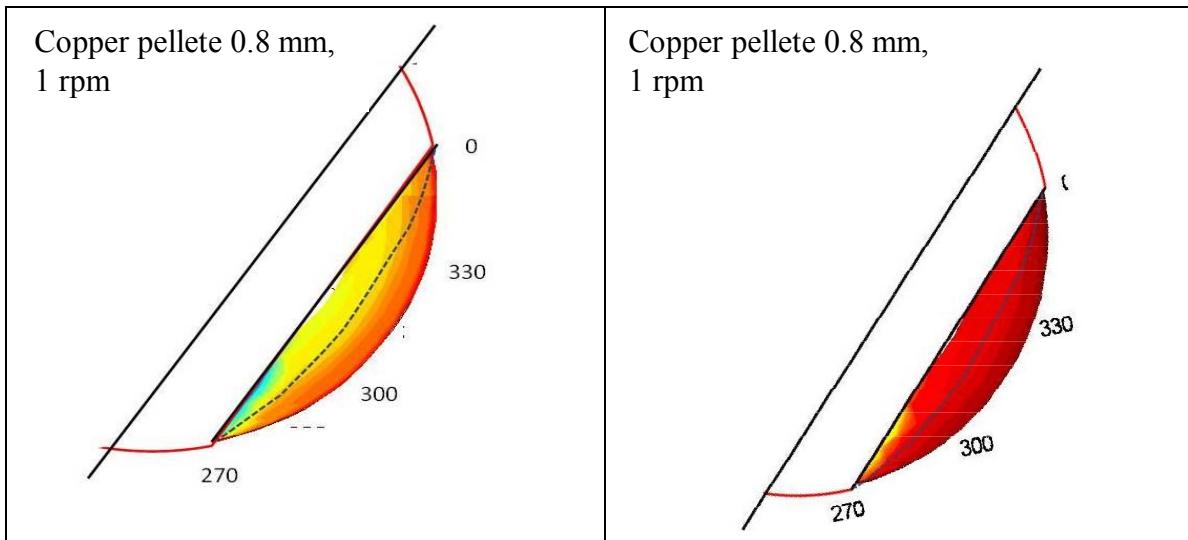


Figure 4.40 & 4.41 Temperature profiles inside the solid bed at 5 and 15 min

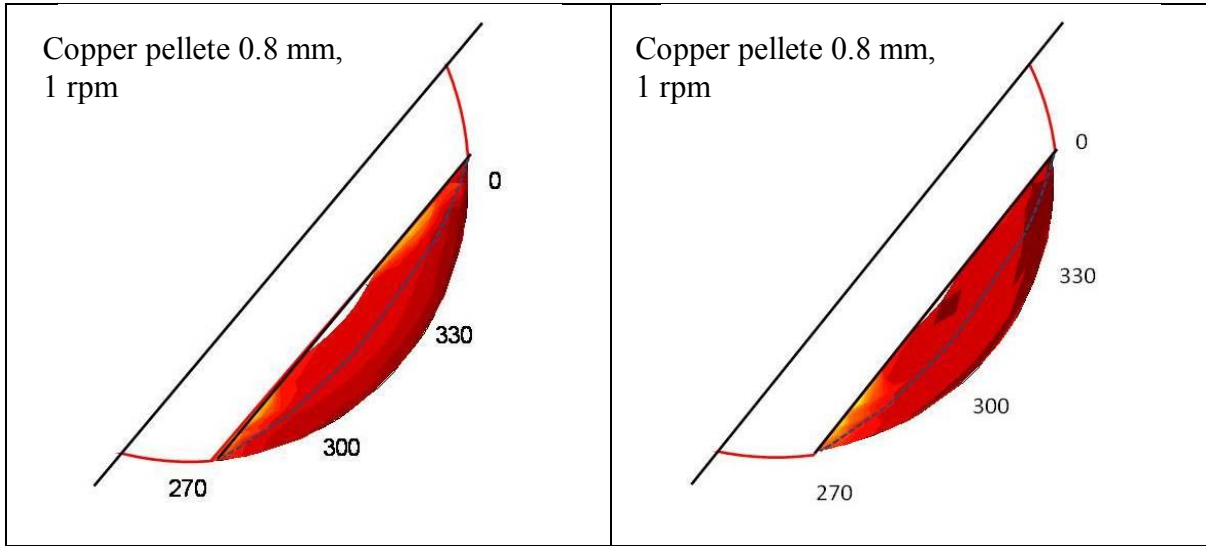


Figure 4.42 & 4.43 Temperature profiles inside the solid bed at 25 and 80 min

#### 4.9 Temperature profiles at various speeds of rotation

Detailed study of temperature distribution inside the agitated bed at various speed of rotations has been done. Similarly, various experiments have been performed with 0.8 mm cylindrical copper pellets, at 10% filling degree. The temperature fluctuations on the internal surface of the kiln wall are presented in figure 4.44.

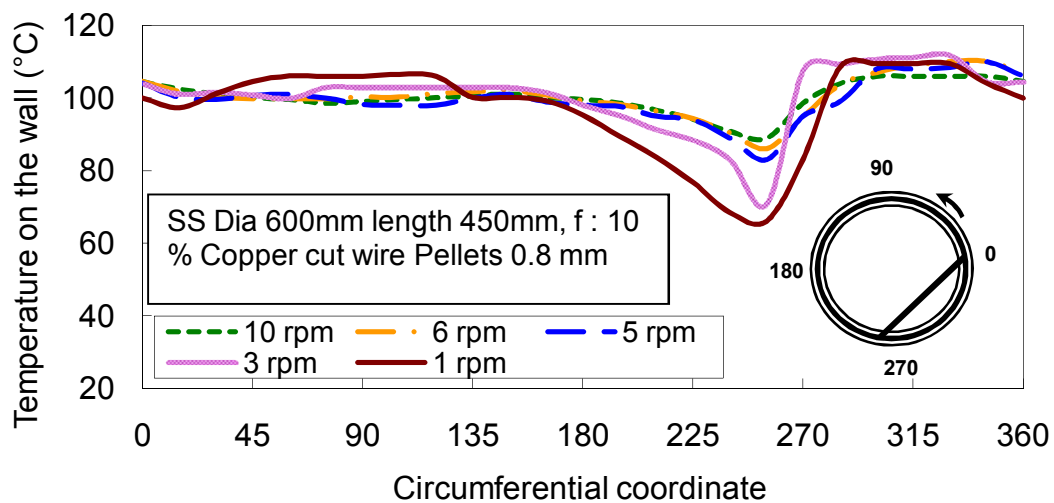


Figure 4.44 Effect of the rotational speed on the temperature fluctuations.

The speed of rotation have been maintained from 1 rpm to 10 rpm. When the kiln speed is increased, decrease in the temperature fluctuation has been observed. The kiln wall has been alternately cooled and heated during each revolution by the hot gas and the cold solid respectively. At lower kiln speed, higher temperature fluctuations have been observed which qualitatively matches with the numerical and the analytical results as shown before. This phenomenon is well explained in [12].

#### 4.10 Heat transfer coefficient from wall to the solid bed

As explained in Chapter number 2, various models for heat transfer are available for calculations of heat transfer coefficient. In the present study, only heat transfer coefficient from wall to solid has been considered. From our experimental plant, we try to calculated heat transfer coefficient from wall to the agitated solid bed. A detailed investigation of the heat transfer coefficient have been carried out. Following table shows the properties of the material used for the experiments,

No	Material	$\lambda$ W/mK	$\rho$ kg/m <sup>3</sup>	$c_p$ J/kgK	$D_p$ mm
1	Quarts sand	0.3	1500	830	0.2
2	Copper pellets	400	8960	385	0.8

Table 4.2 Material properties for the solid used in the rotary kiln

Parameters used for the calculations of experimental heat transfer coefficient are given in the table 4.3.

No	Parameter	Value
1	Rotary kiln : Stainless steel	D 600mm, L450mm, Thickness 2mm
2	Heat source	4 KW
3	Speed of rotation	1rpm to 10 rpm

Table 4.3 Parameter for estimation of heat transfer coefficient

To evaluate the heat transfer coefficient from wall to solid, temperature distribution inside the agitated solid bed have been measured as described before. Mean temperature of the bed is very important to evaluate in the calculations. So following method has been used to evaluate mean temperature of the bed.

#### 4.10.1 Mean temperature of the bed for heat transfer coefficient calculations

Mean temperature of the agitated bed have been calculated as explained in chapter 3. Figure 4.45 represents temperature profile on the wall and inside the agitated solid bed. Mean temperature of the bed has been calculated using equation 4.1. Mean temperature of the bed with respect to the wall temperature has been plotted in figure 4.46. The wall temperature increases exponentially with time. Maximum temperature difference exist at the beginning of the heating.

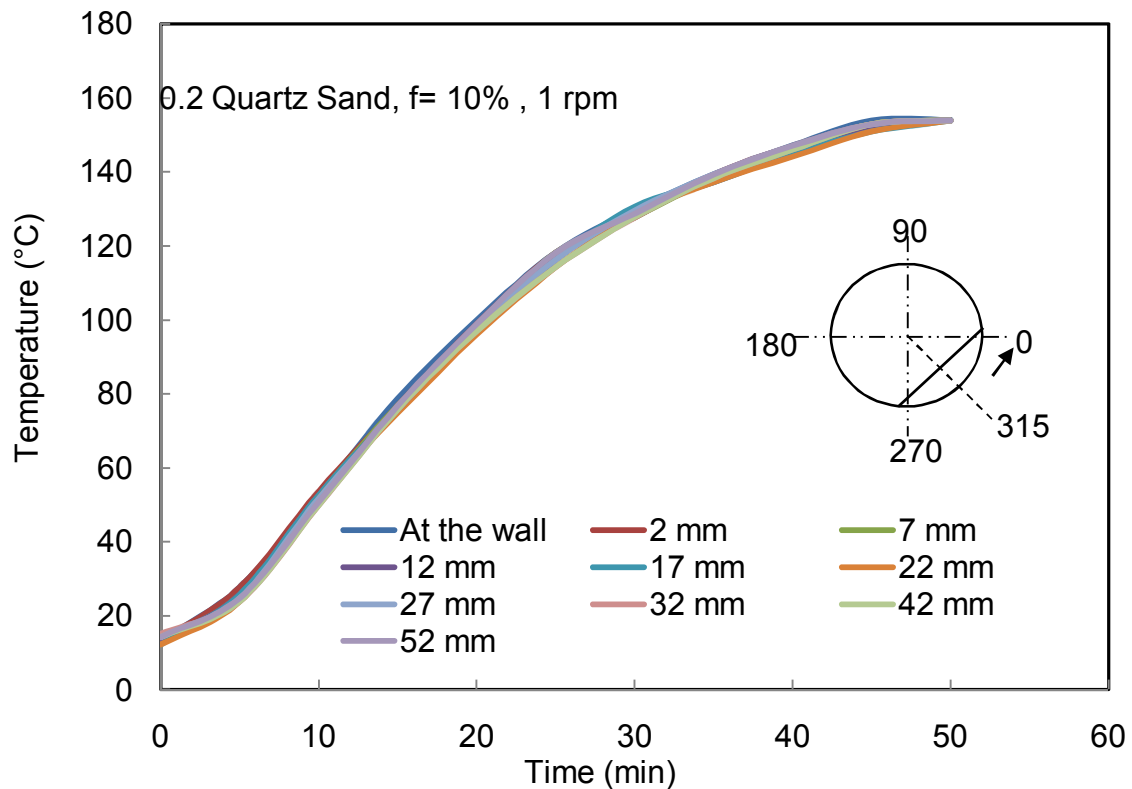


Figure 4.45 Temperature of the agitated bed with time

After continuous heating, the temperature difference between the mean temperature of the bed and the wall temperature of the Rotary kiln reduces. Simultaneously the slope of the curve also decreases with increase in time.

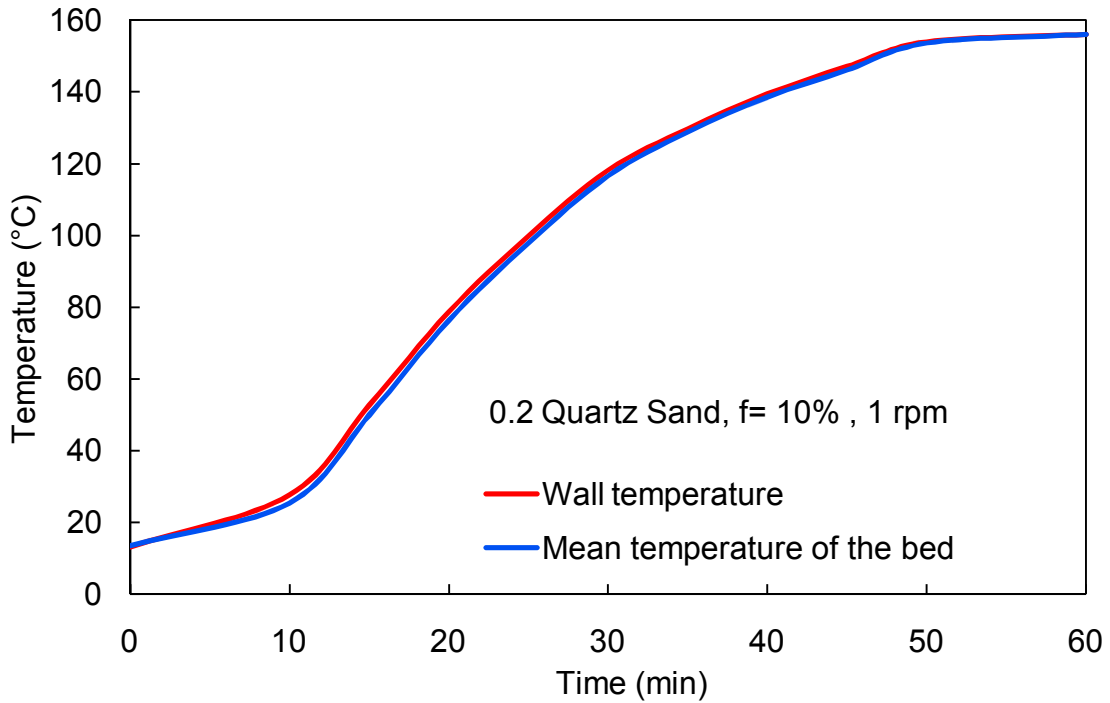


Figure 4.46 Temperature profile on the wall and mean temperature of the agitated solid bed with respect to time

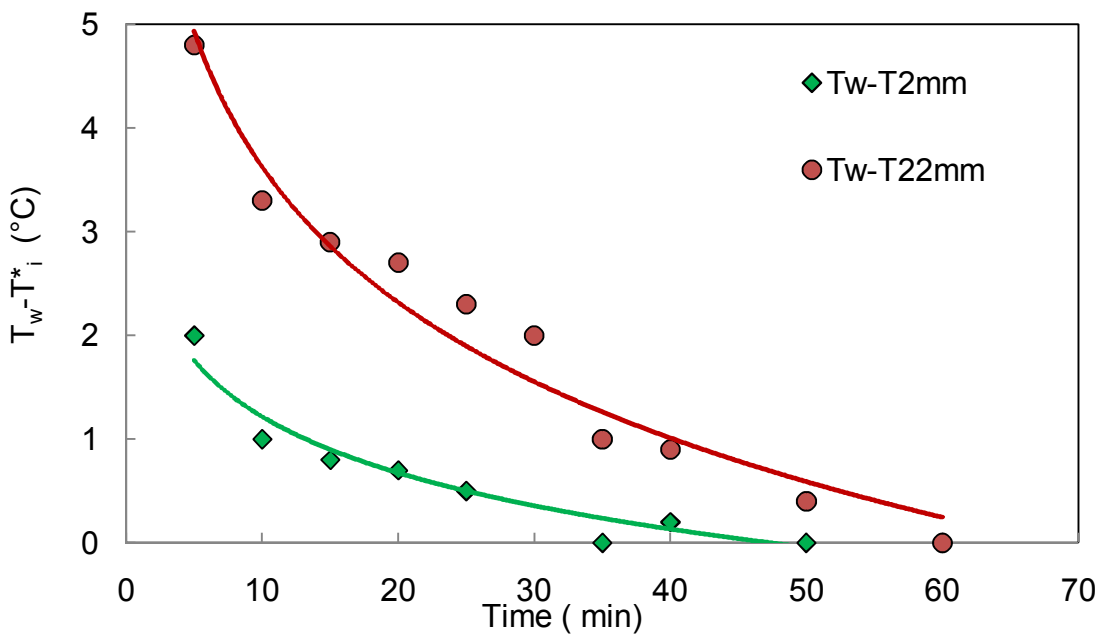


Figure 4.47 Temperature fluctuation inside the agitated solid bed

Temperature fluctuation inside the solid bed with respect to the wall can be clearly seen in figure 4.47. Temperature difference at the wall and the region in the bed at 2 mm and 22 mm has been plotted. The temperature difference between the wall and particular depth inside the solid decreases continuously and attain minimum value. Higher temperature fluctuation between two reference points i.e. at a 2 mm and 22 mm inside the solid, has been observed at the start and later it reduces with time. This temperature fluctuations defines the value of the heat transfer coefficient which is described in the following session.

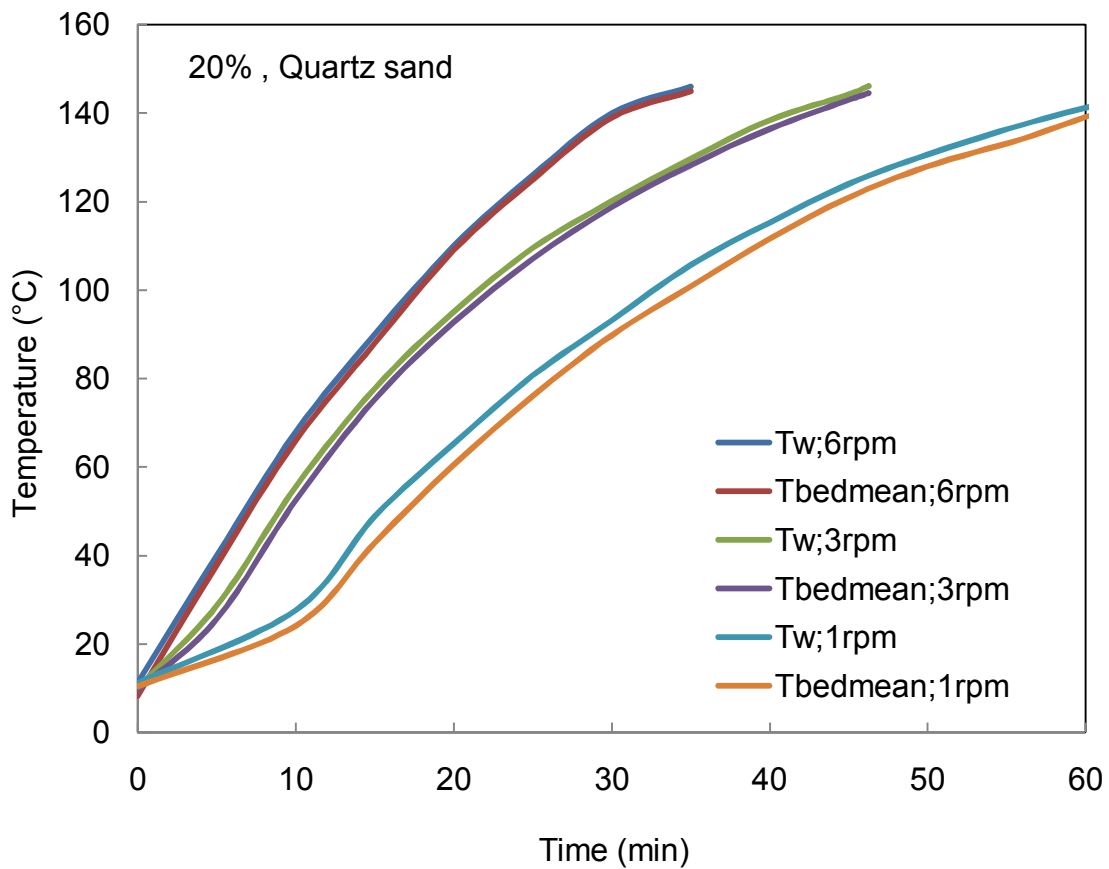


Figure 4.48 Temperature of wall with respect to the mean temperature of the agitated solid bed

Mean temperature of the bed with respect to the wall temperature for 0.2 mm Quartz sand for 20% filling degree at 1, 3 and 6 rpm are as shown in Figure 4.48. It has been observed that slope of the curve increases with increase in the rotational speed.

#### 4.10.2 Evaluation of the wall to solid heat transfer coefficient

A series of experiments have been performed for various rotational speed and filling degree with 0.2 mm of Quartz sand and 0.8 mm of Copper pellets. Calculation of heat transfer coefficient has been done with overall heat balance based on the following considerations.

- Heat gained by the agitating solid bed is equal to the heat supplied to the wall.
- Enthalpy stored inside the wall can be neglected as the thickness of the kiln is 2 mm.

From the overall heat balance; equation 4.2 represent calculation of the heat transfer coefficient form the wall to the solid.

$$\alpha_{WS} \cdot A \cdot (T_W - T_{\text{meanbed}}) = M_S \cdot c_{p,S} \cdot \frac{dT_{\text{meanbed}}}{dt} \quad 4.2$$

Where

$M_S$  = Mass of solid bed (kg)

$c_{p,S}$  = Specific heat capacity (J/Kg K)

$T_W$  = Temperature of the wall (K)

$T_{\text{mean bed}}$  = Mean temperature of the solid bed (K)

$A$  = Area of the solid bed with wall (m<sup>2</sup>)

Heat transfer coefficient has been calculated at various filling degree and at various rotational speeds. It has been observed that heat transfer coefficient increases with increase in speed of rotations.

Experimental calculation of the heat transfer coefficient from wall to solid for 0.2 mm Quartz sand, 20 % filling degree at various speed of rotations has been plotted with respect to time as shown in figure 4.49. Heat transfer coefficient from wall to solid increases with increase in rotational speed. Heat transfer coefficient has been observed in the range of 600 W/m<sup>2</sup>K to 1700 W/m<sup>2</sup>K.

Similarly, heat transfer coefficient from the wall to solid for 0.8 mm copper pellets has been plotted with respect to time as shown in figure 4.50. It has been observed that copper pellets have high heat transfer coefficient. Heat transfer coefficient from wall to solid increases with increase in rotational speed. For high speed of rotation, high heat transfer coefficient has been observed from 900 W/m<sup>2</sup>K to 2400 W/m<sup>2</sup>K

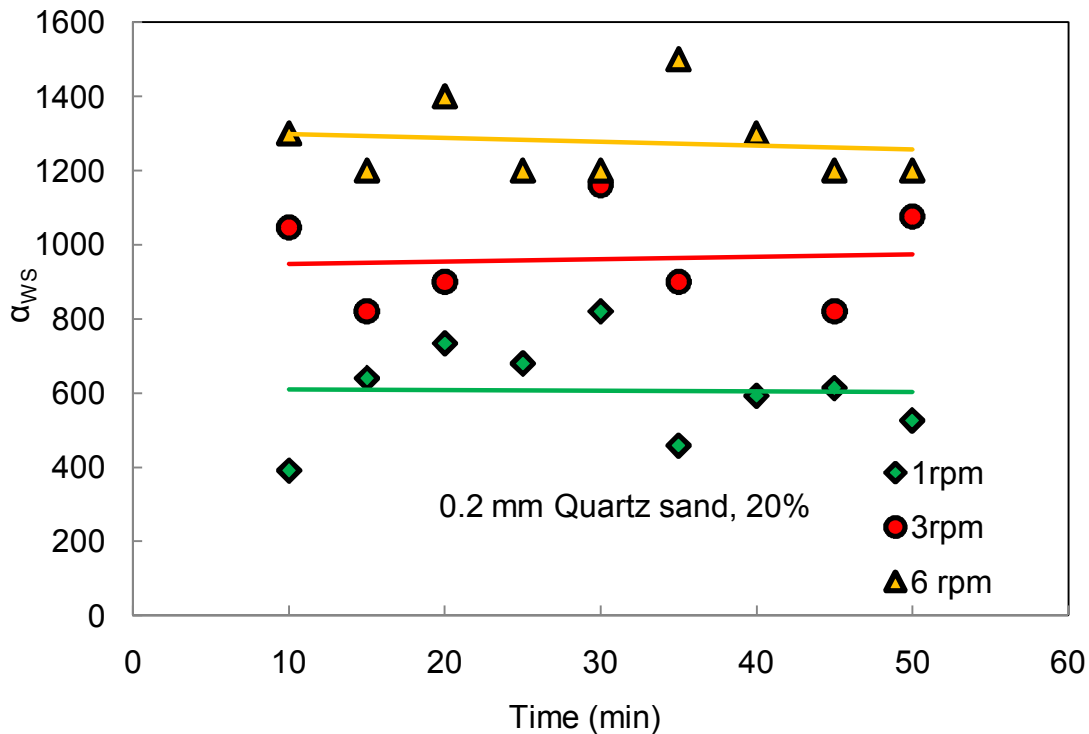


Figure 4.49 Heat transfer coefficient from wall to solid with respect to time at f 20% for Quartz sand

Present calculation of the heat transfer coefficient are based on the assumption as explained in sub section 4.11. For better evaluation of heat transfer coefficient, large amount of data should be evaluated from the experiments. Heat lost from the kiln should be measured perfectly. Also enthalpy stored in the wall should be considered. Heat transfer from the free bed surface should also take part in the overall heat transfer process.

Effect of filling degrees on heat transfer coefficient has been studied and plotted as shown in figure 4.51. A rotational speed of 3 rpm has been maintained throughout the experiment. Wide range of heat transfer coefficients have been observed.

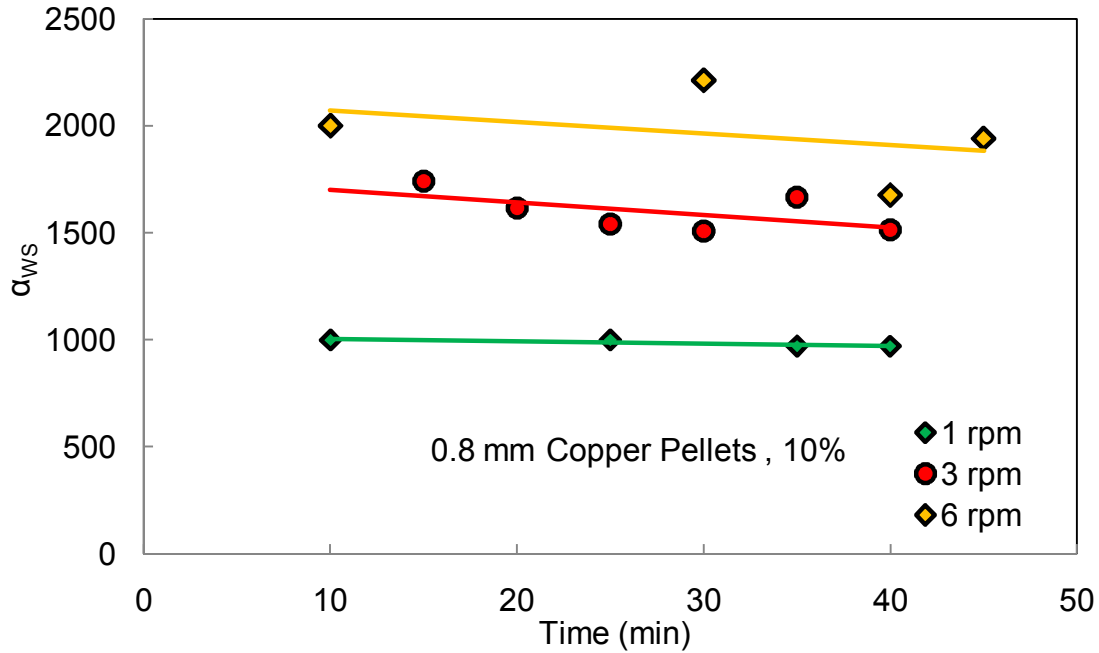


Figure 4.50 Heat transfer coefficient from wall to solid with respect to time at f 10 % for copper

In case of the higher filling degrees, contact time for the particles with the heated wall is also increases. Therefore high values of the heat transfer coefficient has been observed for 10% filling degree than 20% filling degree.

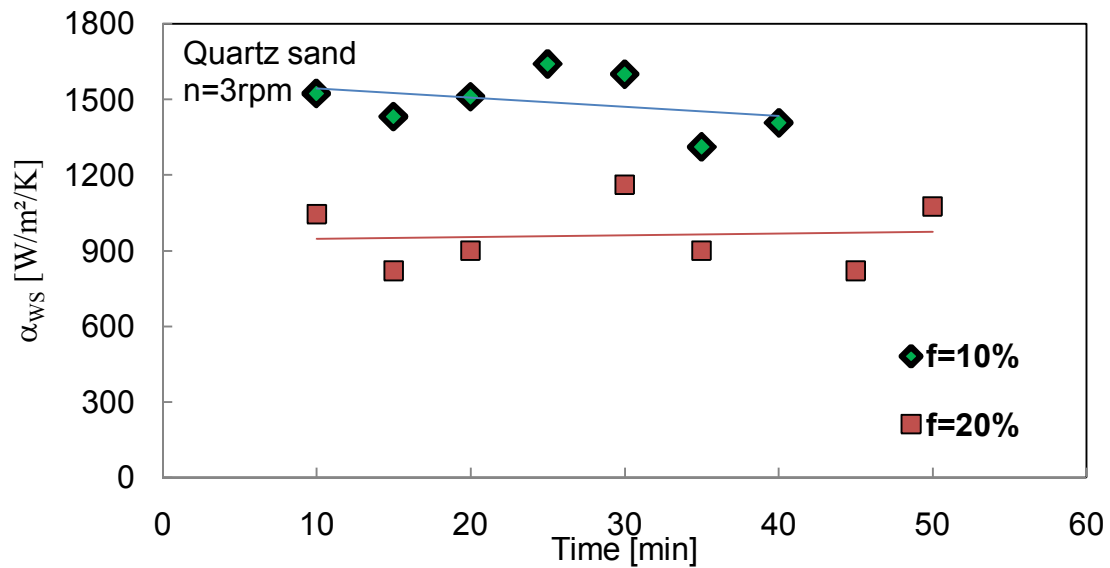


Figure 4.51 Effect of filling degree for heat transfer coefficient from wall to solid with respect to time Quartz sand

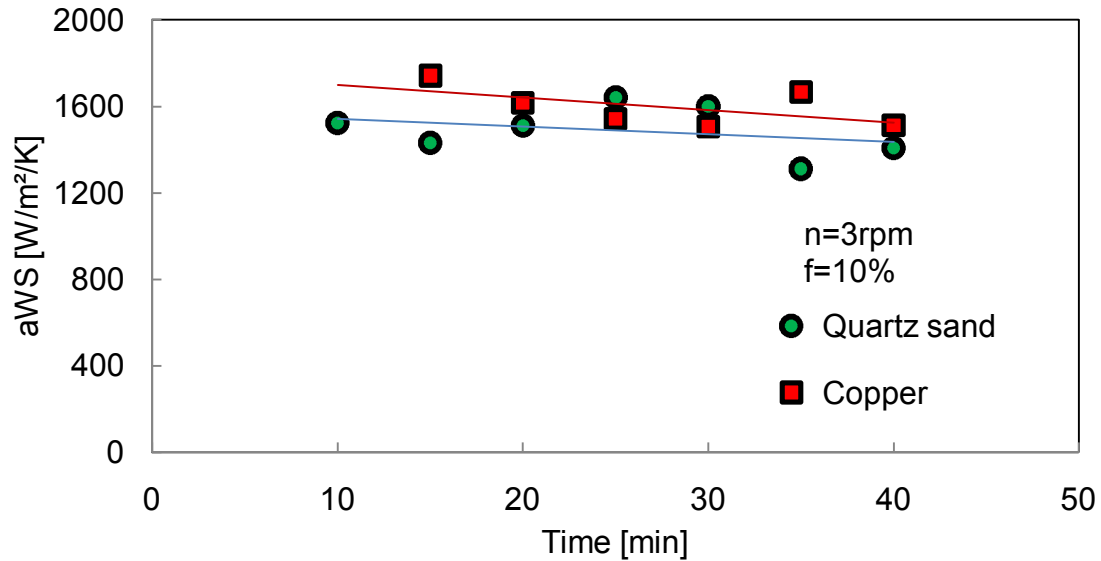


Figure 4.52 Effect of the types of materials on heat transfer coefficient

Effect of the types of materials on heat transfer coefficient have been studied and plotted as shown in figure 4.52. A rotational speed of 6 rpm has been maintained throughout the experiments. Copper pellets has bigger size with higher value of specific heat capacity than quartz sand, so higher value of heat transfer coefficients for copper have been observed. As explained in the review chapter, section 1.9, various authors [5, 6, 7, 8] have used different parameter in their analysis such as drum size, filling degree, rotational speed and also different material of various sizes. A comparison of various available model with the experimental results have been thoroughly carried out. Heat transfer coefficient of the wall to solid for 0.2 mm Quartz sand and for 0.8 mm Copper pellets at various rotational speeds of the kiln have been considered.

The experimental values of heat transfer coefficient for 0.2 mm Quartz sand and for 0.8 mm Copper are compare to the values obtained from the models provided by Tscheng [5], Li et. al. [6], Wes et. al [7] and Lehmborg [8]. It has been observed that the wall to solid heat transfer coefficient from experiments are higher than available models as shown in figure 4.53. This might be because of specific assumptions and calculation methods used in the models. As explained in the section 4.5, hot and cold regions have

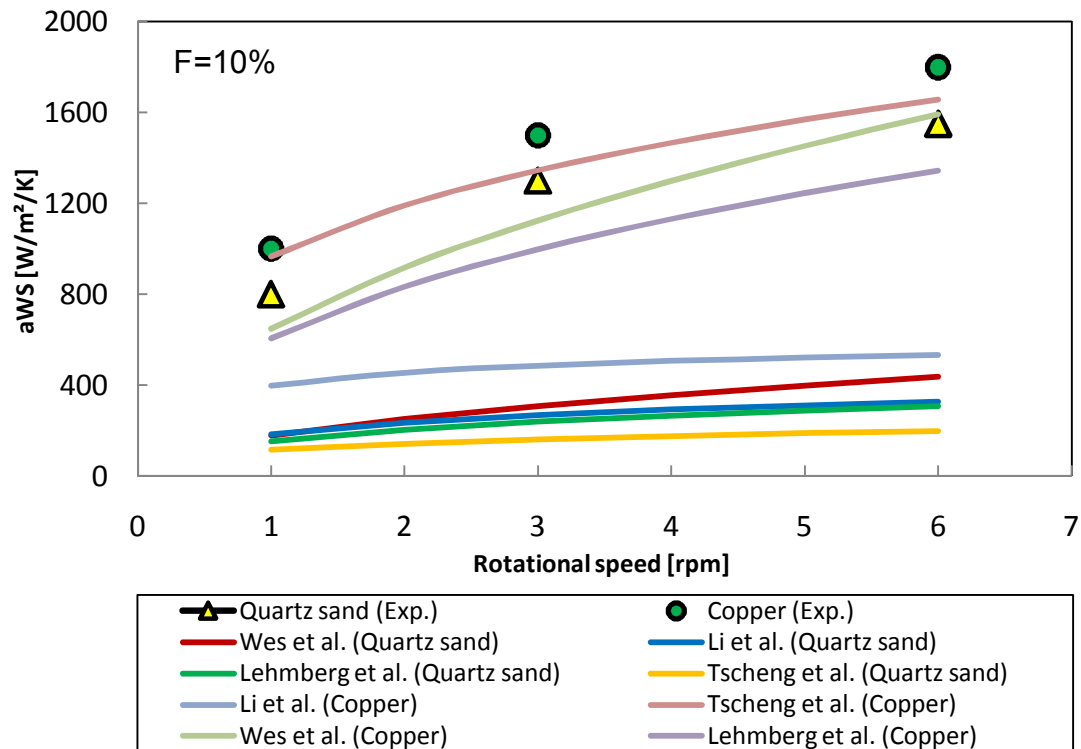


Figure 4.53 Comparison of the experimental and models heat transfer coefficient from wall to solid with number of rotations

been observed in the rotating bed of the solid. Mean temperature of the bed has also been consider for the wall to solid heat transfer coefficient calculations. This explains the need for a improved model for wall to solid heat transfer coefficient. So influence of the mixing should also be considered. Detailed study of the mixing of hot and cold layer for the various solid materials has been carried out and is discussed in Chapter 5.

## Conclusion

Detailed study of temperature distribution across the wall and inside the agitated bed of 0.2 mm Quartz sand and 0.8 mm Copper pellet have been carried out. K type thermoelements (Ni-Cr base) has been selected for temperature measurements as it gives quick response with low reaction time and good anti oxidation qualities. Temperature profiles at the wall and inside the agitated bed have been studied thoroughly. Temperature gradients have been observed high at start of the experiments and it reduces

further with time. Hot and cold regions have been observed. High temperature has been seen at the top region of the kiln perpendicular to the agitated solid bed. This is due to buoyancy of the hot gas inside the kiln.

A new method has been developed to evaluate mean temperature of the bed. Wide ranges of the heat transfer coefficient have been observed for various filling degree. Heat transfer coefficients from wall to solid are high at higher rotational speeds. In our study the heat transfer coefficient obtained from the experimental data for 0.2 mm quartz sand is and for 0.8 mm cylindrical copper pellets has been observed higher than that of the available literature models. Hence a new model has to be considered in future work.

## References

1. N.A. Burley, R.L. Powel, G.W. Burns and M.G. Scroger. Monograph 161, NBS, Washington, DC 20234, 1978.
2. American Society for Testing and Materials, Annual Book of ASTM Standards 1987, Philadelphia, 1907, pp. 242.
3. T.G. Kollie, J.L. Horton, K.R. Carr, M.B. Herskovitz and C.A. Mossman. Temperature measurement errors with type K (Chromel vs Alumel) thermocouples due to short-range ordering in Chromel, Rev. Sci. Instrum. 46 (11) (1975) 1447-1461.1
4. A. Queck, "Untersuchung des gas und wandseitigen wärmetransportes in die Schüttung von Drehrohröfen" PhD thesis , Otto von Guericke Universtiy Magdeburg Germany 2002
5. Tscheng, S.H., and Watkinson, A.P., Convective heat transfer in Rotary Kilns, Can. J. Chem. Chem.Eng, 57, pp. 433-443
6. Li,K.W., and Friday, J.R., Simulation of Coke calciners, Carbons,12,pp.225-231, 1974.
7. Wes, G.W.J., Drinkenburg, A.A. H., and Stemerding, S., Heat transfer in a horizontal Rotary drum reactor, Powder Technology, 13, pp.185-192, 1976
8. Lehmborg, J., Untersuchung zum Wärmeübergang Zwischen der Wand und der Feststoffschicht eines Drehrohrofens, PhD THesis, TU Hannover, Germany, 1975

## Chapter 5

# Mixing Experiments for the Heat of Granular Material in the Agitated Bed of Rotary Kiln

---

### 5.1 Mixing in rotary kiln

The solid shows various forms of motion behaviour during the transport along the axis of a rotary kiln i.e. slipping, cascading and cataracting motion [1, 2, 3]. The transient behaviour between the different motion types were researched by [4, 5] and [6, 7]. Slipping motion is a result of slow rotational speeds and low friction between wall and solid bed. Slipping motion gives no particle mixing in the solid bed hence it is avoided in industrial application. High rotational speeds and high centrifugal force shows a cataracting motion. Therefore the motion of solid bed is discontinuous and partially particles flow into the freeboard which results in an inhomogeneous mixing which is avoided in the industries. The desired bed motion in rotary kilns is the cascading, more precisely the rolling motion. Here the mixing of the particles in the solid bed is efficient

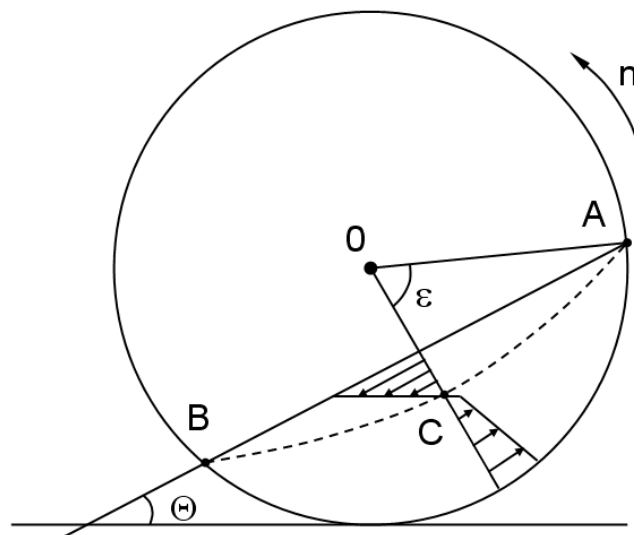


Figure 5.1 Rolling bed motion in a drum

because of the continuous circulation of the bed particles. In the chapter 1, figure 1.4 shows various motions of the solid bed in the cross sectional plane inside the rotary kiln.

Figure 5.1 indicates the rolling bed motion in the cross-section area of a drum. The free solid bed surface is inclined by a typical angle called the dynamic angle of repose ( $\Theta$ ). This slope is characteristic for every solid material and depends only on the particle size, solid density and wall friction. A rolling bed can be divided into two zones. At first the passive or static zone where the particles below the bed are transported in radial direction as a rigid body with the rotation speed of the wall from point B to A. No particle mixing occurs in this zone. After reaching the upper point A the particles flow downwards on the free bed surface in a thin layer – the active or cascading layer – with relatively higher velocities from point A to B. This is the particle mixing zone where the particles offer radial and axial velocity components. The boundary line (dotted line) between the mixing zone and the stagnant zone is approximately symmetric over the vortex point C. For industrial application the mixing of the solid bed is an important fact. Due to a good mixing the product gets homogeneous and the quality rises up. Therefore the following theoretical and experimental determination has been considered.

In the previous work, the mixing behaviour was described by the mixing condition on the drum wall [8]. This was realised with observing different coloured fractions of particles through a transparent wall. Woodle [8] determined the influence of the particle shape and wall friction on the mixing behaviour using drums with a smooth wall which leads to the slipping motion and a rough wall which results in the rolling motion. The mixing time by the rolling motion was ten times higher than the slipping motion. Based on this, an empirical way to estimate the mixing time was developed whereas the frictional coefficients (particle-particle; wall-particle) correlate with the mixing time. He finds out that the particle shape has an essential influence on the mixing time. A same particle shape and particle size for the different mixing components are assumed. During the mixing procedure two or more components are mixed together. In most cases it could be reduced to a two-component-mixture with the relevant component A (e.g. Tracer) and the rest of the solid bed as the component B [9]. The local concentration of the component A

$(X_{i,A})$  has to be measured in the bed. The variance of the measured values describes the goodness of mixture.

$$s^2 = \frac{1}{n} \cdot \sum_{i=1}^n (X_{i,A} - \bar{X}_A)^2 \quad 5.1$$

where  $n$  is the number of sample  $X_{i,A}$  and the concentration  $\bar{X}_A$  is the probability to find tracer particles in an perfect mixture [10]. Equation 5.1 shows the empirical variance which only estimates the unknown real goodness of the mixture; the theoretical variance. Generally a mixing process starts with the complete segregated components. Therefore the starting variance can be appointed as [10],

$$\sigma_0^2 = \bar{X}_A \cdot (1 - \bar{X}_A) \quad 5.2$$

The highest variance of the random mixture by a particle number  $N$  which consists of the whole particles of component A and B is as [11],

$$\sigma_z^2 = \frac{\bar{X}_A \cdot (1 - \bar{X}_A)}{N} \quad 5.3$$

Boss [10] gives a two-dimensional mixing model as shown in figure 5.2: (a) shows the structure of complete segregated components before mixing ( $\sigma_0 = 0.4714$ ); (b) is the random mixture by a random sample of 10 particles per component ( $\sigma_z = 0.1491$ ); (c) shows the perfect mixing of both components ( $\sigma = 0$ ).

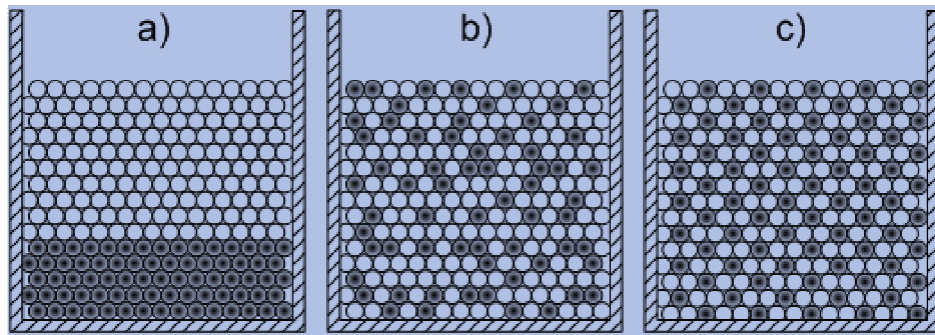


Figure 5.2 Two-dimensional mixing model

Probably to find the tracer particles in an perfect mixture is as shown in equation 5.4

$$\bar{X}_A = 0.33 \quad 5.4$$

In previous research, all authors gave the empirical variance as a representative parameter for the goodness of mixture. For example the model of Yano & Sano which is described by Boss [10] is used in present work:

$$M = 1 - \frac{\sigma^2}{\sigma_0^2} \quad 5.5$$

The deviation of the sample size and the number of samples has to be known in comparison between the different definitions. The goodness of mixture have been described by the model of Yano & Sano. Therefore a value of  $M = 0$  defines complete segregated components as an initial condition. With proceeding mixing the value increased till a range between  $0 \leq M < 1$ . The maximum value of  $M = 1$  stands for perfect mixing (ideal) which cannot be realized because a real mixing process is every time a random mixing.

## 5.2 Model for describing the mixing process

Weydanz [12] developed a model to describe the mixing kinetics with the two-term-equation as follows:

$$s^2(t) = s_0^2 \cdot e^{(-2 \cdot A \cdot t)} + s_\infty^2 \cdot (1 - e^{(-2 \cdot A \cdot B \cdot t)}) \quad 5.6$$

The term at first position shows the time dependence of mixing procedure whereas the second term is characteristic for the segregation effects in the bed. Due to a complete demixing of particles the starting variance  $s_0^2$  is the same like  $\sigma_0^2$ . Parameter A depends on the rotational speed of the drum and the drum construction, therefore it is a process parameter. With superposed segregation effects ( $t \rightarrow \infty$ ) the variance  $s_\infty^2$  follows. The parameter B illustrates the time progression of segregation and shows if segregation effects happened in the mixing zone. Based on Eq. (5.6) Schubert [13] eliminates the disadvantages from Weydanz and proposes Eq. (5.7):

$$s^2(t) = (\sigma_0^2 - \sigma_z^2) \cdot e^{(-2 \cdot A \cdot t)} + \sigma_{\text{sys}, \infty}^2 \cdot (1 - e^{(-2 \cdot A \cdot B \cdot t)}) + \sigma_z^2 \quad 5.7$$

Equation (5.5) shows the correct mixing behaviour with superposed segregation effects and without segregation in the mixing zone. Furthermore the dependence of the sample

size is considered by the parameter  $\sigma_z^2$ . Gonzalez [14] performed experiments with two colours of sand. From his experiments he determined number of rotations of the drum need for the perfect mixing of the material. Hence aim of the present work is to connect the heat transfer mechanism which relates with mixing of solids have to carried out and to determined exact mixing time for perfect mixing.

## 5.3 Experimental setup

### 5.3.1 Cold mixing experiments

The mixing behaviour was determined by Gonzalez [14] in two batch drums with the construction parameters as shown in figure 5.3 a, b :

- Batch drum 1: D = 400 mm, L = 400 mm
- Batch drum 2: D = 400 mm, L = 160 mm

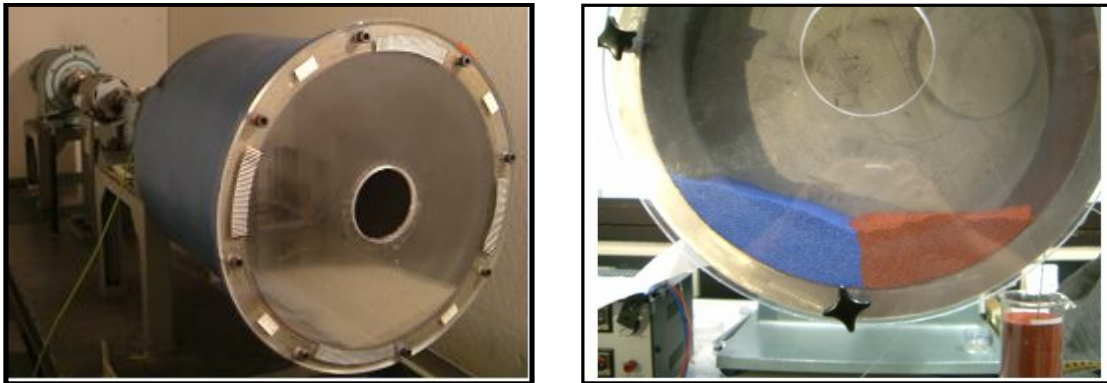


Figure 5.3 Batch drum 1 (a) and batch drum 2 (b) to determine the mixing behaviour

The drums consist of a transparent front side and are driven by an adjustable gear motor. For experimental measurements the rotational speeds are in a range from  $n = 2$  rpm to  $n = 10$  rpm. According to these rotational speeds the rolling motion could be realized for every single measurement.

The employed material is Quartz sand with the specific parameters: (i) bulk density  $\rho_0 = 1500 \text{ kg/m}^3$ , (ii) particle diameter  $d_p = 0.80 \dots 1.00 \text{ mm}$  and (iii) mean particle diameter  $\bar{d}_p = 0.90 \text{ mm}$ .

To measure the mixing behaviour the material was divided into two fractions by colouring the sand into red colour and blue colour as presented in figure 5.3 (b). Consequently the particle size for both fractions was the same. The filling degree of a drum is a function of the geometry of particle and drum construction. In cross section it is defined by the ratio of solid area to the whole drum area  $f = A_s/A_d$  alternatively by the volume ratio  $f = V_s/V_d$ . During the measurements; filling degrees of  $f = 5\%$ ;  $10\%$ ;  $20\%$ ;  $30\%$  were realized in the drums.

A fibre-optic system at which visible white light works as the radiation source was used to determine the deviation of the components after a mixing process. So called dive reflection samplers with small shapes were used because of reducing the influence on the formation of the inner solid bed. On the rod-shaped sensor a drum lens with a visual field of 2 mm diameter was installed. The schematic of measurement system is presented in figure 5.4.

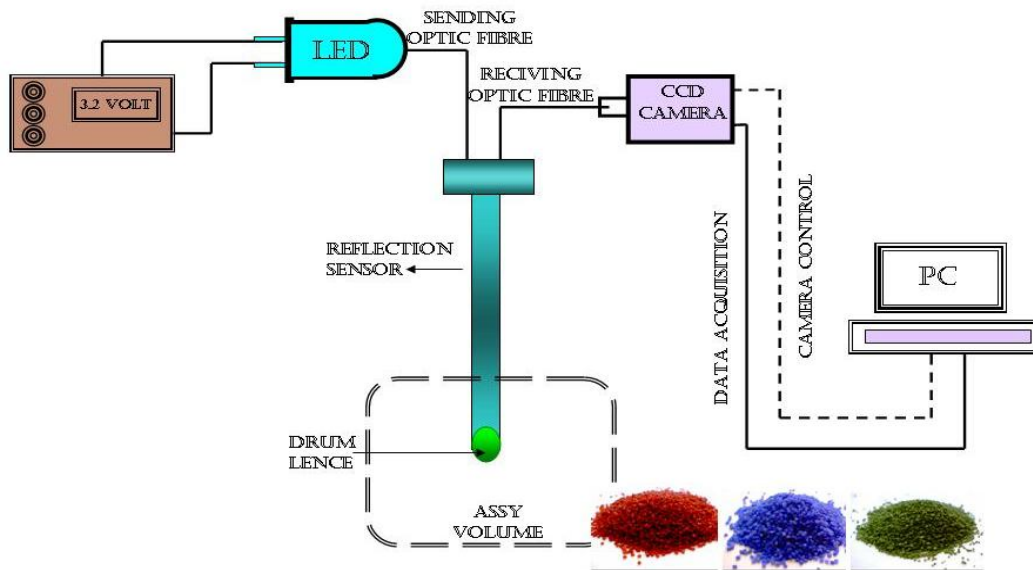


Figure 5.4 Schematic of measuring system with the CCD-camera [14]

By dipping the dive reflection samplers in the bed an assay volume of the bulk is illuminated due to the optic sending fibre (LED). Afterwards the reflected light is conducted via a second fibre – the receiving fibre – to the CCD-Sensor of a line scan camera and the end face of the fibre is recorded. A three line scan CCD-camera “L301bc” from the company Basler Vision Technologies is used whereby the three signals blue (380-530 nm), green (500-620 nm) and red (600-780 nm) are detected. Subsequently the signals were sent to the program XCAP™ Version 2.2 from EPIX Inc. per an adequate frame grabber. The signals were collected to picture data and analysed by the program Image Pro Plus™. The measuring system is explained in detail by Gonzalez [14]

Here the time dependence of the empirical variance is plotted for the filling degrees  $f = 10\%$ ;  $20\%$ ;  $30\%$ . All curves start with a rapid decrease during the first rotations and show a tendency of a constant variance. By reaching this constant value the mixing time and therefore the necessary number of rotations are given. The experimental results for the constant rotational speed  $n = 3$  rpm are listed in table. 5.1.

<b>Filling degree % (n = 3 rpm)</b>	<b>Number of rotations</b>
5	< 1
10	5
20	8
30	12

Table 5.1 Number of rotations for mixing process (cold) [14]

## **5.4 Experimental determination of the mixing in Rotary kiln**

### **5.4.1 Experimental setup for mixing of the hot and cold sand**

Figure 5.5 indicates schematic arrangement of the fixed and the rotating thermoelements in hot and cold bed of solid before mixing. Hot layer of sand has been kept close to the

wall and other same volume of the cold layer of sand is placed on it far from the wall. At this point we start rotary drum with adjusted rotational speed.

Aim of the experiments is to measure the number of rotation required to obtain uniform temperature in the solid bed. Mixing of the solid define heat transfer in the moving bed. Rolling motion is an ideal motion for the heat transfer in an industrial rotary kilns. Experiments were carried out at various rotational speeds from 1, 3 and 6 rpm and filling

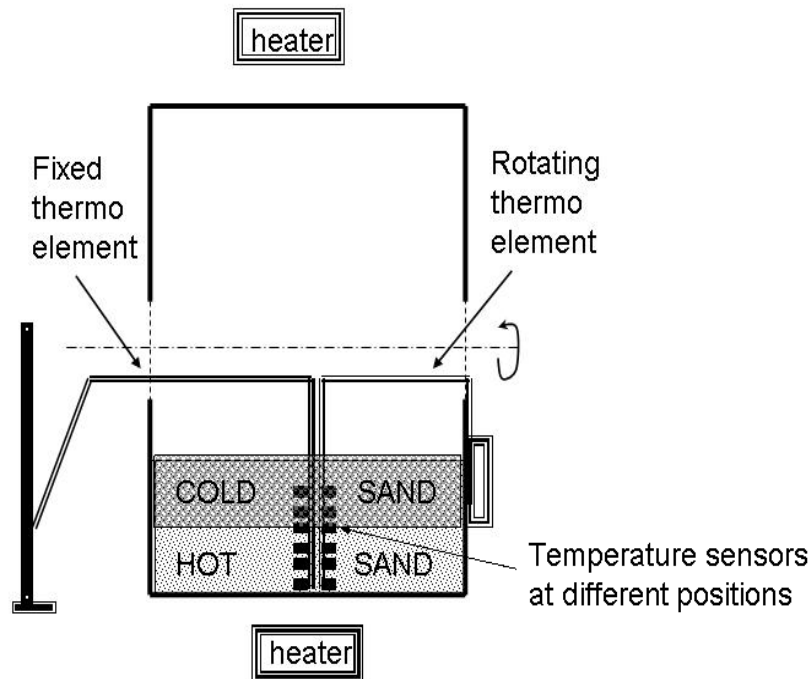


Figure 5.5 Arrangement of fixed and rotating thermoelements in hot and cold bed before mixing

degrees of 10%, 15% and 20%. Quartz sand 0.2 mm haven been heated in rotary kiln at certain temperature, care must be taken that uniform temperature of the sand in the solid bed has been obtained. A second layer of the cold sand at room temperature have been placed slowly on the hot sand layer. By adjusting the specific speed of rotation, temperature distributions inside the solid have been measured. Results of the experiments have been studied thoroughly.

Figure 5.6 represent principle temperature profile for the numbers of rotation for uniform mixing zone for two different temperature layers of sand in rotary kiln. The hot sand loosing heat to the cold sand in contact with it. After certain rotations, a uniform temperature has been obtained. It means that a layer of hot and cold layer sand mixed uniformly.

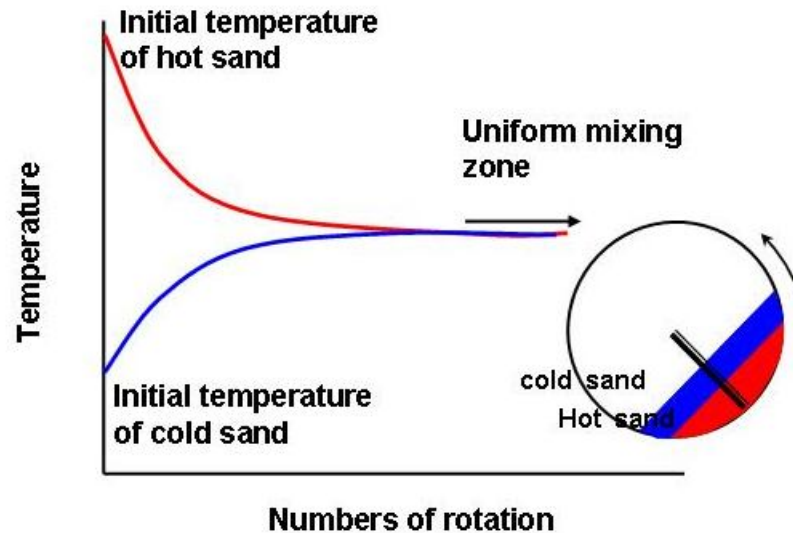


Figure 5.6 Principle temperature profile for the mixing for cold and hot sand experiments.

Experiments have been performed with various filling degree and various rotational speed. Figure 5.7 indicates experimental details and result for the time needed for two layers of the solid beds to achieve an uniform temperature. An experiment with 10% of filling degree of Quartz sand was carried out in which, a hot layer of sand of filling degree 5% at temperature of  $103^{\circ}\text{C}$ , in contact with second layer with filling degree 5% of the sand at room temperature at  $21^{\circ}\text{C}$  inside the rotary kiln. Both hot and cold layer of the sand acquire in total 10% of the filling degree.

By adjusting rotational speed at 6 rpm, fixed temperature measurement sensors were used to measure temperature at the center of the bed at angle of  $45^{\circ}$ . The curves of cold and hot sand have been observed to meet each other at certain time intervals which indicates

that temperature inside the bed is uniformly distributed and almost no temperature gradients exist inside the moving solid bed.

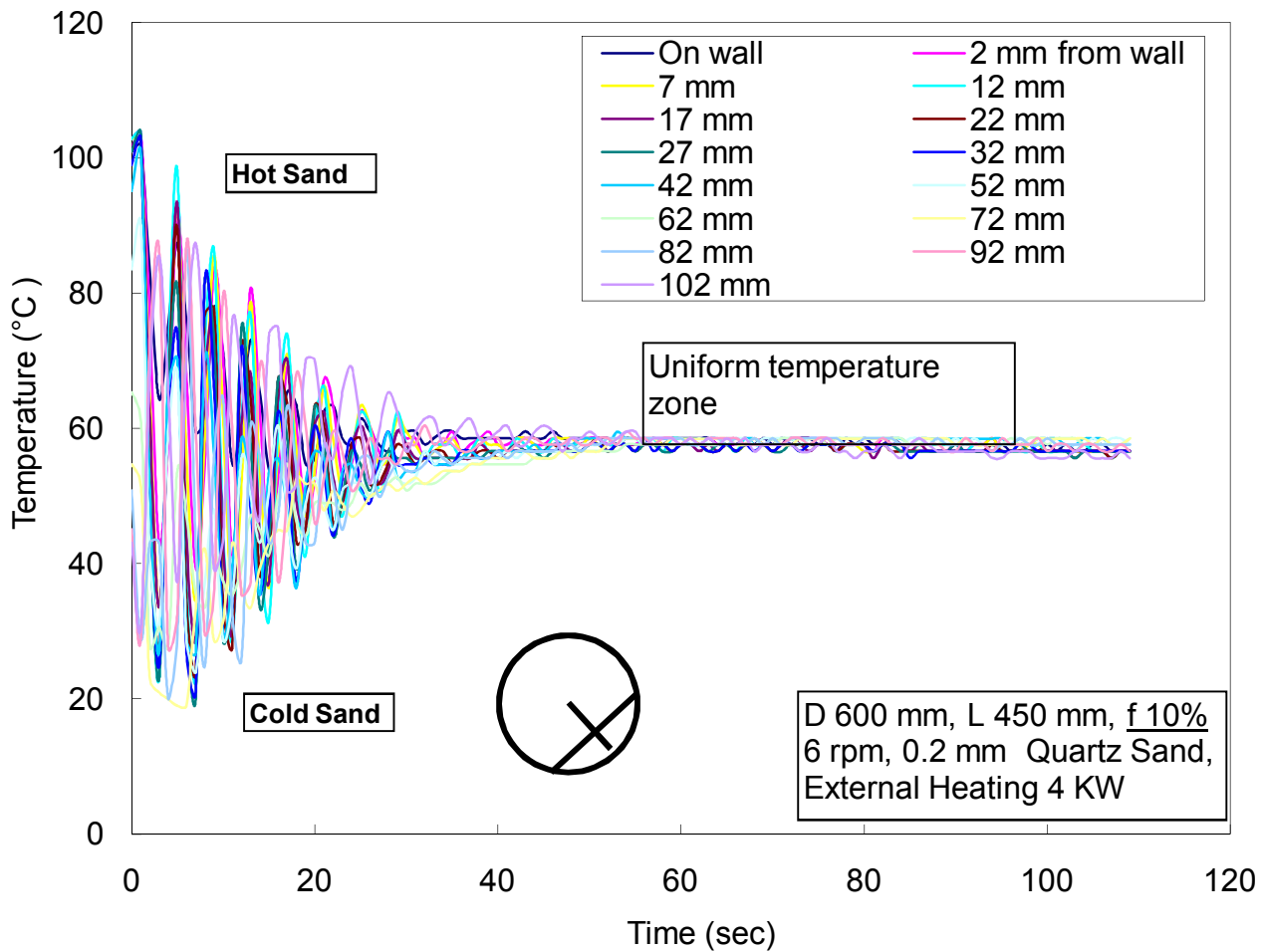


Figure 5.7 Temperature Vs Time for 6 rpm and 10% filling degree.

A series of experiments have been performed at rotational speed of 1, 3, 6 rpm and with different filling degree from 10%, 15% and 20%. The Table 5.2 indicates that for the

Rotational speed (rpm)	Number of rotations		
	f: 10%	f: 15%	f: 20%
1	4	5	6
3	5	6	8
6	7	8	11

Table 5.2 Number of rotations for various filling degrees

filling degree of 10%, 15% and 20% and at various speed of rotation from 1 rpm to 6 rpm have been taken into consideration. Table 5.3 indicates the time in seconds required for the uniform mixing of cold and hot layer of sand at various filling degree and various speed of rotations.

Rotational speed (rpm)	Time in Seconds		
	f: 10%	f: 15%	f: 20%
1	250	300	350
3	100	115	160
6	65	75	105

Table 5.3 Time in second for various rotational speeds and with filling degrees

Nature of the graph for these experiments are as shown bellow from figure 5.8 to 5.15

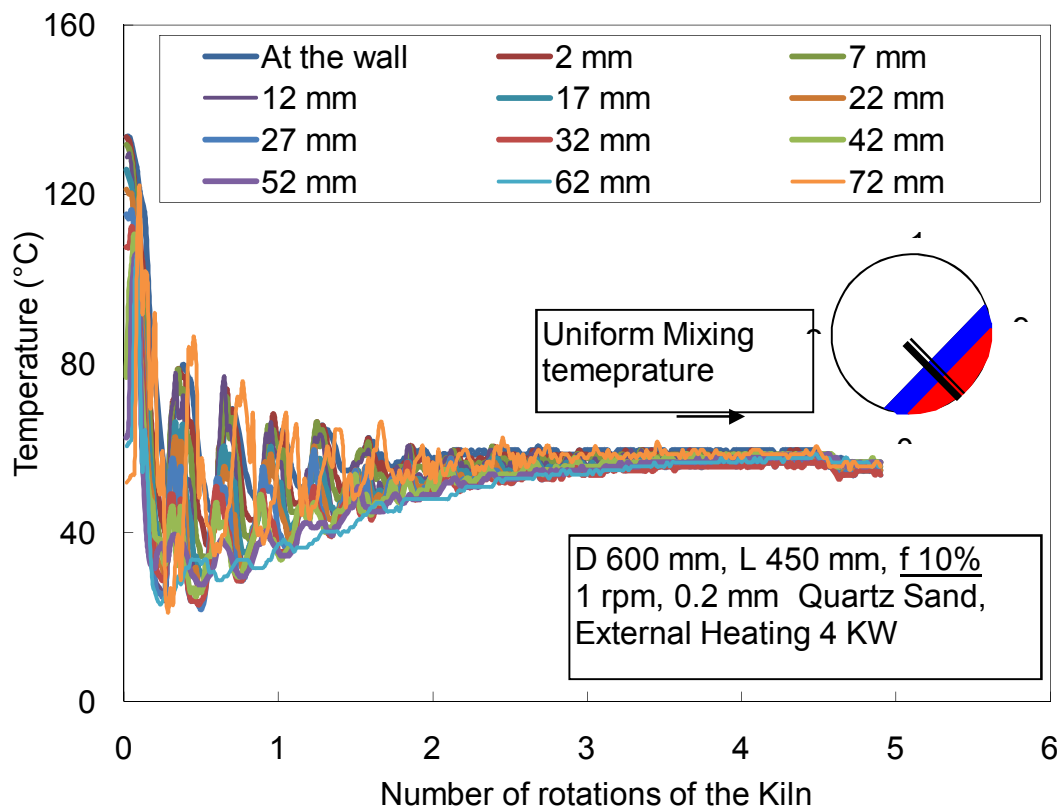


Figure 5.8 Temperature inside the bed with numbers of rotations for 1rpm and 10% filling degree.

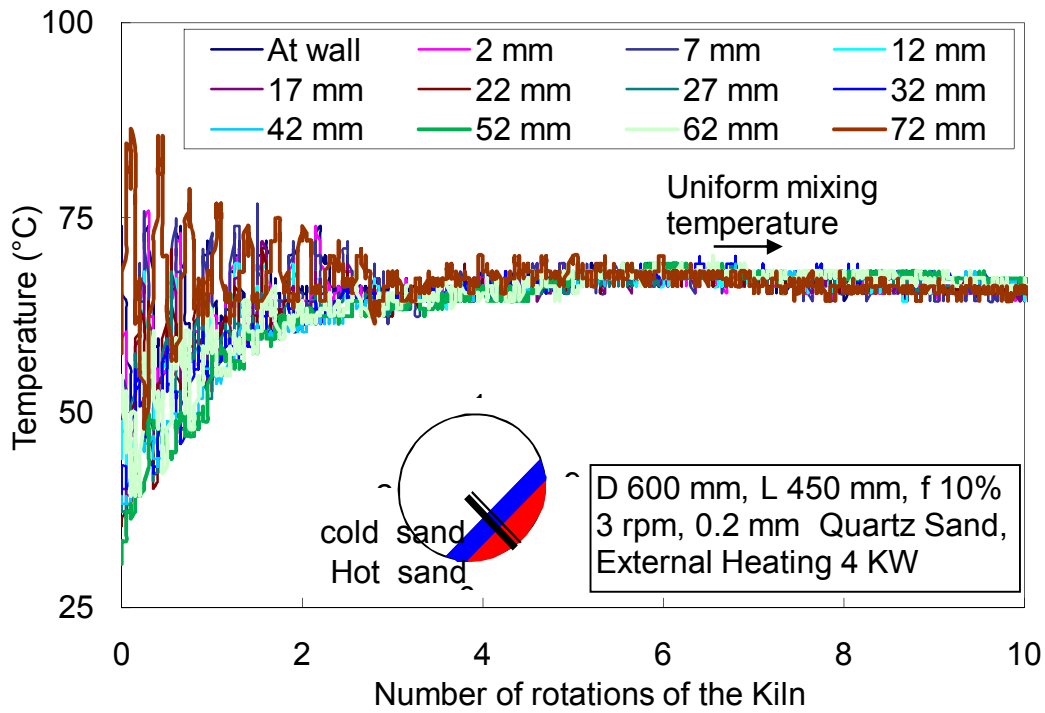


Figure 5.9 Temperature inside the bed with numbers of rotations for 3 rpm and 10% filling degree

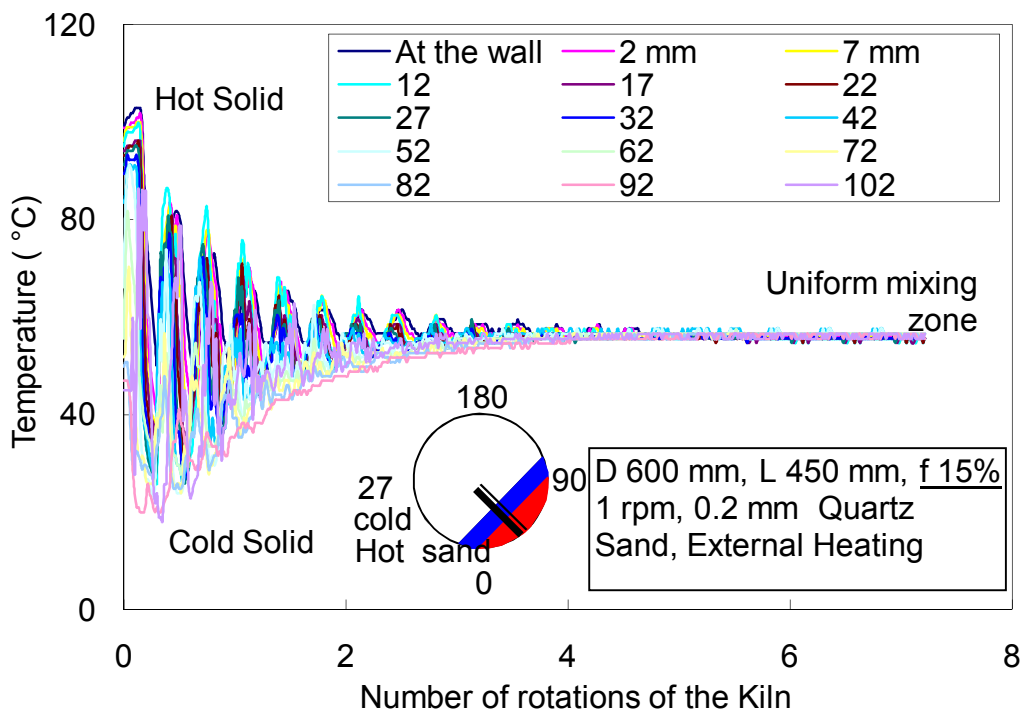


Figure 5.10 Temperature inside the bed with numbers of rotations for 1 rpm and 15% filling degree.

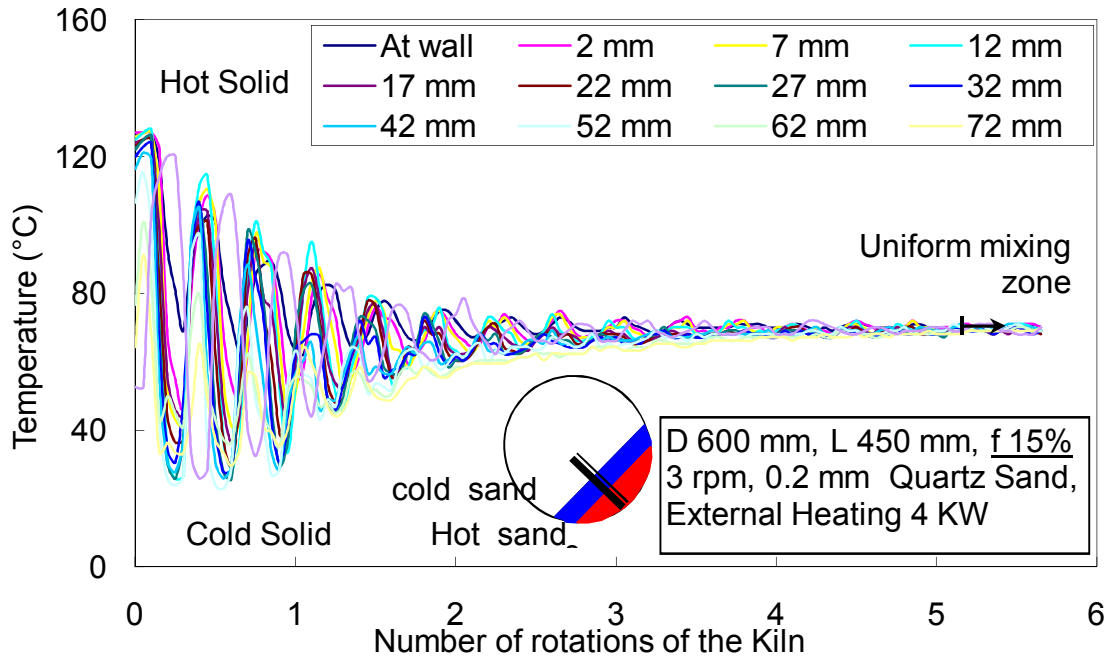


Figure 5.11 Temperature inside the bed with numbers of rotation for 3 rpm and 15% filling degree.

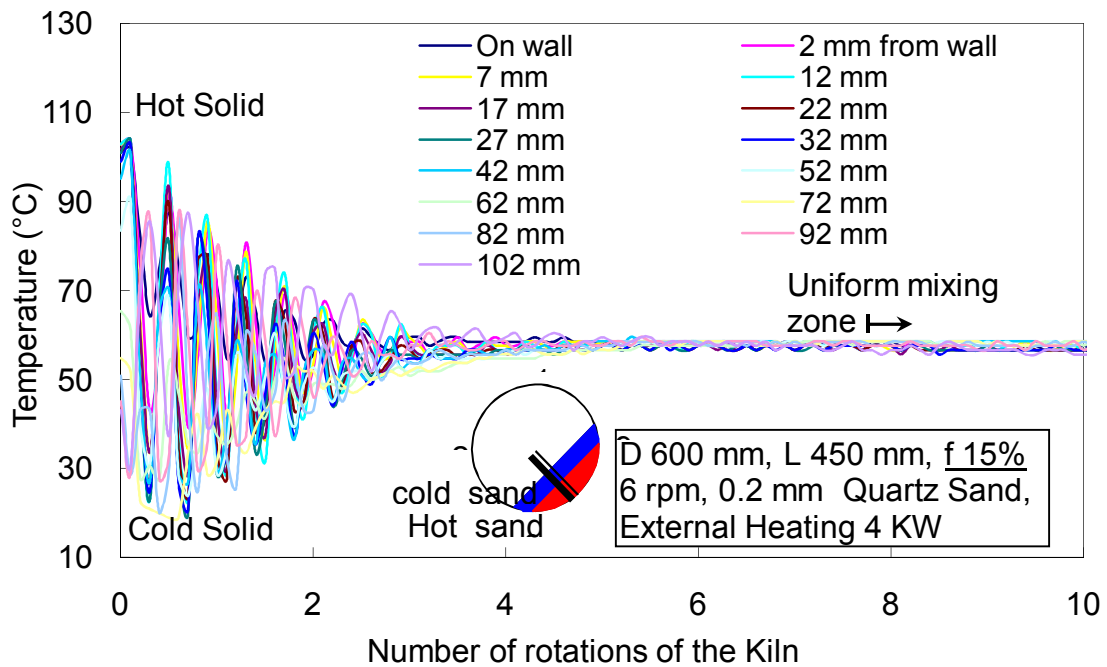


Figure 5.12 Temperature inside the bed with numbers of rotation for 6 rpm and 15% filling degree

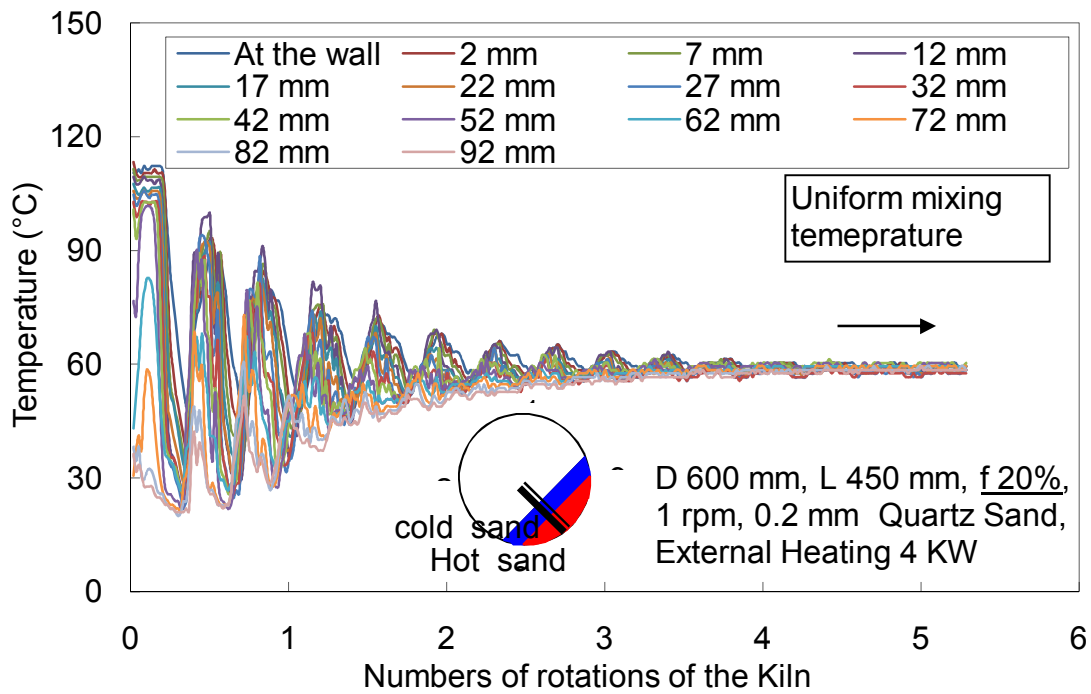


Figure 5.13 Temperature inside the bed with numbers of rotations for 1 rpm and 20% filling degree.

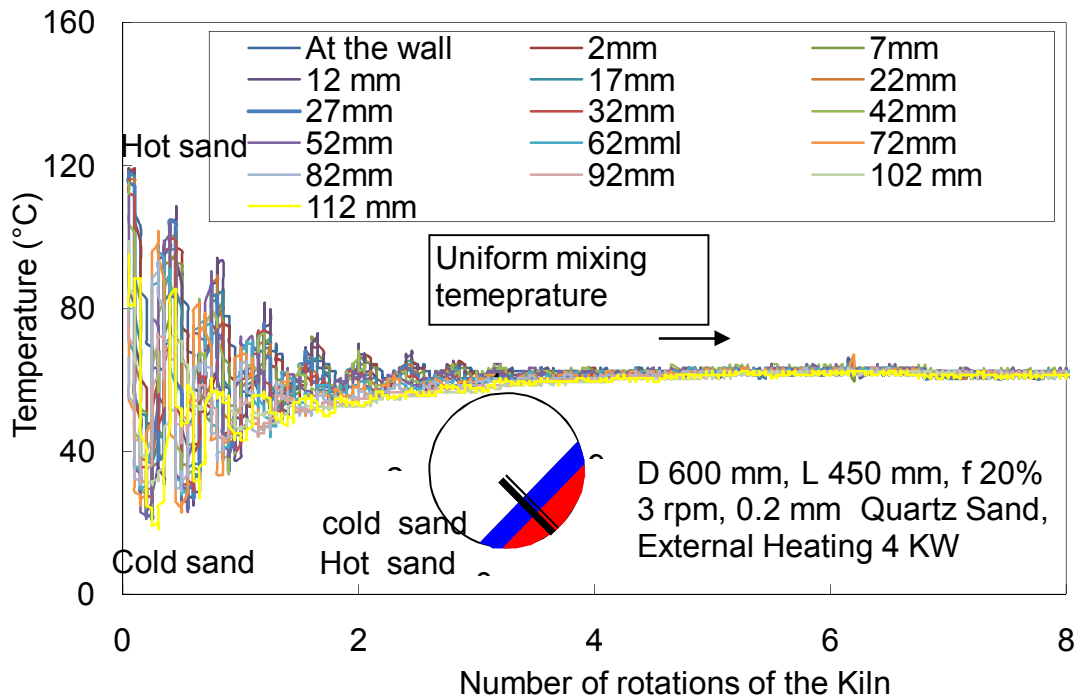


Figure 5.14 Temperature inside the bed with numbers of rotation for 3 rpm and 20% filling degree.

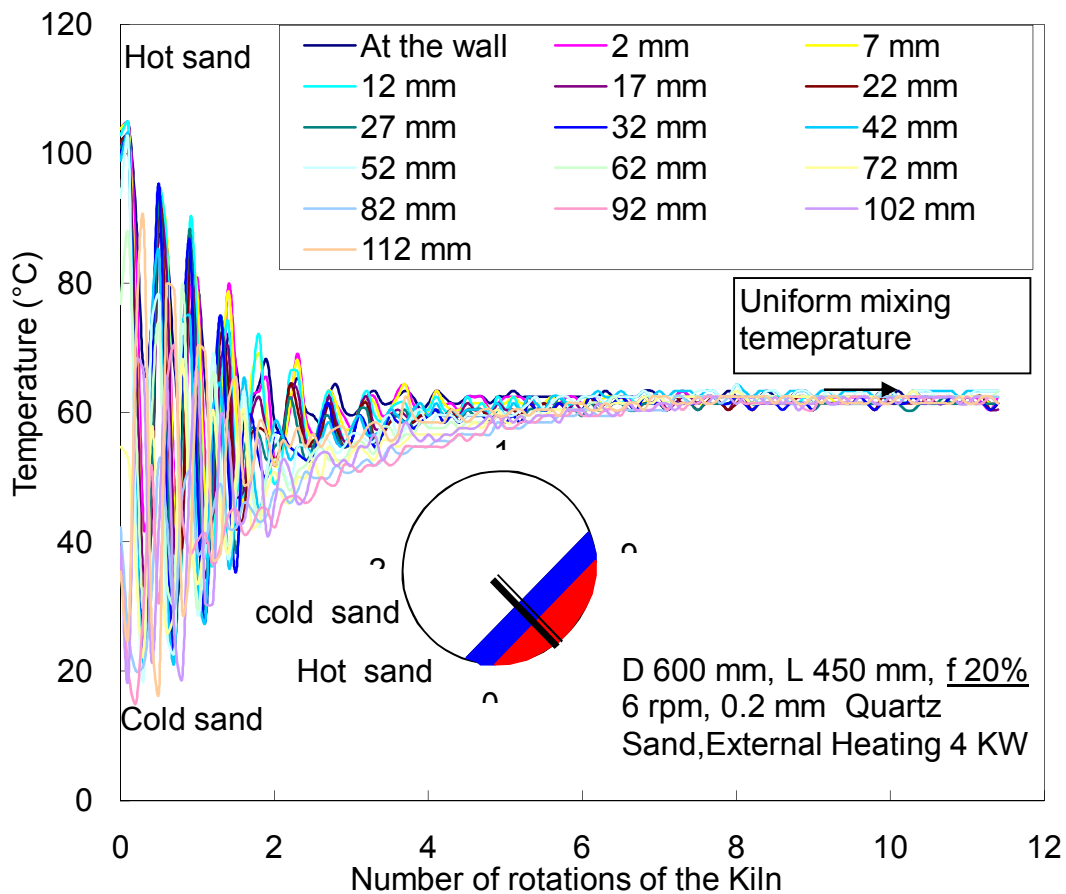


Figure 5.15 Temperature inside the bed with numbers of rotation for 6 rpm and 20% filling degree

A dimensionless temperature has been formed with maximum and minimum temperature of the layer of sand. Dimensionless temperature has been maintained between the range from 0 to 1. Number of rotations needed for the hot and cold layer of the sand with 10%,15% and 20% filling degrees and the rotational speed has been adjusted about 1 rpm, 3 rpm and 6 rpm. These results have already been mentioned in table 5.2

The purpose of diagrams from figures 5.17 to 5.19 are to indicate perfection of the measurement of the exact number of rotations. From the calculations it is observed that when these two curve of hot and cold layer of the sand touch each other, at that point perfection of the mixing of the hot and cold layer of the sand has been observed.

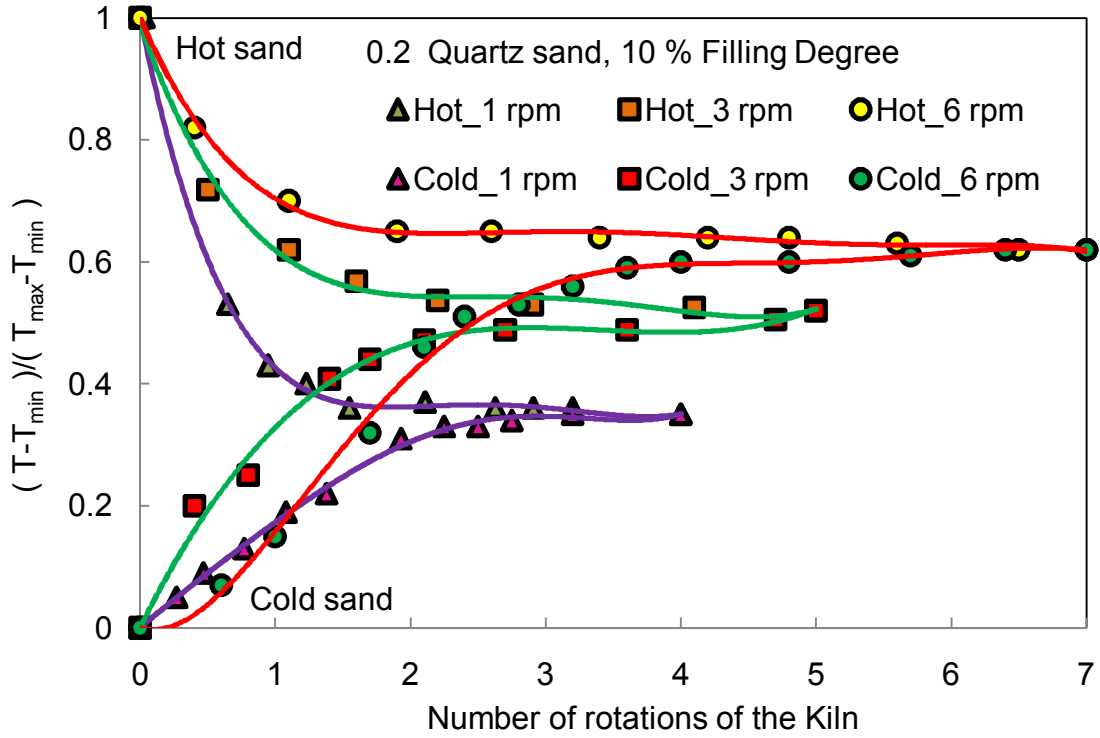


Figure 5.16 Temperature inside the bed with numbers of rotation for 10% filling degree

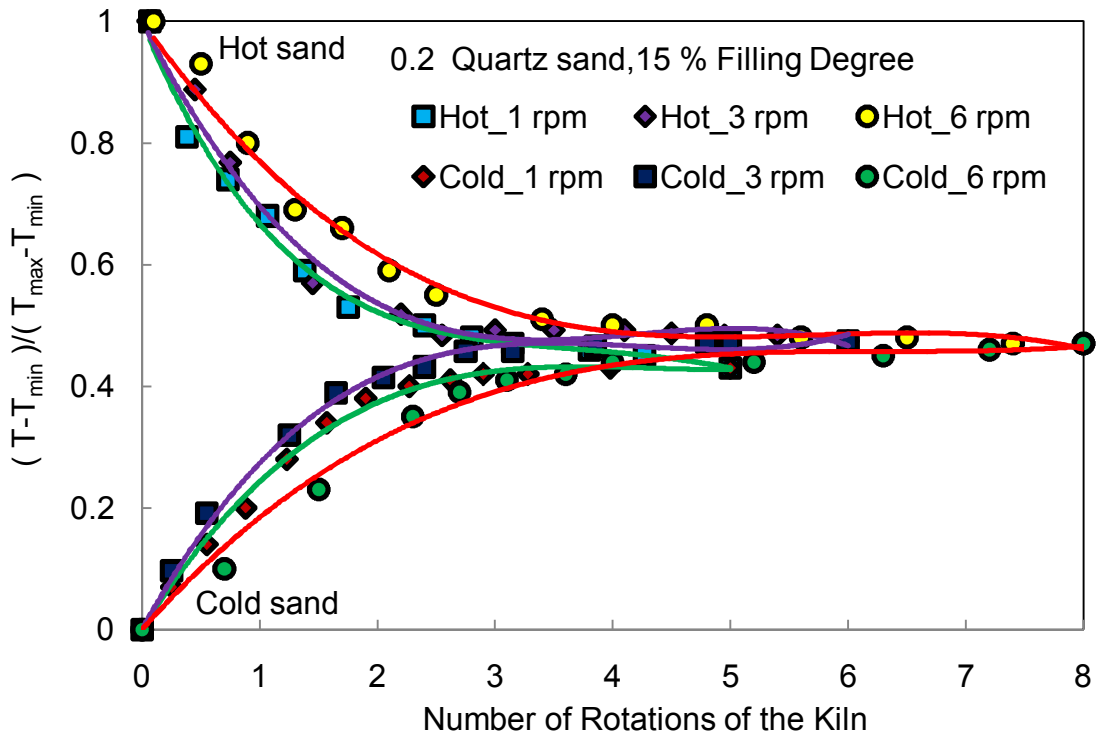


Figure 5.17 Temperature inside the bed with numbers of rotation for 15% filling degree

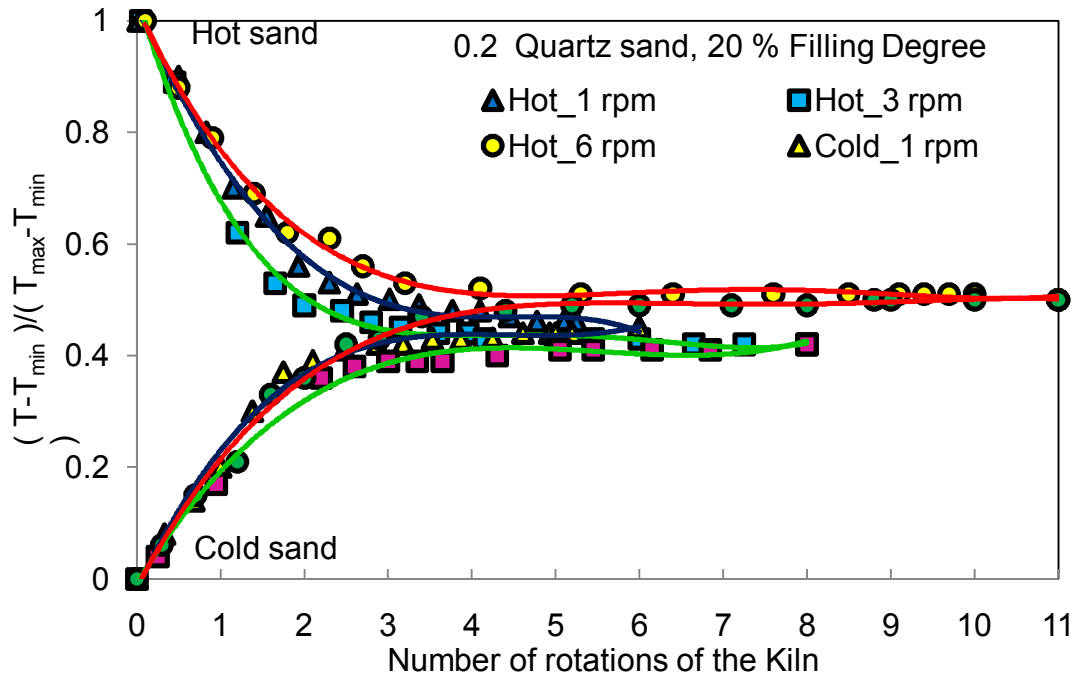


Figure 5.18 Temperature inside the bed with numbers of rotation for 20% filling degree

Figure 5.19 indicates the effect of rotational speed on the mixing time with various filling degrees. As filling degree of the sand increases, the time required for the perfect mixing is also increases. For 1 rpm

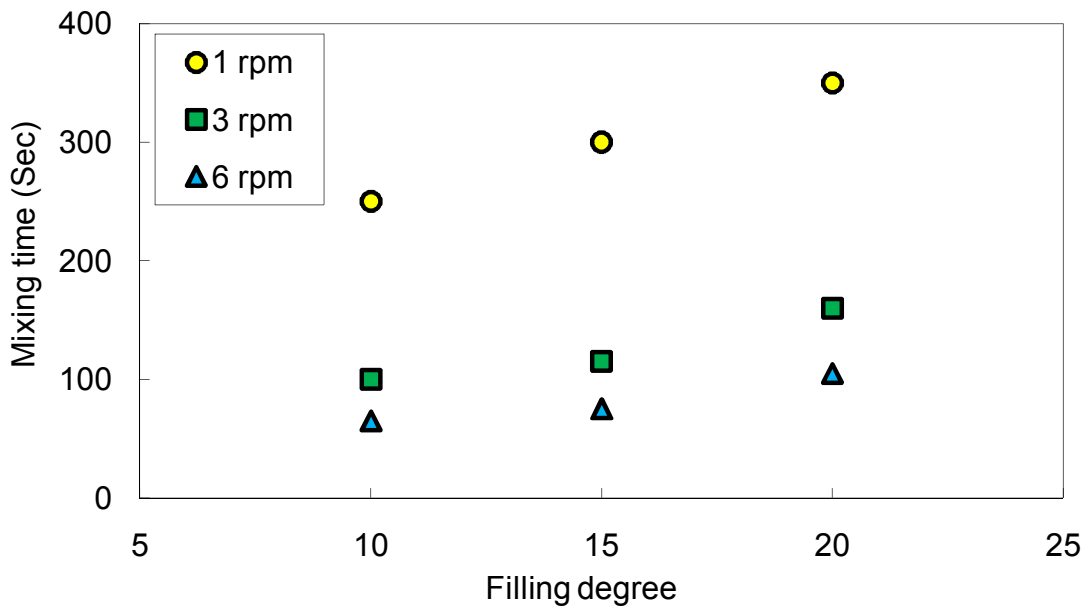


Figure 5.19 Effect of filling degree on mixing time

speed, at 10 % filling degree it take around 250 sec means 4 rotations to get perfect mixing. Table 5.3 indicates the mixing time for different rotational speed at various filling degree. With higher rotation speed mixing time has been reduced.

Motion of the bed plays an important role in the mixing of the particle together. This is a regular application in the chemical, powder processing industries. At higher filling degree up to 20%, for various speed of rotations from 1 rpm to 6 rpm, the results for number of rotations of the kiln with respect to the filling degree at various rotational speed as shown in figure 5.20. With higher filling degrees in the rotating drum the mixing time and respectively the number of rotations for complete mixing increase. This occurs because high rotational speed gives more rotation of the solid bed and which gives more movement of the solid particle and probably to get well mixed is more. Therefore at high rotational speed perfect mixing can be achieved for less time.

For low rotational speed, solid in the bed moves slowly and so it take longer time to be in contact with the cold solid. So mixing time is more.

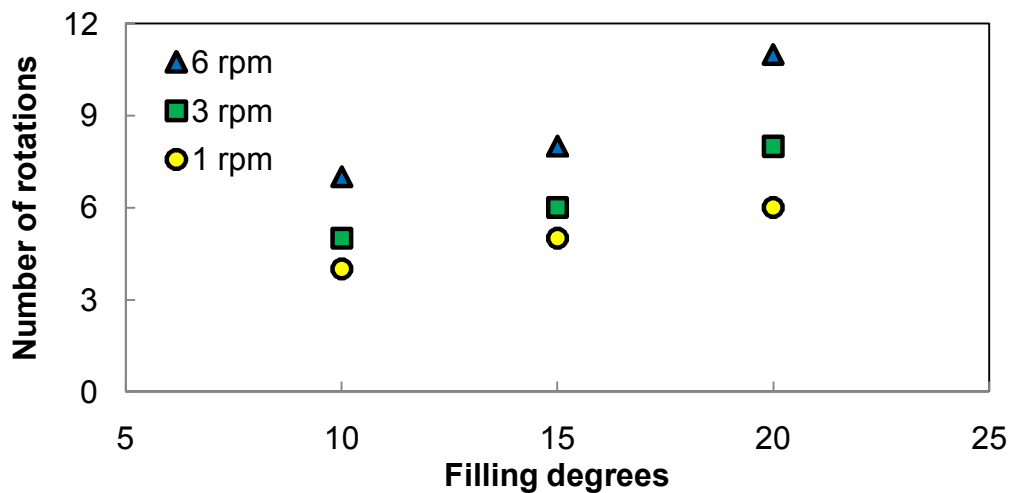


Figure 5.20 Effect of rotational speed on filling degree.

Number of rotation of the solid bed is depends on the rotational speed of the cylinder and filling degree. With higher filling degrees in the rotating drum the mixing time and

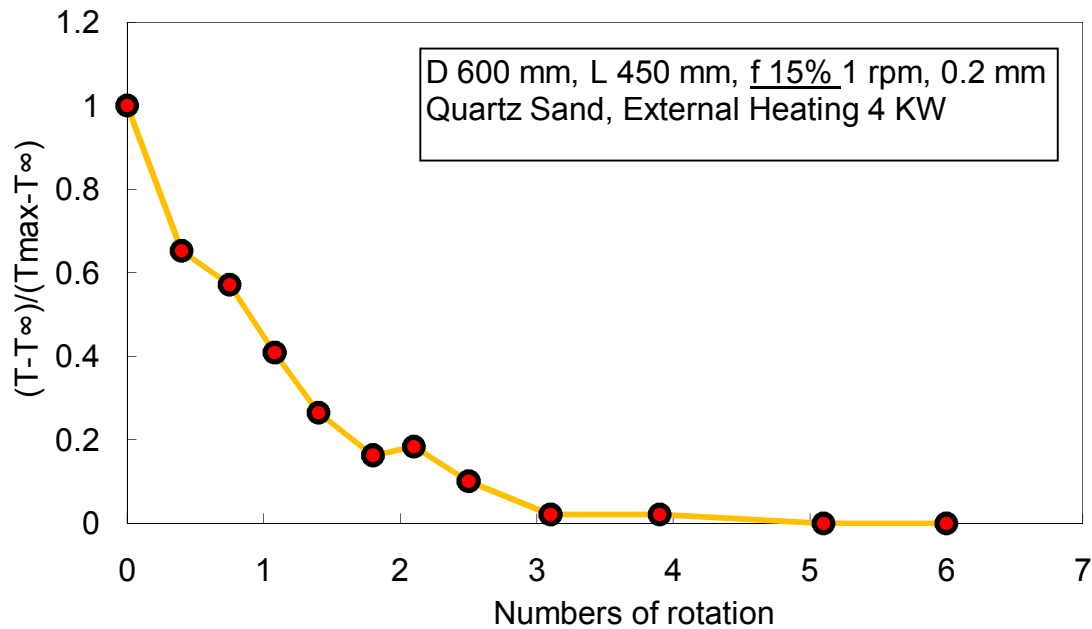


Figure 5.21 Dimensionless temperature with number of rotations of kiln

respectively the number of rotations for complete mixing increases.

Similarly, an uniform mixing can be shown by using another approach. Figure 5.21 shows a plot of dimensionless temperature with number of rotations. Experimental conditions have been mentioned before in this study. This curve meet to the X axis after six bed rotations, it indicates that it needs six rotation for the rotary kiln to get uniform mixing of the hot and sold layer of the sand.

A dimensionless number has been formed to compare the results from the experiments of two different colors of sand particles and with the mixing of hot and cold layer of quartz sand, a comparison have been made as shown in figure 5.22. A formed dimensionless temperature is the ratio of the temperature difference between temperature of bed to the final uniform temperature of the bed with respect to the maximum bed temperature to the final uniform temperature of the bed. Subtraction of this number from unity forms a parameter called goodness of mixture. This parameter varies from zero to one. The value one to this parameter represent perfect mixing. Based on the blue and red colours

mixture [14] it has been observed that at rotational speed of 3 rpm, with 10 % filling degree; a goodness of the mixture can be achieved at 0.78 value with 5 number of rotation of the kiln. Similarly our analysis with hot and cold sand experiments, the number of rotation needed for the both layer of sand to get mixed well are also 5. Here we achieved goodness of mixture value one. The number of rotation to get uniform temperature is increases with increase in the filling degree.

Table 5.4 indicate the summary of the results for 10% and 20% of filling degree. I indicate the results from the experiments of hot and cold layer sand to mix together and II

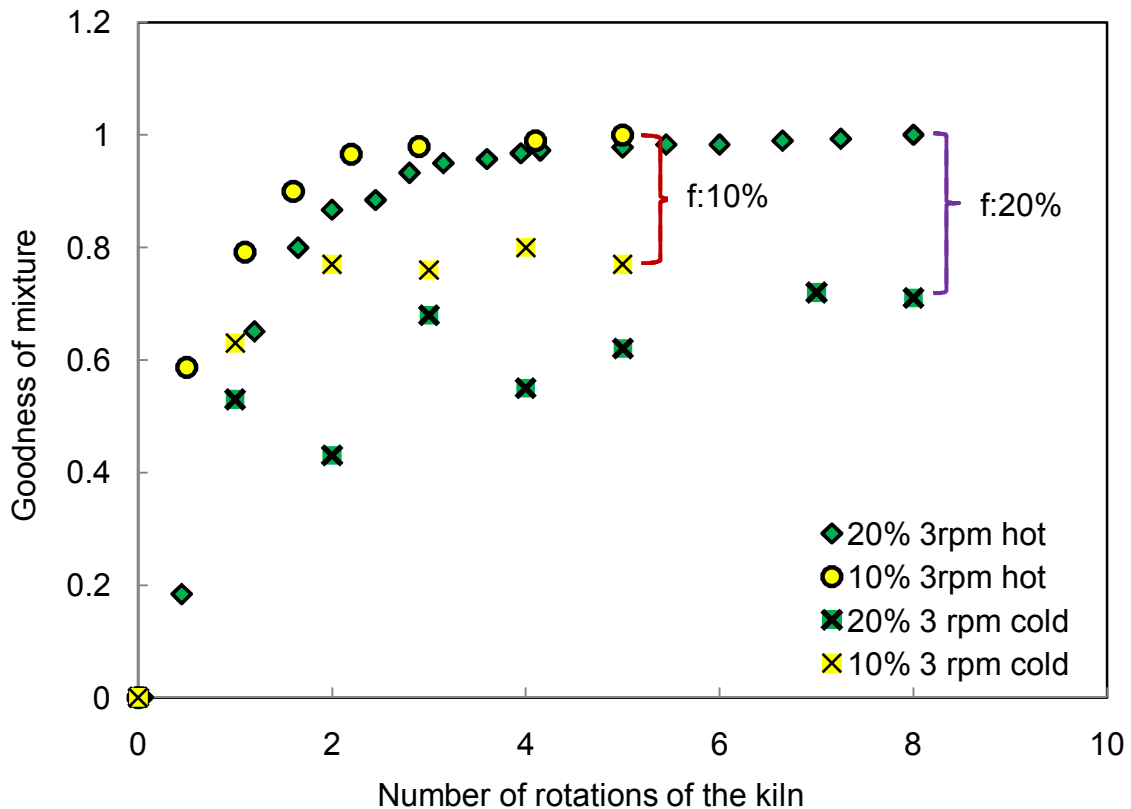


Figure 5.22 Comparison of goodness of mixture with number of rotations

indicates for two different colors particles [14]. It represents comparison of good match of the both experimental results.

<b>Filling degree f</b> <b>n = 3 rpm</b>	<b>Number of rotations</b> <b>I</b>	<b>Number of rotations</b> <b>II</b>
0.10	5	5
0.20	8	8

Table 5.4 Comparison of experimental results for number of rotations

### **5.5 Concept of rotation of the agitated solid bed with respect to the rotation of the rotary kiln.**

As explained before the various type of the motions occurs in the rotary kiln, very limited knowledge about the rotational motion of the bed have found in the literature. Therefore, in the present study, more focus has been given to the measurements of number of rotations of the agitated bed. Rotary kiln rotates with some specific rotational speed, at the same time agitated solid bed inside also rotates depending on the filling degree and the speed of rotation. It is interesting to observe the number of rotation of the agitated solid bed with respect to the kiln rotations.

A series of experiments have been performed with a layer of cold and hot solid at various filling degrees and various rotational speeds. When hot layer of sand get mixed with cold layer of sand, a various fluctuation of the temperature of the plots have been observed.

The fluctuations of the temperature inside the agitated bed are due to the mixing of the hot and cold sand. Each fluctuation of the temperature represents the one rotation of the agitated solid bed. From this study it can be easier to see after how many rotations of the agitated sold bed, an uniform mixing can achieved.

Figure 5.23 represents number of rotation of the rotary kiln needed to achieve the uniform temperature of the overall agitated solid bed with respect to time. Experiments

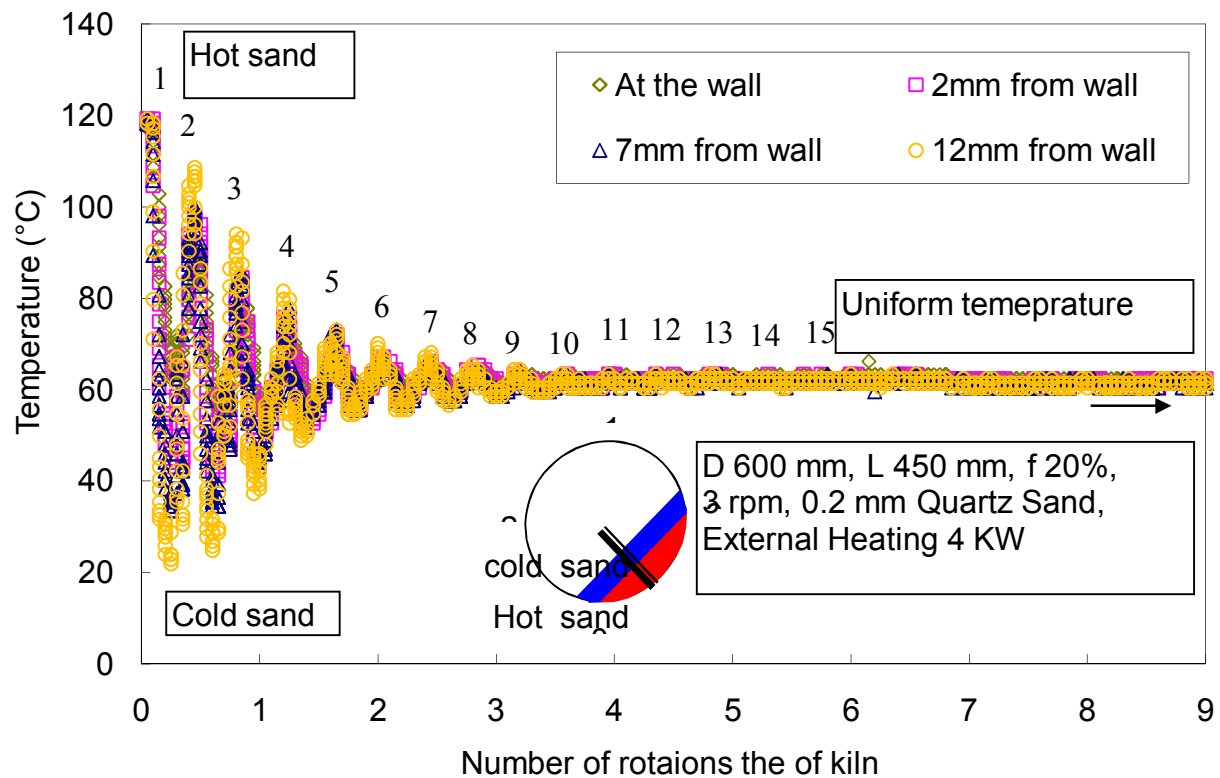


Figure 5.23 Temperature path of rotating solid bed for f:20% and 3 rpm

have been carried out with Quartz sand of 0.2 mm, 20% filling degree with rotational speed of 3 rpm. It has been observed that eight rotation of the rotary kiln gives almost 23 rotation of the agitated solid bed.

More observations of the number of rotation of the solid bed has been made. Figure 5.24 indicates the temperature plot of two thermoelements located at the wall and at 102 mm from the wall at the fixed position of angle 45°. It has been observed that at the rotations speed of 6 rpm and 15% of filling degree, it take 17 rotation of the agitated solid bed at 6 number of rotation of the rotary kiln have been observed.

Similar experiments have been carried out with 1 rpm at similar conditions. figure 5.25 indicates the temperature plot of two thermoelements located at the wall and at 12 mm from the wall at the fixed position of angle 45°. It has been observed that, uniform

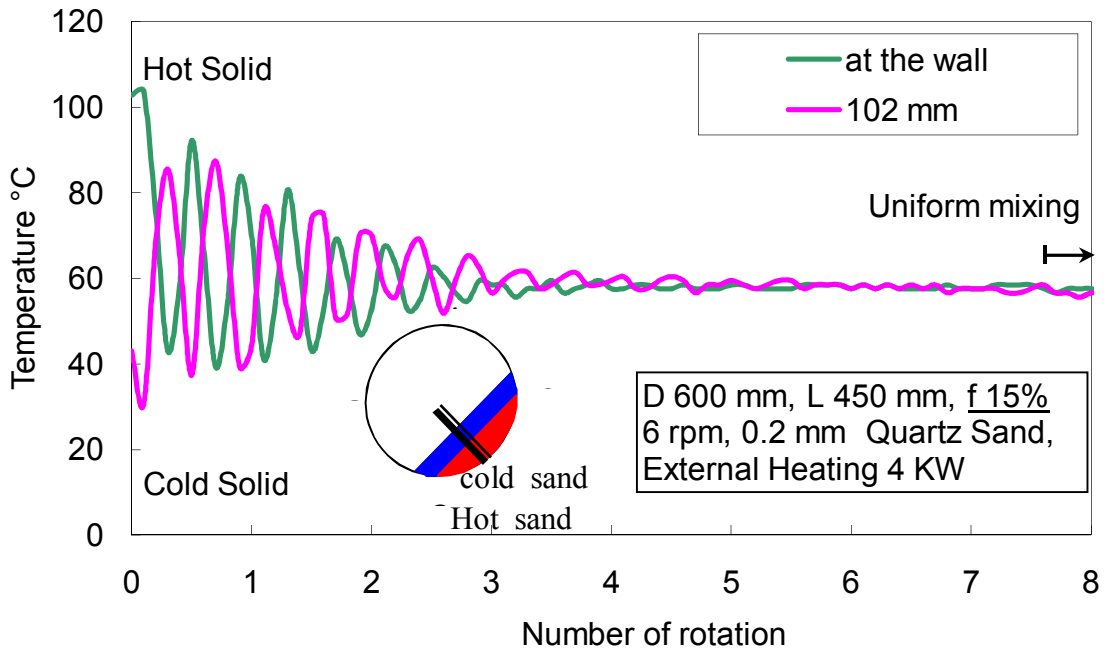


Figure 5.24 Temperature path of rotating solid bed for f:15% and 6 rpm

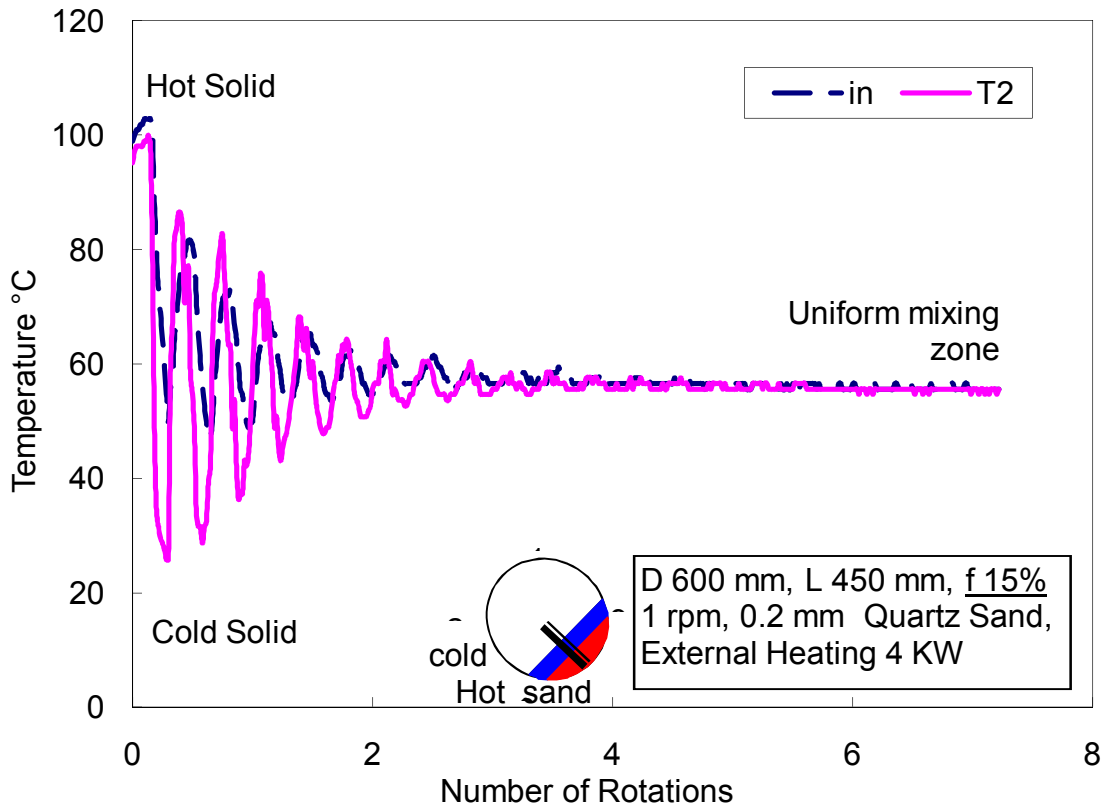


Figure 5.25 Temperature path of rotating solid bed for f:15% and 1 rpm

mixing of the hot layer and cold layer of sand has been achieved at 15 rotation of the agitated solid bed with respect to the 5 rotation of the rotary kiln.

## **5.6 Conclusion**

For the industrial rotary kilns a good mixing of solids represents homogenous products with high quality. A new approach of heat transfer mechanism which relates with mixing of the solids have been carried out successfully. The mixing can be experimentally determined with hot and cold layer of the solid bed. Experiments have been carried out with various filling degrees and rotational speeds. Number of rotations needed for the perfect mixing of the hot and the cold layer of the sand have been studied thoroughly. It has been observed for higher filling degrees, number of rotations for the perfect mixing of hot and cold layer of the sand also high. Mixing time for perfect mixing decreases with increase in rotational speeds.

A new parameter; goodness of mixture has been formulated. It defines at which extent a mixing can be done. These experiments are compared with other experiments which are carried out using solids of two different colours. It has been observed that results with both mechanisms matches perfectly.

Rotation of the agitated solid bed with respect to the rotation of the kiln has been studied thoroughly. This approach can give better understanding of the mixing and heat transfer phenomenon inside the agitated solid bed. More experiments with various filling degrees with different rotational speeds have to be performed for better understanding of the solid bed rotation phenomenon.

## **5.7 References**

- [1] Henein, H., Brimacombe, J.K., Watkinson, A.P., Experimental study of transverse bed motion in rotary kiln, Metallurgical Transaction, 14B, 1983a, 191-205

- [2] Henein, H., Brimacombe, J.K., Watkinson, A.P., The modeling of transverse solids motion in rotary kiln, *Metallurgical Transaction*, 14B, 1983b, 207-220
- [3] Heydenrych, M.D., Greeff, P., Heesink, A.B.M., Versteeg, G.F., Mass transfer in rolling rotary kilns: a novel approach, *Chemical Engineering Science*, 57, 2002, 3851-3859
- [4] Liu, X., Specht, E., Mellmann, J., Slumping-rolling transition of granular solids in rotary kilns, *Chemical Engineering Science*, 60, 2005, 3629-3636
- [5] Liu, X., Specht, E., Guerra Gonzalez, O., Walzel, P., Analytical solution of the rolling-mode granular motion in rotary kilns, *Chemical Engineering and Processing*, 45, 2006, 515-521
- [6] Mellmann, J., Liu, X., Specht, E., Prediction of rolling bed motion in rotating cylinders, *AIChE Journal* 50, 1, 2004, 2783-2793
- [7] Mellmann, J., Specht, E., Mathematical modelling of the transition behaviour between the various forms of transverse motion of bulk materials in rotating cylinders (part 2), *Cement-Lime-Gypsum International*, 54, 2001, 380-402
- [8] Woodle, G.R., Munro, J.M., Particle motion and mixing in a rotary kiln, *Powder Technology* 76, 1993, 241-245
- [9] Sommer, K., *Sampling of powders and bulk material*, Springer-Verlag, Berlin, Heidelberg, 1986
- [10] Boss, J., Evaluation of the homogeneity degree of a mixture, *Bulk Solids Handling*, Vol.6 No.6, 1986, 1207-1214
- [11] Stange, K., Beurteilung von Mischgütern mit Hilfe statistischer Verfahren, *Chemie-Ingenieur-Technik* 26, 3, 1954, 150-155
- [12] Weydanz, W., Zeitlicher Ablauf eines Mischvorganges, *Chemie-Ingenieur-Technik* 32, 5, 1960, 343-349
- [13] Schubert, H., Heidenreich, E., Liepe, F., Neeße, T., *Mechanische Verfahrenstechnik II*, VEB Deutscher Verlag für Grundstoffindustrie, Leipzig, 1979
- [14] Gonzalez, O.G., *Untersuchungen zum Misch- und Transportverhalten von Schüttgütern in Drehrohren*, Dissertation, TU Dortmund, 2008

## CURRICULUM VITAE

**NAME** YOGESH SONAVANE  
**DATE OF BIRTH** 10th April, 1978  
**NATIONALITY** Indian  
**Email** yogeshsonavane2000@gmail.com

### EDUCATION

Doctorate in Engineering (Dr.-Ing.) June. 2006- June 2010  
Otto Von Guericke University Magdeburg, Germany

Master of Technology Oct. 2003-Nov. 2005  
(Chemical and Process Engineering)  
Otto Von Guericke University Magdeburg, Germany

Bachelor of Technology May. 1996-May. 2000  
(Chemical Engineering)  
Pravara Rural College of Engineering, Loni, India

Secondary and Higher sec. school June 1988 - March 1996  
K.B.H. Vidyalay Malegaon camp India

Primary school June 1982 - March 1988  
Bharat Vidyalay Malegaon camp India

### INDUSTRY EXPERIENCE

#### **1) Tech Flow Engineers India Pvt. Ltd. India**

Technical Chemical Engineer From 12/12/01 to 11/12/2002 in research and development department. Gained experience in CAD and ANSYS. Planning, implementation and evaluation of development tasks: from new ideas to commissioning of industrial prototypes

#### **2) Namdev Silicate & Chemical Pvt. Ltd. India**

Technical Chemical Process Engineer from 01/11/2000 to 11/12/2001 in research and development department. Gained experience in process development. Gained experience preparation of reports, projects managing, etc.

### EXPERIENCE AT UNIVERSITY

Otto Von Guericke University Magdeburg, Germany Since May 2006 to June 2010, teaching for Master and PhD students in Heat Transfer and ANSYS

## **PROFESSIONAL PUBLICATIONS AND CONFERENCES**

- **Sonavane Yogesh** and Specht E, “Study of temperature profile in the case of pilot scale externally heated rotary kiln”, Conference of AIChE spring meeting, Tampa, Florida USA 2009.
- **Sonavane Yogesh** and Specht E., “Numerical modelling of the rotary kilns in the industrial processes by using ANSYS (Finite Element Method), Conference DSL Rome Italy June 2009.
- Herz F., **Sonavane Y.**, Specht E., Bensmann, S; Walzel, P “Mixing behaviour of granular material in the agitated bed of rotating drums”, Bulk Solids & Powder- Science & Technology. Vol 4 (2009) No 3, page 109-116
- Herz F., **Sonavane Y.**, Specht E., Bensmann, S; Walzel, P “Mixing behaviour for the mass and heat of granular material in the agitated bed of rotating drums”, Conference MCGM China, September 2009
- **Sonavane Yogesh** and Specht E., “Numerical analysis of heat transfer in wall of the rotary kiln using finite element method ANSYS, Seventh international conference on Computational Fluid Dynamics in Mineral and Process industries Melbourne, Australia, December 2009.